Exploring parity-time ($\mathcal{PT}$)-symmetry in Nonlinear Optics

Samit Kumar Gupta

A thesis
Submitted for the Degree of

Doctor of Philosophy

Department of Physics
Indian Institute of Technology Guwahati
Guwahati-781 039, India

June 2016

Exploring parity-time ($\mathcal{PT}$)-symmetry in Nonlinear Optics

Samit Kumar Gupta

A thesis
Submitted for the Degree of

Doctor of Philosophy

Supervisor

Dr. Amarendra Kumar Sarma

Department of Physics
Indian Institute of Technology Guwahati
Guwahati-781 039, India

June 2016

Proclamation

I hereby declare that the contents of the Thesis are results of authentic scientific pursuits and have not been submitted for consideration for any other degree in this institute or any other university. Apart from the collaboration as mentioned in the text of the Thesis and the Acknowledgements, it does not contain any results of others.

Samit Kumar Gupta
Dept. of Physics, IIT Guwahati June 2016

Certificate

It is certified that the work contained in this Thesis work entitled as, "***Exploring parity-time ($\mathcal{PT}$)-symmetry in Nonlinear optics***" by Mr. Samit Kumar Gupta, a student in the Department of Physics, Indian Institute of Technology Guwahati was carried out under my supervision and has not been submitted elsewhere for award of any degree.

Dr. Amarendra Kumar Sarma
Dept. of Physics, IIT Guwahati

June 2016

Dedicated to my beloved parents, Shree Ram Bahadur Gupta (late) and Smt. Sumitra Gupta, "***RamSumi***"

Acknowledgements

I feel immensely happy and grateful to convey my gratitude to all of you who have contributed to this thesis in their unique way.

First of all, my sincere gratitude goes to my PhD Supervisor, Dr. Amarendra Kumar Sarma for his excellent and inspiring guidance over the span of my PhD thesis work. His careful, systematic and punctual way of supervision has enabled me to carry out a timely completion of my PhD thesis. It is needless to say that his highly professional guidance is a rare blend of critical mentorship and affectionate guardianship for nurturing a novice mind. I have learned a lot from his guidance not only towards my PhD thesis work, but also towards general way of life. His intuitive vision and friendly kind approach has been impactful even in the difficult times. This has been instrumental to shape my own professional as well as the personal outlook to a significant extent. The freedoms in thinking and carrying out my research activities have given me self-confidence and motivation for further life.

I would like to convey my cordial gratitude towards my PhD thesis Doctoral Committee members: Dr. Alika Khare, Dr. Tarak Nath Dey and Dr. Anupam Saikia for their valuable comments, suggestions and support during the review seminars and presentations. I also express my gratitude to Dr. Debasish Borah for his useful suggestions.

I extend my sincere gratitude to the present and the past Heads of the Department for their full support and different kinds of facilities. I extend my cordial thanks and gratefulness to all the Faculty members of the department for their care and support during my PhD life. My thanks also go Mr. Basab for his system managements help in the numerical lab and the non-teaching staff members of the department.

The financial support provided through a research fellowship by the Ministry of Human Resource and Development (MHRD) of India is gratefully acknowledged.

I am grateful to my senior group-mates Dr. Manirupa Saha and Dr. Parvendra Kumar for their encouragement and support. I also thank my junior group-mates Mr. Jyoti P. Deka,

Mr. Koushik Paul, Mr. Subhadeep Chakraborty and Ms. Bijita Sarma for their helps and informal discussions. I also thank Ms. Rajitha and Mr. Sujay for their support and useful discussions.

I thank my seniors Dr. Supriyo Roy, Dr. Bappaditya Pal, Ramesh Ghosh, Biswajit Karmakar and Anabil Gayen and Nasir Alam for their suggestions and supports.

I thank my friends Arindam Mal, Arindam Ghosh, Aryaman, Mohosin, Kartik, Debasish, Sandeep, Gyan, Ranganadh, Bipul Mahesh, Sougata and DK for their supports and company. My sincere gratitude also goes to Bulbuli and Sagarika in this regard.

Finally, I pay my whole-hearted respect and gratitude towards my family whose unconditional love and support has always inspired me to take up a career in the science. I proudly remember and respect the hard work and the dreams that my parents carried in their eyes for me. I sincerely pay my regards and respect to my elder brother Amit, my sisters Rupa, Mita and Nirupa for their love and support. Their unwavering faith and belief in me has motivated me to go forwards in the midst of all kinds of situations.

Although, strictly speaking I am not a theist, but I believe that there is a unifying and universal consciousness that connects humanity with trust, respect and integrity: God. I thank Him for his blessings in my life.

Abstract

One of the most fruitful strategies in optics research is to investigate the implications of concepts and mathematics used in seemingly very different fields of physics such as quantum field theory and high-energy physics. One such recent concept widely explored in the context of optics is the so-called Parity-time (PT) symmetry. PT Symmetry can be realized in an optical system with judicious manipulation of optical loss and gain. In fact, this may result in achieving new classes of synthetic structures with altogether new physical behavior and novel functionality. PT-symmetry is no longer a theoretical concept only; it has been demonstrated experimentally numerous times in optical and other physical systems. This thesis work explores the idea of parity-time-symmetry in different types of optical structures and systems in the context of nonlinear optics. These include quadrimer waveguides, nonlinear Bragg structure, ring-resonator system, nonlocal Schrödinger system and negative-index metamaterials. Our studies on parity-time symmetric quadrimer waveguide explore the effects of the nonlinearity and the dispersions on the PT-phase transition of the system. In another nonlinear quadrimer configuration, with a different coupling scheme, we have addressed the issue of parity-time symmetry from attractor perspective. Next, we report analytical traveling solitary wave solutions for the forward and the backward waves in a nonlinear PT-symmetric Bragg grating structure. We predict the existence of bright solitary wave solution below the PT-threshold for forward wave and dark solitary wave solution above the PT-threshold for backward wave. In a definite parametric regime, the existence of optical rogue waves (ORWs) has been elucidated. In another work, in the recently discovered nonlocal nonlinear Schrodinger system with parity-time symmetric nonlinearity we have studied the Peregrine Soliton (PS) dynamics. Due to prototypical analogy between the Peregrine solitons and the rogue waves, we numerically confirm that an initial PS excitation could yield Peregrine rogue wave (PRW) in the broken PT-phase. In the single ring resonator system, we find that simple alterations in the parity-time (PT) symmetric synthetic coupler structures could result in a dynamically controllable algorithm for the chaotic dynamics inherent in the system. We have also shown the dependence of the period doubling point upon the input amplitude, emphasizing on the dynamical aspects. Finally, a theoretical study has been performed in order to explore the parity-time (PT)-symmetry in optical

negative-index material with parametric amplifier settings. In this study we have exploited the notion of parity-time (PT)-symmetry in order to address the issue of optical loss. It has been found that the strength of the signal can be significantly enhanced if the system is operated beyond the PT-threshold point. It is shown that the aforementioned behavior is robust against small deviation from the exact phase-matching condition or the PT-symmetry.

Contents

List of Figures

Chapter 1

Introduction

"The average quantum physicist on the street believes that a quantum-mechanical Hamiltonian must be Dirac Hermitian (invariant under combined matrix transposition and complex conjugation) in order to guarantee that the energy eigenvalues are real and that time evolution is unitary. However, the Hamiltonian $H = p^2 + ix^3$*, which is obviously not Dirac Hermitian, has a real positive discrete spectrum and generates unitary time evolution, and thus it defines a fully consistent and physical quantum theory. Evidently, the axiom of Dirac Hermiticity is too restrictive. While* $H = p^2 + ix^3$ *is not Dirac Hermitian, it is PT symmetric; that is, invariant under combined space reflection P and time reversal T. The quantum mechanics defined by a PT-symmetric Hamiltonian is a complex generalization of ordinary quantum mechanics. When quantum mechanics is extended into the complex domain, new kinds of theories having strange and remarkable properties emerge. Some of these properties have recently been verified in laboratory experiments. If one generalizes classical mechanics into the complex domain, the resulting theories have equally remarkable properties"*-**C. M. Bender** [1]

1.1 Background

The idea of the real and positive eigen-spectra of the non-Hermitian Hamiltonian $H = \hat{p}^2 + \hat{x}^2 + i\hat{x}^3$, where $\hat{p}$ and $\hat{x}$ are momentum and position operator respectively, came through discussions between two leading mathematical physicists of the world, Dr. Daniel Bessis of Texas Southern University, USA and Dr. Jean Zinn-Justin of Saclay Nuclear Research Centre, France who, at that time, were studying Lee-Yang edge singularity using renormalization group methods. Using moment methods, D. Bessis conjectured [2] upon the real and positive eigen-spectra of the non-Hermitian Hamiltonian. But, the studies on the reality of the eigen-spectra of the non-Hermitian Hamiltonians date back to some earlier times as pointed out by C. M. Bender [3]. These studies includes: early investigations upon Reggeon field theory [4] on the cubic quantum-mechanical Hamiltonian

$H = \hat{p}^2 + i\hat{x}^3$; work by Caliceti et al. [5] where it was claimed that the non-Hermitian Hamiltonian $H = \hat{p}^2 + i\hat{x}^3$ possesses real eigen-values. Until C. M. Bender, there was no rigorous and comprehensive proof of the conjecture by Bessis. He along with Stefan Boettcher, in their seminal paper [6] claimed that the real and positive eigen-spectra of the above-mentioned Hamiltonian were due to the parity-time (PT)-symmetry. The perturbative delta expansion technique [7] was employed to study the eigen-spectra of the system. In this work [6], they have considered a class of quantum-mechanical Hamiltonians designated by: $H = \hat{p}^2 + m^2\hat{x}^2 - (i\hat{x})^N$, where N is real. With respect to N and m they have discussed various phases of the system. They found that when $m = 0$, the spectrum of H shows three different spectral behaviors: i) for $N \geq 2$, H results in an infinite, discrete, entirely real and positive eigen-spectrum, ii) for $1 < N < 2$ this produces finite number of real and positive eigenvalues while an infinite number of complex conjugate pairs of eigenvalues, iii) for $N \leq 1$ it gives entirely complex eigen-spectra. $N = 2$ is the phase transition point. For $m \neq 0$, the spectrum of H involves another transition at $N = 1$ in addition to $N = 2$. Afterwards, this novel idea of parity-time (PT)-symmetry has been studied extensively in quantum field theory [8-13], non-Hermitian Anderson models [14], open quantum systems [15,16] and metamaterials [17] etc. Though the impact of parity-time symmetry is still debated in these areas, optics has recently turned out to be a testing ground for PT-related notions after the first experimental observation of parity-time symmetry in optics [18]. Since then, the concept of parity-time symmetry is experimentally and theoretically exploited in various contexts [19-24].

The notion of PT-symmetry entered into optics due to the isomorphism between the paraxial equation of diffraction and the Schrödinger equation in quantum mechanics, as explained later. It is worthwhile to mention that, the possibility of realizing PT-symmetry in optics was first proposed by Ruschhaupt, Delgado and Muga [25]. They have shown that Maxwell equations, for an electromagnetic wave travelling along a planar slab waveguide filled with gain and loss media in contiguous regions, could be approximated in a parameter range by a Schrödinger Equation with a PT-symmetric scattering potential. This theoretical proposition stimulated great deal of experimental studies pertinent to parity time (PT)-symmetry. It is appropriate to mention a few of them here. Guo et al. [13] demonstrated the observation of

PT-symmetry breaking and loss induced optical transparency in a pseudo-Hermitian optical guiding potential. In 2010, C. E. Rüter et al. [18] have shown the first ever experimental observation of the behavior of a PT optical coupled system based on Fe-doped $LiNbO_3$ being shone by Ar^+laser beam. This work has shown the spontaneous PT-symmetry breaking and power oscillations behaviors violating left-right symmetry (non-reciprocity). In another experimental report [19], A. Regensburger et al. have discussed about the nature and dynamics of light transport in large-scale temporal lattices respecting parity time (PT)-symmetry. They found that when these periodic lattice structures are operated near to their exceptional points, they could be used as a unidirectional invisible media. G. Vemuri et al. [26,27] studied parity-time (PT)-symmetry in tunable waveguide arrays and lattices. They reported quantum effects as well, in optical waveguide arrays [28]. In [20], L. Feng et al. have demonstrated the reflectionless unidirectionality on a chip-scale optical metamaterial close to the parity-time (PT)-symmetry breaking point paving the way for on-chip PT-Metamaterials and other relevant optical devices. Experimentally J. Schindler et al. [21] have demonstrated realization of a parity time (PT)-symmetric system based on coupled pair of modes of an active LRC circuits, in which one arm experiences amplification and the other one attenuation. Yet in another work, N. Bender et al. [22] have studied the asymmetric transport mechanism using parity-time (PT)-symmetric nonlinearity in an electronics system made of a pair of coupled Van der Pol oscillators. They also have provided corresponding optical analogue. In a dissipative microwave billiards system, S. Bitner et al. [23] have studied both theoretically and experimentally the PT-symmetry and the PT phase transition phenomena. N. M. Chtchelkatchev et al. [24] have studied both theoretically and experimentally the contribution of fluctuation to the superconductivity and the phenomena of PT-symmetry breaking in the temperature evolution. All these studies have virtually exploded PT-symmetry based research in condensed matter and optical systems in last few years.

In fact, one of the most fruitful strategies in optics research is to investigate the implications of concepts and mathematics used in seemingly very different fields of physics such as quantum field theory and high-energy physics. As stated earlier, one such concept widely explored in the context of optics is the so-called Parity-time symmetry (PT Symmetry). In

designing an optical system nature demands that one can only resort to the following three basic "ingredients": refractive index, gain, and loss. Researchers and engineers have cleverly used various gain mechanisms to boost weak signals and index contrast, e.g. in the so-called photonic crystals, to their advantages. But, loss is usually considered as a disadvantage and is avoided as far as possible, since it degrades the efficiency of the structures employed to perform useful operations. It is perhaps for this particular reason that researchers have never intentionally explored the combination of gain and loss as a duality of useful ingredients in device and materials engineering. Recently, as already discussed, an alternate viewpoint is emerging which aims at manipulating absorption through a judicious design that involves the combination of delicately balanced amplification and absorption mechanisms. This results in achieving new classes of synthetic structures with altogether new physical behavior and novel functionality. In fact, optical media with delicately balanced gain and loss, characteristic of systems with joint parity-time (PT) symmetry, have been reported [18], showing intriguing functionality. Recently, various linear and nonlinear PT-symmetric optical structures have been demonstrated theoretically and experimentally. It has been realized that PT symmetry can enable effects, behavior and applications that would have been impossible in a standard passive optical structure, such as breakdown of the left–right symmetry and power oscillations [29], unidirectional invisibility [30], broad-area PT single-mode lasers [31], and coherent perfect absorbers [32-34]. PT symmetry has also been explored in the context of nonlinear optics by various research groups. To mention a few, they include the effect of nonlinearity on beam dynamics in PT-symmetric potentials [35], stable dark solitons in dual-core waveguides [36], dynamics of a chain of interacting PT-invariant nonlinear dimers [37], and Bragg solitons in nonlinear PT-symmetric periodic potentials [38].

Drawing inspiration from the fact that optics has become the testing ground for the idea of Parity-time (PT)-symmetry, in this thesis we investigate various aspects of Parity-time (PT)-symmetry in a variety of physical systems including coupled waveguides systems, Bragg grating structures, ring-resonators systems and nonlocal Schrödinger system with parity-time (PT)-symmetric nonlinearity, negative index media with parametric amplifier settings. We have employed both theoretical and numerical approach to study these systems.

1.2 Basics of PT-symmetry

Parity (P) and Time-reversal (T) symmetries are fundamental notions in physics. They are represented by their actions on the position operator ($\hat{x}$) and momentum operator ($\hat{p}$). $\hat{P}$ is a linear operator which inverses both space and momentum:

$$\hat{x} \to -\hat{x} \quad \text{and } \hat{p} \to -\hat{p}, \tag{1.1}$$

On the other hand, $\hat{T}$ represents an antilinear operator that reverses the time $t \to -t$ and is defined as:

$$\hat{x} \to \hat{x},\ \hat{p} \to -\hat{p} \text{ and } i \to -i \tag{1.2}$$

Recently, systems that do not obey P and T symmetries separately but respect the combined PT symmetry, is attracting lots of attention. Such systems are described by a Hamiltonian (H) which commutes with the combined PT operator: $[H, PT] = 0$. Bender and Boettcher [6] pointed out that such Hamiltonians can in general be non-Hermitian and still they may exhibit entirely real spectra. In optics, the idea of PT-symmetry entered owing to the mathematical isomorphism of quantum Schrödinger equation to paraxial equation of diffraction. To understand it, let us consider the usual Schrödinger equation of quantum mechanics:

$$i\hbar \frac{\partial \psi}{\partial t} = -\frac{\hbar^2}{2m}\frac{\partial^2 \psi}{\partial x^2} + V(x)\psi \tag{1.3}$$

Here, $\hbar$ is the reduced Planck's constant, ψ is the wave function, m is the mass of the particle and $V(x)$ is the potential. In the usual quantum mechanics $V(x)$ is a real function and consequently the corresponding Hamiltonian becomes Hermitian. But, if $V(x)$ is a complex function, the time independent Hamiltonian: $H = \frac{\hat{p}^2}{2m} + V(x)$ is obviously non-Hermitian. However, if this Hamiltonian satisfy the relation $[H, PT] = 0$, i.e. H is PT-symmetric, then it is straightforward to see that we must have $V(x) = V^*(-x)$. This implies that the real part of the potential is an even function of x, while the imaginary part of the potential function is an odd function of x, i.e. $V_R(x) = V_R(-x)$ and $V_I(x) = -V_I(-x)$. Thus, the Hamiltonian

must have the form: $\widehat{H} = \frac{\hat{p}^2}{2m} + V_R(x) + i\lambda V_I(x)$, $\lambda > 0$ in order to be PT-symmetric. It turns out that as long as $\lambda < \lambda_{th}$, where λ_{th} is some threshold value, the Hamiltonian shows entirely real eigen-spectra. On the other hand if $\lambda > \lambda_{th}$, the eigenspectrum ceases to be real and include complex eigenvalues as well. Now, let us consider the paraxial equation of diffraction in optics:

$$i\frac{\partial E}{\partial z} + \frac{1}{2k}\frac{\partial^2 E}{\partial x^2} + k_0 n(x)E = 0 \tag{1.4}$$

Here, E is the electric field envelope, $k_0 = 2\pi/\lambda_0$, λ_0 is the wavelength in vacuum, $k = k_0 n_0$ and n_0 is the background refractive index. The isomorphism between Eq. (1.3) and (1.4) is quite evident. Also, it is clear that the optical medium can be said to possess parity-time symmetry provided: $n(x) = n^*(-x)$ or $n_R(x) = n_R(-x)$ and $n_I(x) = -n_I(-x)$. It is well known that, the real part of the refractive index is responsible for dispersion while the imaginary part of refractive index is responsible for gain or loss in the optical medium [39]. So it is evident that if one engineers gain and loss in a media, it is possible to design a PT-symmetric system artificially. In fact this was what done in the seminal work of Rüter et al. [18]. The idea of PT-symmetry in the context of optics may be more clearly understood by considering the case of linear optical coupler.

Let us consider a symmetric coupler with one arm having loss and the other one having gain, as shown in Fig.1.1.

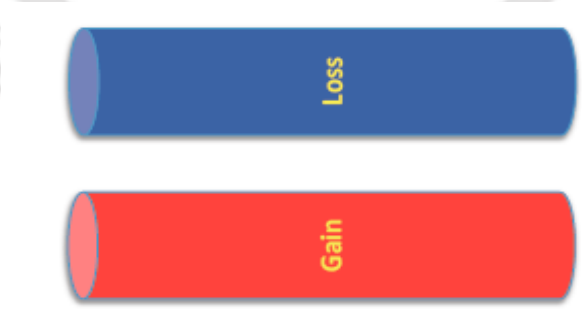

Figure 1.1: A basic nonlinear coupler with loss in first core and equal gain in second one.

The propagation dynamics of the coupler can be modeled by the normalized generalized coupled differential equations:

$$i\frac{\partial a_1}{\partial z} = -iga_1 - ka_2 \tag{1.5a}$$

$$i\frac{\partial a_2}{\partial z} = iga_2 - ka_1 \tag{1.5b}$$

Here a_1 represent the slowly varying pulse envelope in the first core with loss while a_2 represent the corresponding component in the second core with gain. g and k are respectively the normalized gain/loss and the linear coupling parameter. Here 'z' is scaled as $z = z_{ns}/L_D$, where z_{ns} is the propagation distance without scaling and , L_D= dispersion length = $T_0^2/|\beta_2|$, where T_0=pulse-width. The linear coupler is parity-time (PT) symmetric, as the system satisfies the condition: $[H,\ PT] = 0$ where the Hamiltonian, H and the parity operator, P, are defined as follows:

$$H = \begin{pmatrix} -ig & -k \\ -k & ig \end{pmatrix} \tag{1.6}$$

$$P = \begin{pmatrix} 0 & 1 \\ 1 & 0 \end{pmatrix} \tag{1.7}$$

The eigenvalues, λ, of this system can be found, via a direct diagonalization, as: $\lambda = \pm\sqrt{k^2 - g^2}$. It is easy to see that λ is real for $g < k$ and becomes imaginary for $g > k$. The sharp transition from a real to a complex spectrum takes place at $g_{PT} = k$, known as PT-threshold. It is also known as the exceptional point [18]. As the gain/loss parameter g increases above g_{PT}, the eigenvalues become complex and the system enters into the so-called broken PT-symmetric phase. If the system is kept below the threshold, its supermodes could be identified as:

$$|1\rangle = [e^{i\theta/2} \quad e^{-i\theta/2}]^T\ , \quad |2\rangle = [ie^{-i\theta/2} \quad -ie^{i\theta/2}]^T$$

where, $\theta = sin^{-1}(g/k)$. None of the supermodes experiences gain/loss and they remain neutral and oscillate during propagation. On the other hand, if the system is kept above the exceptional point, the supermodes are:

$$|1\rangle = [e^{-\theta/2} \quad -ie^{\theta/2}]^T, \quad |2\rangle = [e^{\theta/2} \quad -ie^{-\theta/2}]^T$$

where $\theta = cosh^{-1}(g/k)$. In this case, the PT symmetry is spontaneously broken: the eigenvectors are no longer PT-invariant and are not any more eigenfunctions of the PT operator. It is interesting to note that the two supermodes coalesce at the exceptional point, a typical signature of a PT-symmetric system. The peculiarities of PT-symmetric regimes can be observed from Fig. 1.2, where we plot the spatial evolution of power in both the waveguides when power is initially launched in the first waveguide, here it is a loss waveguide.

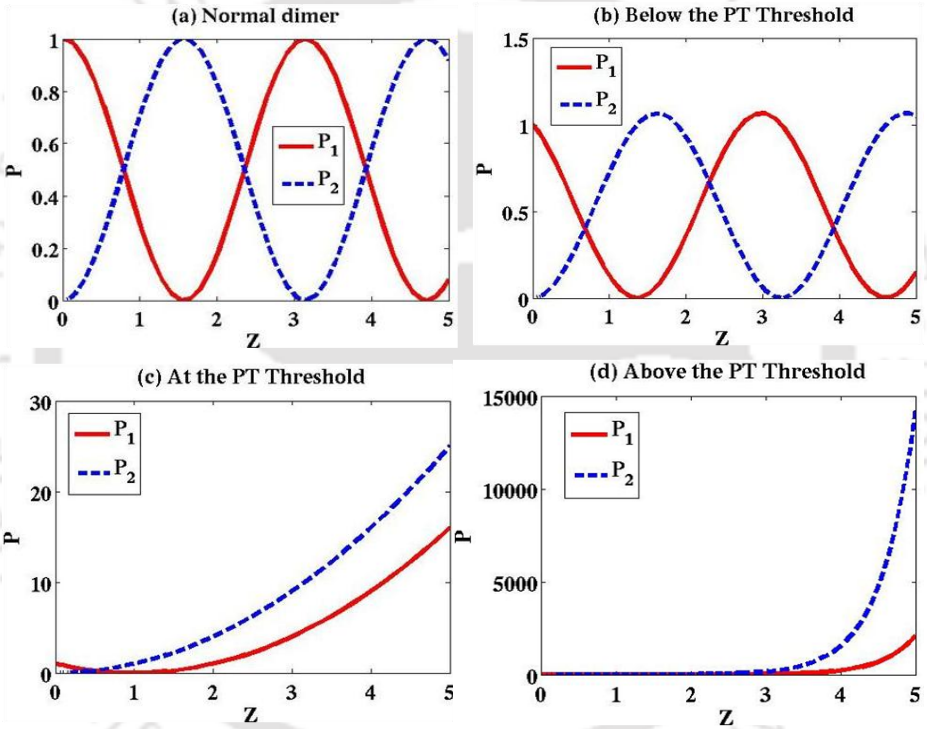

Figure 1.2: Spatial evolution of optical power in the coupler with k = 1 (a) g = 0 (b) g = 0.25 (c) g = 1 (d) g = 1.5.

It can be seen that below the PT-threshold, optical power oscillates between the two waveguides. However ***at*** and ***above*** the threshold exponential increase in power is observed, this increase is, obviously, larger in the gain waveguide. Fig. 1.3 depicts the contour plots of

the intensity profiles of the fields when a Gaussian field with unit amplitude is launched in the first waveguide. The simulated results are in conformity with the ones in Fig. 1.2.

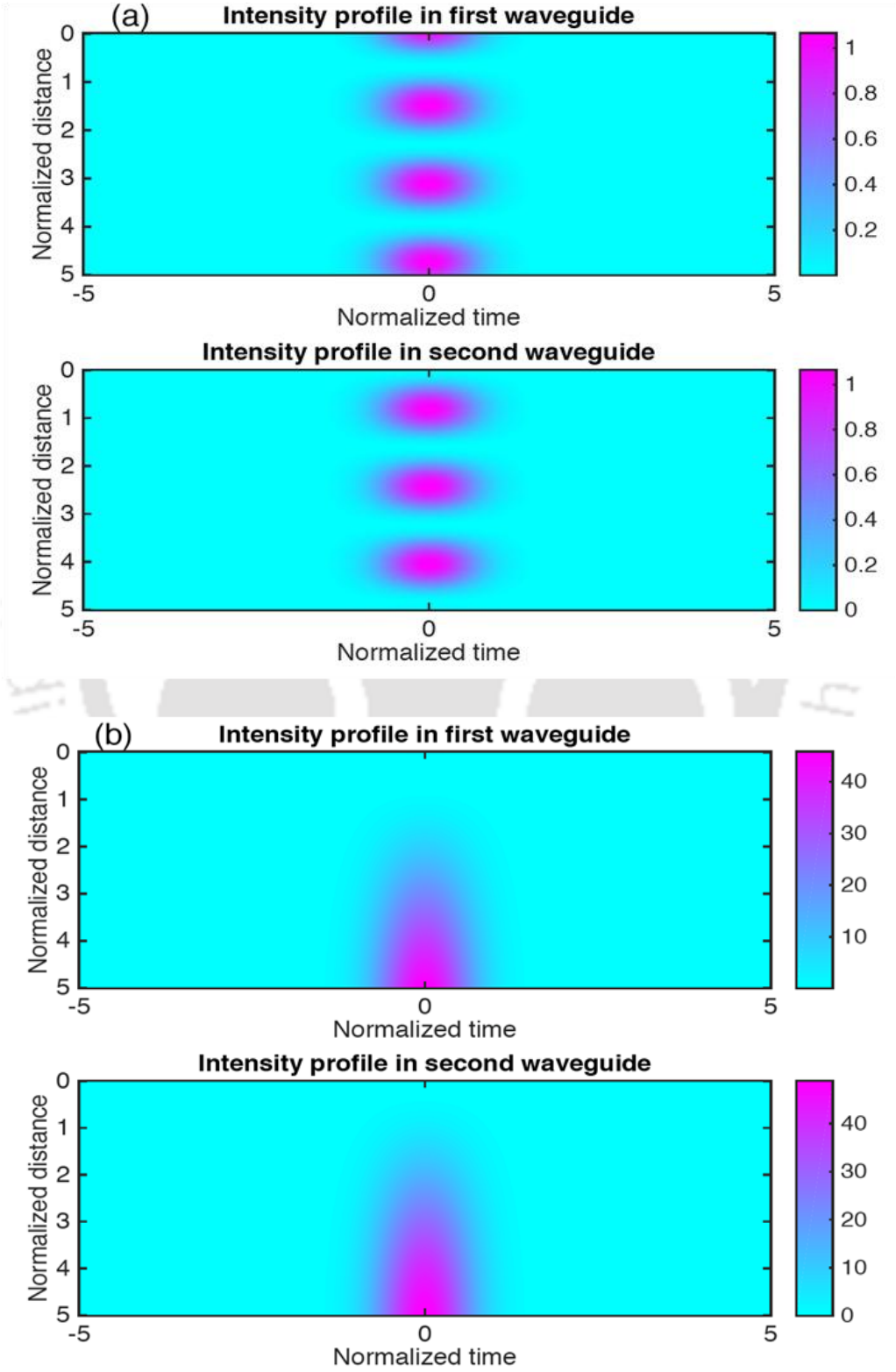

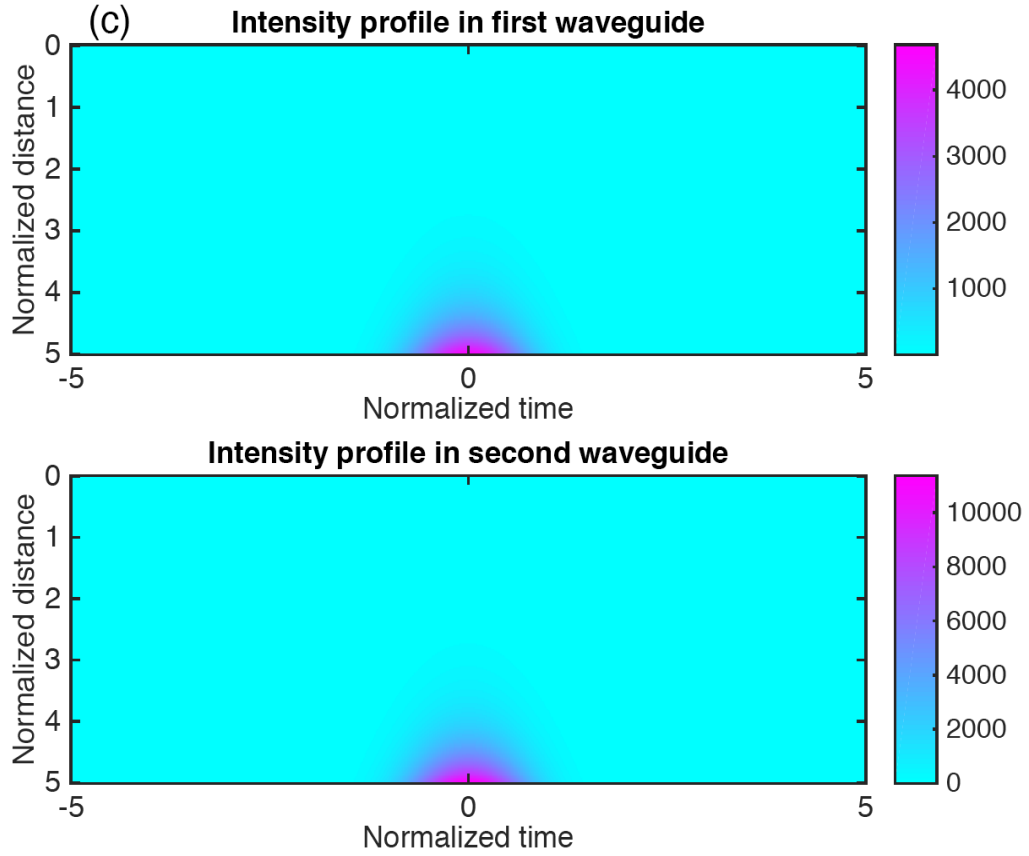

Figure 1.3: Contour plots of intensity profiles in the waveguides in the coupler (a) Below the PT-threshold (b) At the PT-Threshold (c) Above the PT-Threshold.

An intuitive picture of PT-symmetry was put forward by Carl M. Bender et al. [40]. Let us consider two boxes positioned at $x = -a$ and $x = a$. The box at $x = a$ is a sink which absorbs energy at some rate and the one at $x = -a$ is a source that radiates energy at the same rate. If the system is isolated i.e. the boxes are not coupled sufficiently strong enough to each other, then the system cannot be in equilibrium. It is because the energy in the left box will decay down to zero whereas the energy in the right box will grow into infinity. The corresponding energies in the two modes are complex. Now, if the two boxes are coupled strongly enough then the system can equilibrate and the corresponding energy will be real.

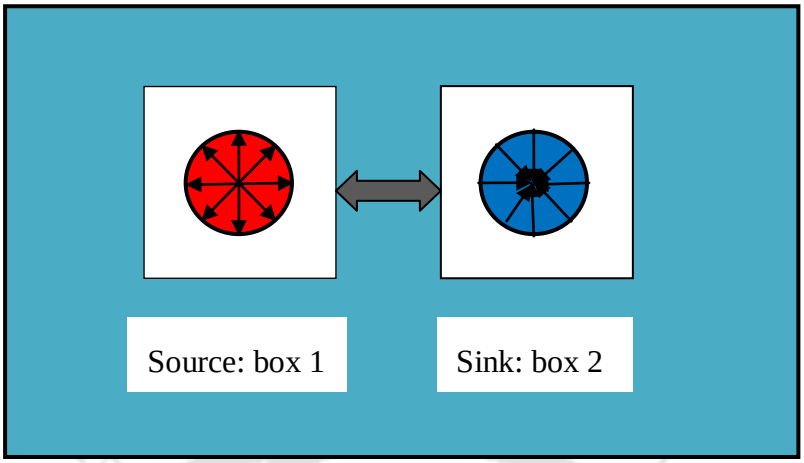

Figure 1.4: The source-sink model. In this case, the boxes are sufficiently coupled to each other so that the corresponding modes in them can equilibrate.

The time evolution of the one-component system in box 1 (source) can be described by the Schrödinger equation:

$$i\frac{d\psi(t)}{dt} = H\psi(t) \tag{1.8}$$

Here, $H = [E_1] = [\rho e^{i\phi}]$, where $\rho > 0$ and $0 < \phi < \pi$. The solution of Eq. (1.8) is: $\psi(t) = \psi\,(0)e^{-iE_1 t}$, with $\mathrm{Im}(\mathrm{E}_1) < 0$. Similarly, for box 2 (sink) we have: $H = [E_2] = [\rho e^{-i\phi}]$.

The solution to the Schrödinger equation yields, $\psi(t) = \psi\,(0)e^{-iE_2 t}$ with $\mathrm{Im}(\mathrm{E}_2) > 0$. The entire system can be described as:

$$H = \begin{bmatrix} \rho e^{i\phi} & 0 \\ 0 & \rho e^{-i\phi} \end{bmatrix} \tag{1.9}$$

This Hamiltonian is not Hermitian but it is PT-symmetric with the parity operator defined in Eq. (1.7). However, the composite system is not in equilibrium since the eigenfunctions of the system on the left grows exponentially in time being a source while the one on the right decays exponentially in time, being a sink. The whole system can equilibrate if we couple them sufficiently strong so that the following Hamiltonian now represents the system:

$$H = \begin{bmatrix} \rho e^{i\phi} & k \\ k & \rho e^{-i\phi} \end{bmatrix} \tag{1.10}$$

The eigenvalue of this new system will be real when $k^2 > \rho^2 sin^2(\phi)$ resulting into equilibrium state of the system. In this case, the system is said to be in the unbroken PT-phase. The eigenvalues are imaginary when $k^2 < \rho^2 sin^2(\phi)$. The system in this case is said to be in broken PT-phase. The critical point is defined as: $k_{cr}^2 = \rho^2 sin^2(\phi)$. It marks the transition point separating the broken and the unbroken PT phases.

1.3 Organization of the Thesis

The contents of the chapters in the remaining part of the present thesis are described briefly as follows:

Chapter 2: The chapter starts with an introduction to the coupled mode theory generally applicable to the coupled waveguides systems followed by the literature reviews pertinent to Parity-time (PT)-symmetry. We have studied a closed form PT-symmetric quadrimer optical waveguide structure. The beam dynamics of the structure have been studied numerically. The effect of inclusion of nonlinearity and dispersion was also briefly investigated and discussed. Further, we report a study on a closed-form nonlinear parity-time symmetric optical quadrimer waveguides system with a specific coupling scheme. The system yields power saturation behavior in the modes, which may be attributed to the inherent attractor in the system. A detailed analysis has been provided to confirm the attractor aspect of the system. This work also addresses a crucial issue regarding choice of initial conditions while carrying out numerical simulation for such systems.

Chapter 3: The chapter begins with a literature survey on the index-gratings, particularly Bragg grating structures with reference to the Massive Thirring Model (MTM). This chapter is devoted to the study of travelling wave solutions in a Parity-time (PT)-symmetric nonlinear Bragg grating structure. We observe that there is an infinite number of traveling-wave solutions, either solitary or of cnoidal type, depending on the parameter values of the system. The effects of the coupling constant, gain/loss parameter and the traveling-wave speed on the evolution dynamics of the solutions have been discussed. We have found a bright-solitary-wave solution below the PT-threshold for forward waves and a dark-solitary wave solution above the PT-threshold for backward waves. Depending on some suitable

choice of the parameter values of the system, the existence of ORWs has been elucidated.

Chapter 4: This chapter starts a discussion on the recently proposed continuous nonlocal Schrödinger Equation model with Parity-time (PT)-symmetric nonlinearity by Ablowitz and Musslimani [107] with relevant literature reviews. Taking the general solitons on the finite background ansatz as the initial excitation, a numerical study has been carried out with special emphasis given to the Peregrine soliton dynamics. Since, the Peregrine solitons have been seen as a rogue-wave prototype for a long time, we numerically confirmed that an initial PS excitation could yield PR wave in the broken PT-phase. Upon numerical computation, we observe the appearance of low-intense Kuznetsov-Ma (KM) soliton trains in the absence of transverse shift and well-localized high-intense Peregrine Rogue waves in the presence of transverse shift in a definite parametric regime. In the earlier case, the PT-symmetry is unbroken, whereas in the later case the PT-symmetry is broken.

Chapter 5: In this chapter, we show the possibility of controlling the dynamical behavior of a single fiber ring (SFR) resonator system with the fiber being an amplified (gain) channel and the ring being attenuated (loss) nonlinear dielectric medium. Our model is based on the simple alterations in the parity time symmetric synthetic coupler structures proposed recently in Ref. [173]. The system has been modeled using the transfer matrix formalism. We find that this results in a dynamically controllable algorithm for the chaotic dynamics inherent in the system. We have also shown the dependence of the period doubling point on the input amplitude, emphasizing on the dynamical aspects. Moreover, the fact that the resonator essentially plays the role of a damped harmonic oscillator has been elucidated with the non-zero intensity inside the resonator due to constant influx of input light.

Chapter 6: This short chapter discusses PT-symmetry in optical negative-index metamaterials in parametric amplifier settings with $\chi^{(2)}$ nonlinearity. The study aims to address the nontrivial issue of optical losses in such systems and suggests the judicious operation of the system above the PT threshold can result desirable enhancement of the signal field.

Chapter 7: Finally, in this chapter we summarize the results and the analyses of the problems addressed in this thesis work. Possible future perspectives of this trendy field of research have been elucidated.

Chapter 2

Parity-time-symmetric optical quadrimer wave-guides systems*

2.1 Introduction

Since the first experimental demonstration of parity-time (PT) symmetry in optics is demonstrated in an optical coupler [18], coupled waveguides and its variants have been studied quite extensively. It is interesting to note that even though parity-time (PT)-symmetry has been investigated in many complex optical structures in various contexts, simple structures like dimer, trimer and quadrimer are still continued to be explored [41-47]. This may be owing to the fact that these PT-symmetric oligomers may act as building blocks for complex PT-symmetric structures or lattices. Thus, understanding dynamics of such simple structures may be quite useful for practical applications [48]. In this direction, in their work [41] the authors have revisited the PT-symmetric dimer structure and provided in-detail study on the PT-symmetric oligomers structures including trimer, periodic trimer and quadrimer configurations. The existence, stability and the dynamics of the stationary solutions have been elaborated. In an attempt to understand the complexity of the dynamics, as more sites were added, this study opens up new ways towards the realization of PT-symmetric lattices. In another work [42], the authors have studied the two-site (dimer) and three-site (trimer) PT-symmetric configurations with linear and nonlinear gain/loss profiles.

---

*Part of the results of this Chapter have been published in the following papers: S. K. Gupta and A. K. Sarma, "*Parity-time-symmetric closed form optical quadrimer waveguides*," J. Mod. Opt. **61**, 227 (2014); S. K. Gupta, J. P. Deka and A. K. Sarma, "*Nonlinear parity-time symmetric closed-form optical quadrimer waveguides: attractor perspective*," Eur. Phys. J. D **69**, 199 (2015).

This study shows the existence of the symmetric and anti-symmetric stationary solutions and their bifurcations phenomena (e.g. spontaneous symmetry breakings). K. Li et al. [43] have revisited the trimer system studying its regular branches of solutions and their bifurcations, instabilities and ghost states. J. D'Amboise et al. [44] have introduced the staggered PT-symmetric ladder structure with cubic nonlinearity studying the families of discrete solitons and their stability regions. W. Walasik et al. [45] on the other hand have considered finite-size multimode PT-symmetric couplers in which they have investigated the phase transition behaviors. The study shows that the nonlinear oscillatory response of the system can be controlled by three parameters: gain/loss parameter, input light intensity and the nature of the input excitations. A generalized PT-symmetric system with time-periodic gain/loss profile has been considered in [46] exploring various types of modes. S. V. Suchkov et al. [47] have investigated dynamics of the solitons in a chain of interacting dimers which are parity-time (PT)-symmetric. In their study, a comparative analysis has been carried out between the stationary soliton solutions and the solitons of the discrete nonlinear Schrödinger (DNLS) equation. In this work, we study a closed form PT-symmetric quadrimer optical waveguide structure. Apart from gain and loss, another important component of the optical systems is the consideration of the nonlinearity. When nonlinearity is included, the Hamiltonian describing the system does not commute with the PT operator. As a consequence of this, there are nonlinear solutions that continue to exist beyond the linear PT-symmetry threshold. All the studies mentioned earlier indicate that the PT-symmetric oligomers systems could be important test-grounds for the existence, stability and propagation dynamics of optical solitons. In this connection, we find it quite reasonable to study the existence, stability and dynamics of the stationary solutions in PT-symmetric oligomers systems. In this context, it is appropriate to mention that several authors have studied closed- form quadrimer structures in various contexts [49-52]. K. Li et al. [49] explored basic 2-D plaquette configurations and looked for stationary solutions, their stability and bifurcations. D. A. Zezyulin et al. [50] have shown that one can simulate transformations among parity-time symmetric systems, without affecting their pure real linear spectra, via rearrangements of waveguide arrays with gain and losses. However, the nonlinear properties of these systems undergo significant changes under such transformations. In ref. [51] K. Li et al. have proposed a PT-symmetric coupler whose

arms are birefringent waveguides, as a realistic physical model which leads to the so called quadrimer. They have investigated the role of PT symmetry on the stability and the dynamical properties of the modes with different polarizations. I. V. Barashenkov et al. [52], have shown the PT-symmetry breaking phenomena in a necklace of coupled optical waveguides. The study by Y. Lumer et al. [53] has demonstrated the effect of nonlinearity on the systems with periodic parity-time (PT)-symmetry. The study reveals that the nonlinearity can help in transitioning the system between broken and the unbroken PT-symmetry regimes. In another study [54], phase transitions in wick-rotated PT-symmetric models were discussed where it has been shown that the system (wick-rotated PT-symmetric dimer) can possesses stationary or periodic solutions. It is appropriate to mention here that similar model without wick-rotation has been studied [55-57], where co-existence of periodic and unbounded solutions was predicted in the broken PT-phase. These studies inspire us to look into and investigate upon the stationary solutions in a PT-symmetric quadrimer system from an attractor [58] point of view.

In this chapter we have considered closed-form optical quadrimer structures. We have studied the role of nonlinearity and dispersions upon the spatio-temporal evolutions of the optical fields in detail. Beam dynamics of the system has been elucidated via numerical computation. We have also shown the attractor perspective of the stationary solutions of the PT-symmetric quadrimer structure with a specific coupling scheme. This establishes the fact that initial conditions play a vital role in the subsequent evolution dynamics of the optical fields.

2.2 PT-Symmetric Quadrimer

We consider a quadrimer system depicted in Fig. 2.1.

The optical-field dynamics in the system is described by the following evolution equations:

$$\frac{da}{dz} = -i\,H\,a \tag{2.1}$$

where, $a(z) = [a_1(z), a_2(z), a_3(z), a_4(z)]$ with $a_j(z)$ representing the field amplitude in the j-th waveguide and H is the Hamiltonian (under the tight-binding approximation):

$$H = \begin{bmatrix} ig & -k & -\gamma & -\beta \\ -k & -ig & -\delta & -\eta \\ -\gamma & -\delta & ig & -\alpha \\ -\beta & -\eta & -\alpha & -ig \end{bmatrix} \tag{2.2}$$

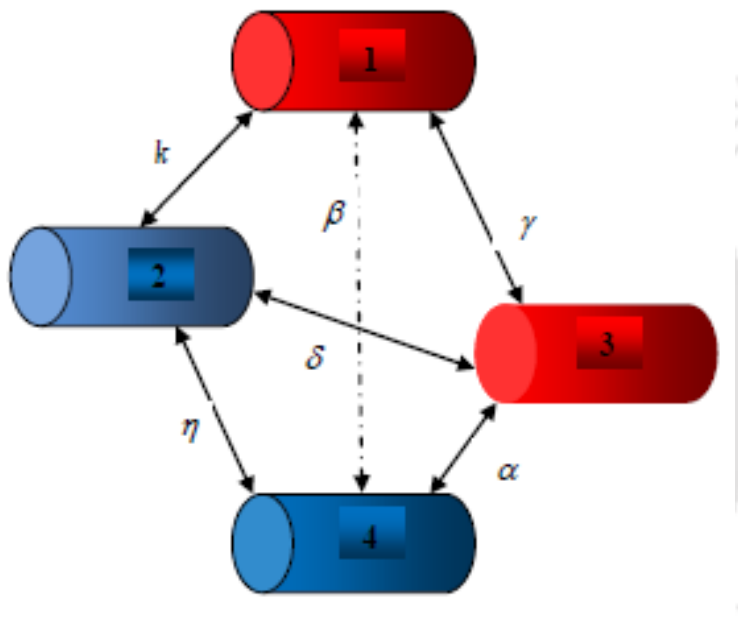

Figure 2.1: Schematic representation of a quadrimer optical waveguide system. Waveguides 1 and 3 have gain (+g) while waveguides 2 and 4 have loss (-g). The coupling coefficients between various waveguides are also shown.

Here, g is the loss/gain coefficient and $[k, \alpha, \eta, \gamma, \delta, \beta]$ are the coupling coefficients between various waveguides as depicted in Fig. 2.1. The system is PT symmetric if $[H, PT] = 0$, where P is a space-reversal linear operator and T performs element wise complex conjugation [18]. It is straightforward to find that the system is PT-Symmetric under the condition: $k = \alpha$ and $\gamma = \eta$ (see *Appendix A*). It is to be noted that, the PT-symmetry of the system is independent of the values of the coupling co-efficient δ and β. In rest of the analy-

sis, we ignore the couplings between waveguide 1 and 4 and between 2 and 3, by setting $\delta = \beta = 0$ in Eq. (2.2). A direct diagonalization of the Hamiltonian gives the following set of four eigenvalues:

$$\lambda = \pm\gamma \pm \sqrt{k^2 - g^2} \tag{2.3}$$

The eigenvalues are real as long as the gain/loss parameter g is smaller than some critical value, also called the exceptional point [18] $g_{PT} = k$. As the gain/loss parameter g increases above g_{PT}, the eigenvalues become complex and the system enters into the so-called broken PT-symmetric phase. If the system is kept below the critical point, its four supermodes could be identified as (see *Appendix B*):

$$|1\rangle = [-e^{i\theta} \;\; 1 \;\; e^{i\theta} \;\; -1\,]^T, \qquad |2\rangle = [1 \;\; e^{i\theta} \;\; -1 \;\; -e^{i\theta}]^T,$$

$$|3\rangle = [e^{i\theta} \;\; -1 \;\; e^{i\theta} \;\; -1\,]^T, \qquad |4\rangle = [e^{-i\theta} \;\; 1 \;\; e^{-i\theta} \;\; 1\,]^T \tag{2.4}$$

Here $\theta = sin^{-1}(g/k)$. None of the supermodes experiences gain/loss and they remain neutral and oscillate during propagation. On the other hand, if the system is kept above the exceptional point, the supermodes are (see *Appendix B*):

$$|1\rangle = [1 \;\; ie^{-\theta} \;\; -1 \;\; -ie^{\theta}]^T, \qquad |2\rangle = [-ie^{\theta} \;\; 1 \;\; ie^{\theta} \;\; -1]^T,$$

$$|3\rangle = [-ie^{\theta} \;\; 1 \;\; ie^{\theta} \;\; 1]^T, \qquad |4\rangle = [1 \;\; ie^{\theta} \;\; 1 \;\; ie^{\theta}]^T \tag{2.5}$$

where $\cosh(\theta) = g/k$. In this case, the PT-symmetry is spontaneously broken: two of the modes experience amplification while the other two decay exponentially with the propagation distance. It is interesting to note that two of the four supermodes above and below the critical point coalesce at the exceptional point, a typical signature of a PT-symmetric system [59]. In the following section, we discuss the beam dynamics of the system. We also discuss the role of the nonlinearity and dispersion on the beam dynamics.

2.2.1 Beam dynamics: Numerical simulations

In order to understand the beam dynamics of the system, we solve Eq. (2.1) numerically, subject to the following initial conditions:

$$a_1(z) = 1,\ a_2(z) = a_3(z) = a_4(z) = 0 \tag{2.6}$$

The simulation results are depicted in Fig. 2.2. In Fig. 2.2 (a), we depict the power evolutions, in each of the waveguides, for the case of a normal quadrimer system with $g = 0$.

On the other hand, Fig. 2.2 (b)-(d) shows the power evolutions of the PT symmetric quadrimer in all the three regimes: below the critical point, at the critical point and above the critical point. Please see the figure caption for the details. One significant effect displayed by PT-symmetric waveguides is the appearance of nonreciprocal wave propagation [60]. In fact, the structure considered in this work also exhibits non-reciprocity, even in the presence of nonlinearity and dispersion. Our numerical investigation shows that the beam propagation is quite sensitive to the initial condition.

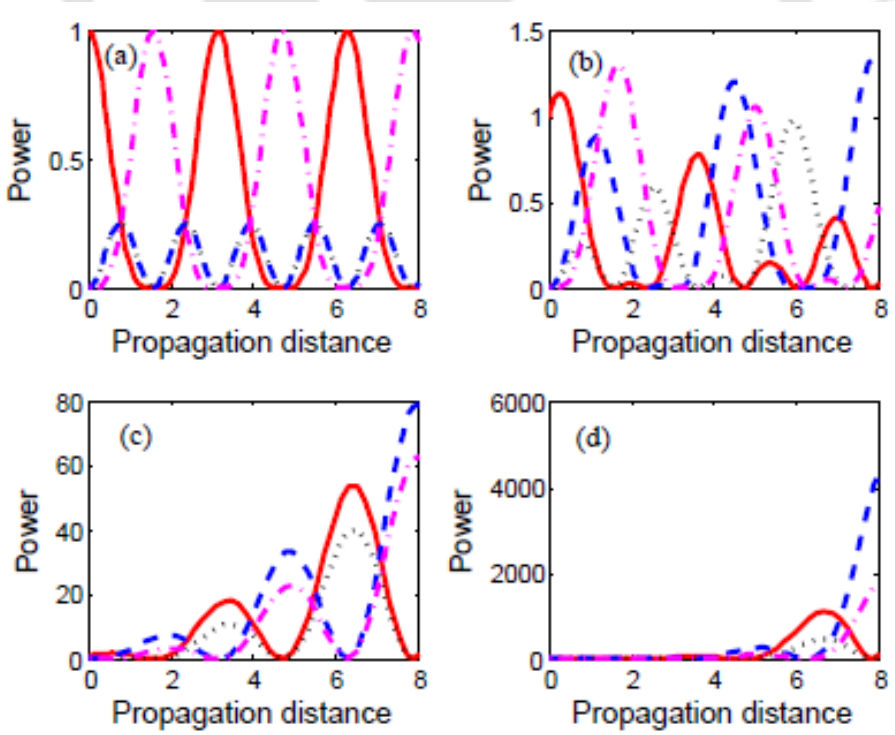

Figure 2.2: Spatial evolution of power in each site of the quadrimer with k = 1 and γ = 1. The solid red curve refers to site 1, dotted black refers to site 2 and dashed blue refers to site 3 while dashdot magenta corresponds to site 4. (a) normal quadrimer with g = 0, (b) g = 0.5 below the critical point, (c) g = 1.0 at the critical point, (d) above the critical point.

The role of nonlinearity on the propagation dynamics may be investigated very quickly through direct numerical simulations of the following coupled equations:

$$\frac{da_1}{dz} = ika_2 + i\gamma a_3 + ga_1 + i|a_1|^2 a_1 \tag{2.7a}$$

$$\frac{da_2}{dz} = ika_1 + i\gamma a_4 - ga_2 + i|a_2|^2 a_2 \tag{2.7b}$$

$$\frac{da_3}{dz} = ika_4 + i\gamma a_1 + ga_3 + i|a_3|^2 a_3 \tag{2.7c}$$

$$\frac{da_4}{dz} = ika_3 + i\gamma a_2 - ga_4 + i|a_4|^2 a_4 \tag{2.7d}$$

Results of direct numerical integrations, subject to the initial conditions (2.6), have been shown in Fig. 2.3.

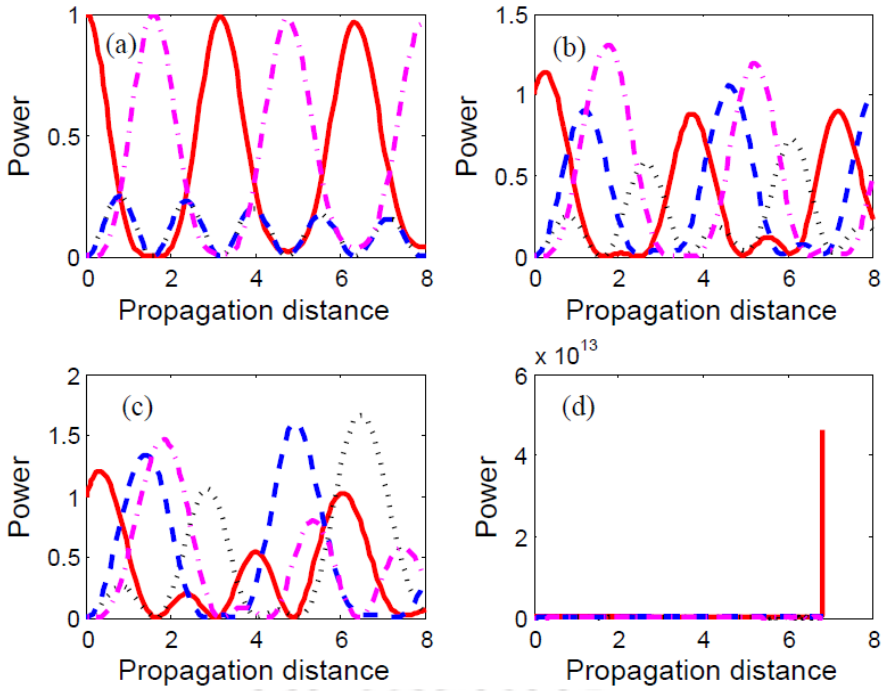

Figure 2.3: Spatial evolution of power in each of the sites of the quadrimer with k = 1 and γ = 1 in the presence of nonlinearity. The solid red curve refers to site 1, dotted black refers to site 2 and dashed blue refers to site 3 while dashdot magenta corresponds to site four. Here, (a) g = 0 for normal quadrimer, (b) g = 0.5, (c) g = 0.6, (d) g = 0.7.

The presence of nonlinearity shifts the critical point of the system. As could be seen from Fig. 2.3(d), as the gain/loss parameter '*g*' increases, at a certain value of the parameter there is

an abrupt PT phase transition and power keeps on building exponentially in one of the waveguides (for the parameters chosen for the current simulation, this value is nearly 0.7, i.e. $g_{CR} \approx 0.7$). This could be understood easily using the source-and-sink model of Ref. [61]. If the coupling of the waveguides is sufficiently strong, then the system is in equilibrium and one could observe Rabi-like oscillation. On the other hand, when the coupling becomes too weak, the Rabi oscillations ceases and the system is no longer able to maintain equilibrium resulting in exponential increase in power in one of the waveguides and exponential decrease in others.

It may be useful to study the effects of dispersion on the beam dynamics of the quadrimer structure. To do so, we consider Eq. (2.7) without the nonlinear terms and including the so-called group velocity dispersion terms.

$$\frac{da_1}{dz} = \frac{i}{2}\sigma_1 \frac{d^2 a_1}{d\tau^2} + ika_2 + i\gamma a_3 + ga_1 \tag{2.8a}$$

$$\frac{da_2}{dz} = \frac{i}{2}\sigma_2 \frac{d^2 a_2}{d\tau^2} + ika_1 + i\gamma a_4 - ga_2 \tag{2.8b}$$

$$\frac{da_3}{dz} = \frac{i}{2}\sigma_3 \frac{d^2 a_3}{d\tau^2} + ika_4 + i\gamma a_1 + ga_3 \tag{2.8c}$$

$$\frac{da_4}{dz} = \frac{i}{2}\sigma_4 \frac{d^2 a_4}{d\tau^2} + ika_3 + i\gamma a_2 - ga_4 \tag{2.8d}$$

Here σ_i is the so-called group velocity dispersion (GVD) parameter in the *j*-th waveguide. Eq. (2.8) could also be written in the frequency domain, by defining the Fourier transform, $\tilde{a}_j(z,w) = \int_{-\infty}^{\infty} d\tau \exp(i\omega\tau)\, a_j(z,\tau)$. Now, we would like to consider the following three cases which we find particularly interesting:

Case 1: Sites have equal dispersion

Let the magnitude of the GVD parameter to be the same in all the waveguides. We can easily find the set of four eigenvalues of the corresponding Hamiltonian to be: $\tilde{\lambda} = \alpha \pm \gamma \mp \sqrt{k^2 - g^2}$, where $\alpha = |\sigma|\omega^2/2$. It is worthwhile to note that if dispersion is taken into

account, the PT symmetry threshold of the system remains unaffected, irrespective of the sign of the parameter σ. A pulse launched at a site, as expected, gets broadened during its evolution. This is illustrated in Fig. 2.4, where a Gaussian pulse is launched at site 1.

Case 2: Sites have alternate dispersion

If the waveguides are chosen to have alternate dispersion, say site 1 has normal dispersion $(+\sigma)$ while site 2 has anomalous dispersion $(-\sigma)$ and so on, then system has the following set of eigenvalues:

$$\tilde{\lambda} = \pm\gamma \pm \sqrt{k^2 + (\alpha + ig)^2} \tag{2.9}$$

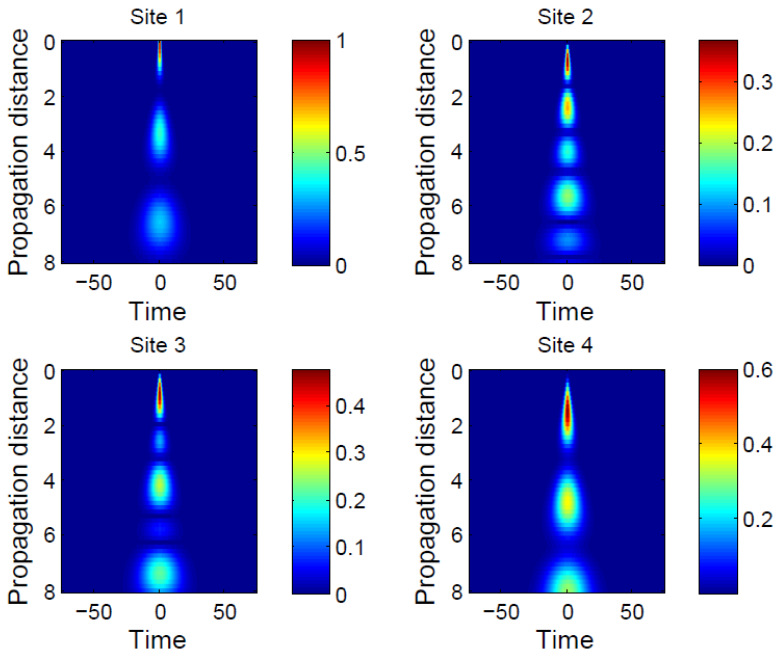

Figure 2.4: Contour plots for evolution of intensity in each site of the dispersive quadrimer.

Clearly, the eigenvalues are purely complex and the quadrimer structure does not exhibit PT-symmetry at all.

Case 3: Site 1 and 2 with normal dispersion while site 3 and 4 with anomalous dispersion or vice-versa.

In this case the system has the following set of eigenvalues:

$$\tilde{\lambda} = \pm\sqrt{\alpha^2 - g^2 + k^2 + \gamma^2 \mp \sqrt{(k^2 - g^2)(\alpha^2 + \gamma^2)}} \tag{2.10}$$

It is easy to see that, here, eigenvalues become purely real for $k = g$, on the other hand if $k < g$ the eigenvalues become complex. Hence we may conclude that the dispersive quadrimer of case 3 is PT symmetric for $g < g_{TH} = k$. Moreover, it seems dispersion may play a fundamental role in the beam dynamics of the structure.

It may be interesting to investigate the combined effect of both nonlinearity and dispersion on the evolution of an optical pulse. To do so, we add the so-called anomalous group velocity dispersion term, in normalized units, to Eq. (2.7), thereby making it a system of coupled nonlinear Schrodinger equation (CNLSE) [62]:

$$\frac{da_1}{dz} = \frac{i}{2}\frac{d^2a_1}{d\tau^2} + ika_2 + i\gamma a_3 + ga_1 + i|a_1|^2a_1 \tag{2.11a}$$

$$\frac{da_2}{dz} = \frac{i}{2}\frac{d^2a_2}{d\tau^2} + ika_1 + i\gamma a_4 - ga_2 + i|a_2|^2a_2 \tag{2.11b}$$

$$\frac{da_3}{dz} = \frac{i}{2}\frac{d^2a_3}{d\tau^2} + ika_4 + i\gamma a_1 + ga_3 + i|a_3|^2a_3 \tag{2.11c}$$

$$\frac{da_4}{dz} = \frac{i}{2}\frac{d^2a_4}{d\tau^2} + ika_3 + i\gamma a_2 - ga_4 + i|a_4|^2a_4 \tag{2.11d}$$

The above set of equations are solved numerically by launching a fundamental soliton in site 1, keeping rest of the sites empty.

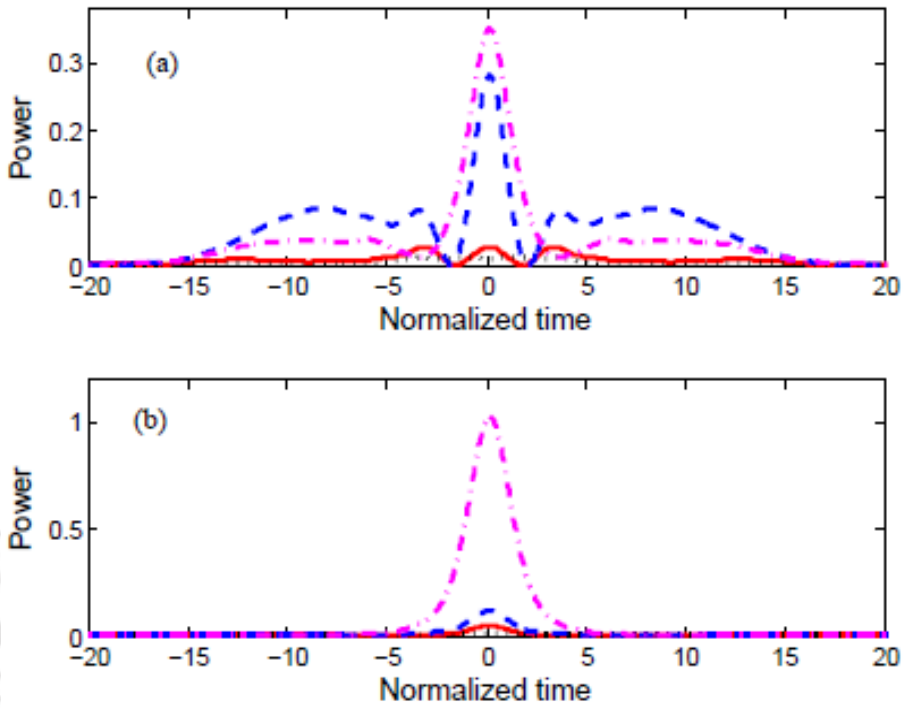

Figure 2.5: Output power in each of the sites of the quadrimer with k = 1 and γ = 1 in the presence of nonlinearity and dispersion. The solid red curve refers to site 1, dotted black refers to site 2 and dashed blue refers to site 3, while dashed-dot magenta refers to site 4.

Fig. 2.5 depicts the simulation results. At the outset we simulate the CNLSE with $g = 0.7$. Fig. 2.5(a) plots the output power of the fields. It could be seen that the PT-phase transition is avoided with the introduction of dispersion into the system. Fig. 2.5(b) depicts the output profiles of the fields with $g = 0.3$. The corresponding contour plots for spatio-temporal evolution is shown in Fig. 2.6. It can be that the soliton launched initially in site 1 is getting switched to site 4 at the end of the given propagation distance. In fact with judicious choice of the propagation length of the quadrimer, one can obtain the soliton at the desired site. The PT-Symmetric quadrimer considered in this work may be exploited for various applications such as tunable 4×4 spatial optical switch [63] and soliton switching [64]. Recently the stability of solitons in a dimer has been investigated [65] and similar analysis may be carried out for the case of a quadrimer also. However, we have checked the stability of solitons in the quadrimer system numerically and find that the soliton is stable as long as the order of the soliton, N, lies in the range: $0.85 < N < 1.2$.

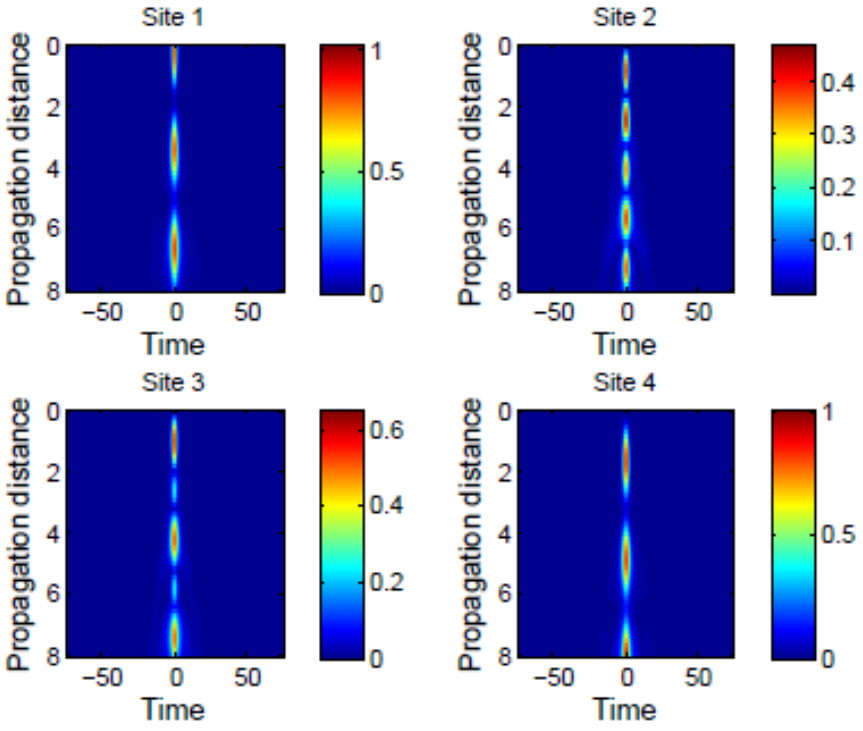

Figure 2.6: Contour plots for evolution of intensity in each site of the quadrimer corresponding to the case in Fig. 2.5(b).

2.3 Nonlinear PT-Symmetric Quadrimer waveguide: Attractor perspective

Next, we consider a closed-form parity-time (PT)-symmetric quadrimer waveguides structure with a specific coupling scheme. This specific coupling yields unique linear eigen-spectrum subject to the choice of various coupling parameters. On the other side, in nonlinear regime, a detailed nonlinear analysis has been conducted to characterize the power saturation behaviors in the different sites. Upon thorough inspection, we confirm that the saturation points correspond to the attractors of the system. It is noteworthy that the power saturation behavior in the oligomers system has been reported in completely different settings, for example, dimer and trimer systems with linear and nonlinear gain/loss distribution [42] and a wick rotated dimer [54]. On the other hand, in our work, the saturation behavior of the nonlinear

quadrimer system has been investigated in detail on attractor aspect. This work also addresses a crucial issue regarding choice of initial conditions while carrying out numerical simulation for such systems.

The schematic of the PT-symmetric quadrimer configuration is shown in Fig. 2.7. The Hamiltonian of the system (linear case) under the tight-binding approximation is given by:

$$H = \begin{bmatrix} ig & 0 & -\alpha & -\beta \\ 0 & -ig & \gamma & -\delta \\ -\alpha & \gamma & ig & 0 \\ -\beta & -\delta & 0 & -ig \end{bmatrix} \tag{2.12}$$

Here the parity operator of the system is given by:

$$P = \begin{bmatrix} 0 & 0 & 0 & 1 \\ 0 & 0 & 1 & 0 \\ 0 & 1 & 0 & 0 \\ 1 & 0 & 0 & 0 \end{bmatrix} \tag{2.13}$$

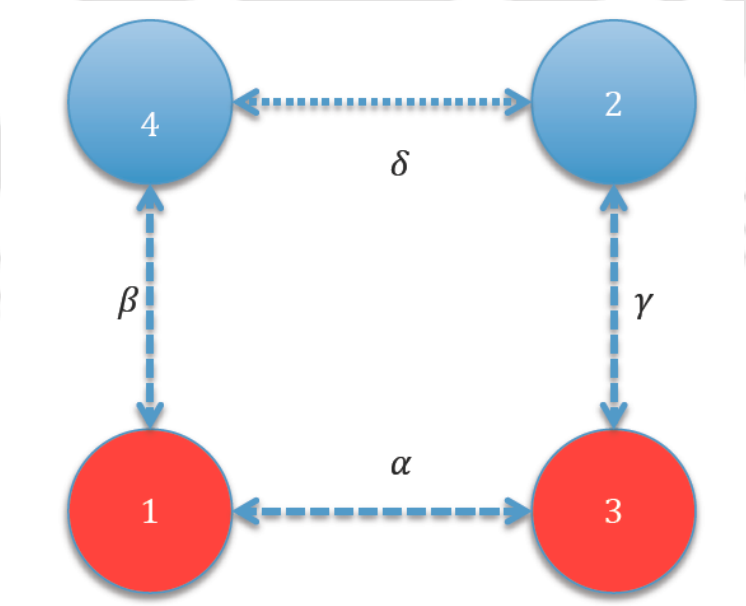

Figure 2.7: Schematic diagram of the optical quadrimer configuration. Waveguides 1 and 3 are gain–guides (+g) and waveguides 2 and 4 are loss-guides (-g). The coupling coefficients between various waveguides are also shown.

We find that the system under consideration is PT-symmetric when $\alpha = \delta$. Direct diagonalization of the Hamiltonian yields the following eigenvalues:

$$\lambda_{1,2} = \pm\frac{\sqrt{f_1+f_2}}{\sqrt{2}},\ \lambda_{3,4} = \pm\frac{\sqrt{f_1-f_2}}{\sqrt{2}} \tag{2.14}$$

where, $f_1 = -2g^2 + \beta^2 + \gamma^2 + 2\delta^2$

$$f_2 = \sqrt{\beta^4 - 2\beta^2\gamma^2 + \gamma^4 - 16g^2\delta^2 + 4\beta^2\delta^2 + 8\beta\gamma\delta^2 + 4\gamma^2\delta^2} \tag{2.15}$$

It is well known that if the system is in the unbroken PT-regime, all the eigenvalues are real while if all or some of the eigenvalues are complex the system is in broken-PT symmetric regime [18]. In order to investigate the *PT*-threshold of the system, in Fig. 2.8 we plot the appropriate eigen-spectrum of the system, taking the following coupling parameters: $\alpha = \delta = 2, \beta = 1$and $\gamma = 4$.

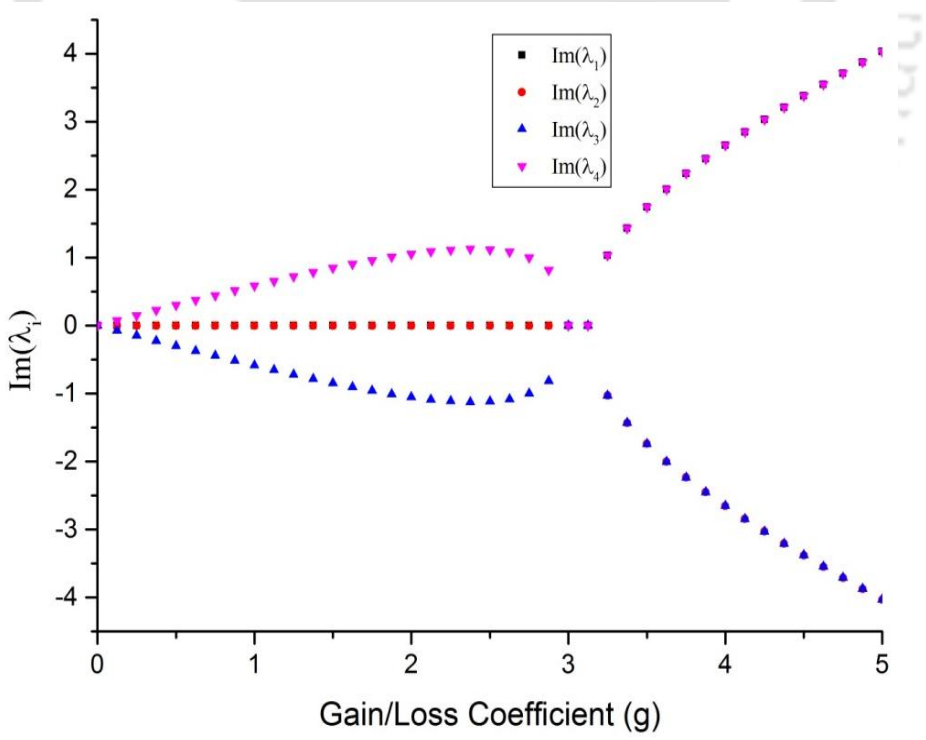

Figure 2.8: Eigen-spectrum of the linear system vs. loss/gain parameter.

It is easy to see that we have a narrow region in g where all the eigenvalues are real, i.e. a region of unbroken PT-symmetry while outside this region PT-symmetry is broken. For the chosen set of parameters, we obtain two PT-thresholds, namely $g_{th} = 3.0$ and $g_{th} = 3.125$. On the other hand, in nonlinear regime, the propagation dynamics of the system are described by the following set of coupled nonlinear equations:

$$\frac{da_1}{dz} = ga_1 + i\alpha a_3 + i\beta a_4 + i|a_1|^2 a_1 \tag{2.16a}$$

$$\frac{da_2}{dz} = -ga_2 + i\gamma a_3 + i\delta a_4 + i|a_2|^2 a_2 \tag{2.16b}$$

$$\frac{da_3}{dz} = ga_3 + i\alpha a_1 + i\gamma a_2 + i|a_3|^2 a_3 \tag{2.16c}$$

$$\frac{da_4}{dz} = -ga_4 + i\beta a_1 + i\delta a_2 + i|a_4|^2 a_4 \tag{2.16d}$$

It is assumed that each of the waveguides exhibits Kerr-nonlinearity of equal strength. We now carry out a linear stability analysis of the nonlinear quadrimer system. The set of four coupled Eqs. (2.16) can be rewritten, using the prescription, say: $a_1 = x_1 + ix_2$, $a_2 = x_3 + ix_4$, and so on, as follows:

$$\dot{x}_1 = gx_1 - \alpha x_6 - \beta x_8 - (x_1^2 + x_2^2)x_2; \dot{x}_2 = gx_2 + \alpha x_5 + \beta x_7 + (x_1^2 + x_2^2)x_1 \tag{2.17a}$$

$$\dot{x}_3 = -gx_3 - \gamma x_6 - \alpha x_8 - (x_3^2 + x_4^2)x_4;\ \dot{x}_4 = -gx_4 + \gamma x_5 + \alpha x_7 + (x_3^2 + x_4^2)x_3 \tag{2.17b}$$

$$\dot{x}_5 = gx_5 - \alpha x_2 - \gamma x_4 - (x_5^2 + x_6^2)x_6; \dot{x}_6 = gx_6 + \alpha x_1 + \gamma x_3 + (x_5^2 + x_6^2)x_5 \tag{2.17c}$$

$$\dot{x}_7 = -gx_7 - \beta x_2 - \alpha x_4 - (x_7^2 + x_8^2)x_8;\ \dot{x}_8 = -gx_8 + \beta x_1 + \alpha x_3 + (x_7^2 + x_8^2)x_7 \tag{2.17d}$$

This enables us to evaluate the fixed points of the system and carry out the linear stability analysis. Afterwards, we seek to find the nonlinear dynamics of the system about its fixed points. The Jacobian, J, of the coupled system with these new variables, after linearization, is worked out to be:

$$J = \begin{bmatrix} J_1 & J_2 \\ J_3 & J_4 \end{bmatrix} \tag{2.18}$$

Here,

$$J_1 = \begin{pmatrix} g - 2x_1x_2 & -x_1^2 - 3x_2^2 & 0 & 0 \\ 3x_1^2 + x_2^2 & g + 2x_1x_2 & 0 & 0 \\ 0 & 0 & -g - 2x_3x_4 & -x_3^2 - 3x_4^2 \\ 0 & 0 & 3x_3^2 + x_4^2 & -g + 2x_3x_4 \end{pmatrix},$$

$$J_2 = \begin{pmatrix} 0 & -2 & 0 & -1 \\ 2 & 0 & 1 & 0 \\ 0 & -4 & 0 & -2 \\ 4 & 0 & 2 & 0 \end{pmatrix}, \quad J_3 = \begin{pmatrix} 0 & -2 & -2 & 0 \\ 2 & 0 & 0 & 4 \\ 0 & -1 & -1 & 0 \\ 1 & 0 & 0 & 2 \end{pmatrix} \text{ and}$$

$$J_4 = \begin{pmatrix} g - 2x_5x_6 & -x_5^2 - 3x_6^2 & 0 & 0 \\ 3x_5^2 + x_6^2 & g + 2x_5x_6 & 0 & 0 \\ 0 & 0 & -g - 2x_7x_8 & -x_7^2 - 3x_8^2 \\ 0 & 0 & 3x_7^2 + x_8^2 & -g + 2x_7x_8 \end{pmatrix}.$$

It is possible to obtain considerable insight into the behavior of the system from the determinant of the Jacobian and its eigenvalues evaluated at various values of the g parameter. We have chosen $g = 2.5$ for the rest of the analysis. It is easy to see that $x_i = 0$ is the most trivial fixed point of the system. The corresponding eigenvalues of the Jacobian are (3.7081i, -3.7081i, 3.7081i, -3.7081i, 1.1180, 1.1180, -1.1180, -1.1180). In passing, it is worthwhile to note that our investigation shows that for $0 < g < 3$ and $g > 3.125$, the fixed point $x_i = 0$ is hyperbolic, as the Jacobian has complex eigenvalues. On the other hand, in the unbroken PT- symmetric regime, i.e. $3 < g < 3.125$, the Jacobian has purely imaginary eigenvalues, which indicates that the fixed point $x_i = 0$ is non-hyperbolic. Due to the presence of real positive eigenvalues, we can infer that this is an unstable fixed point. Clearly, choice of initial conditions in numerical simulations or power launching condition at the input ends of the waveguides, in the context of experiments now becomes a highly nontrivial issue. For example, choosing the initial condition such as: $(a_1 = 1, a_2 = a_3 = a_4 = 0)$ would result in huge perturbation in the fixed point. Using the Newton-Raphson method, we have obtained the following non-trivial fixed point of the system which is correct upto five decimal places: $(-0.95224, 0.82349, 1.29818, 1.26033, 0.35102, -1.77497, -1.25158, -0.13579)$ with error tolerance set at 10^{-10}. The determinant of the Jacobian evaluated at the above mentioned fixed point is $\approx 1.6786 \times 10^{-7}$. From the infinitesimal value of the determinant, it can be inferred that it is not an invertible matrix. Hence, the system is not exactly linear in the vicinity of the fixed point. On the other hand, the correspo-

nding eigenvalues of the Jacobian are purely imaginary. This implies that these fixed points are non-hyperbolic. This in turn means that only a numerical solution of the nonlinear system will give us the appropriate picture of the propagation dynamics of the optical fields along the length of the waveguide. We numerically solve Eq. (2.17) with perturbed fixed point as our initial conditions. For our simulation the fixed point perturbation is chosen to be: 10^{-5}. We find that the system does have an attractor. This could be clearly seen from Fig. 2.9.

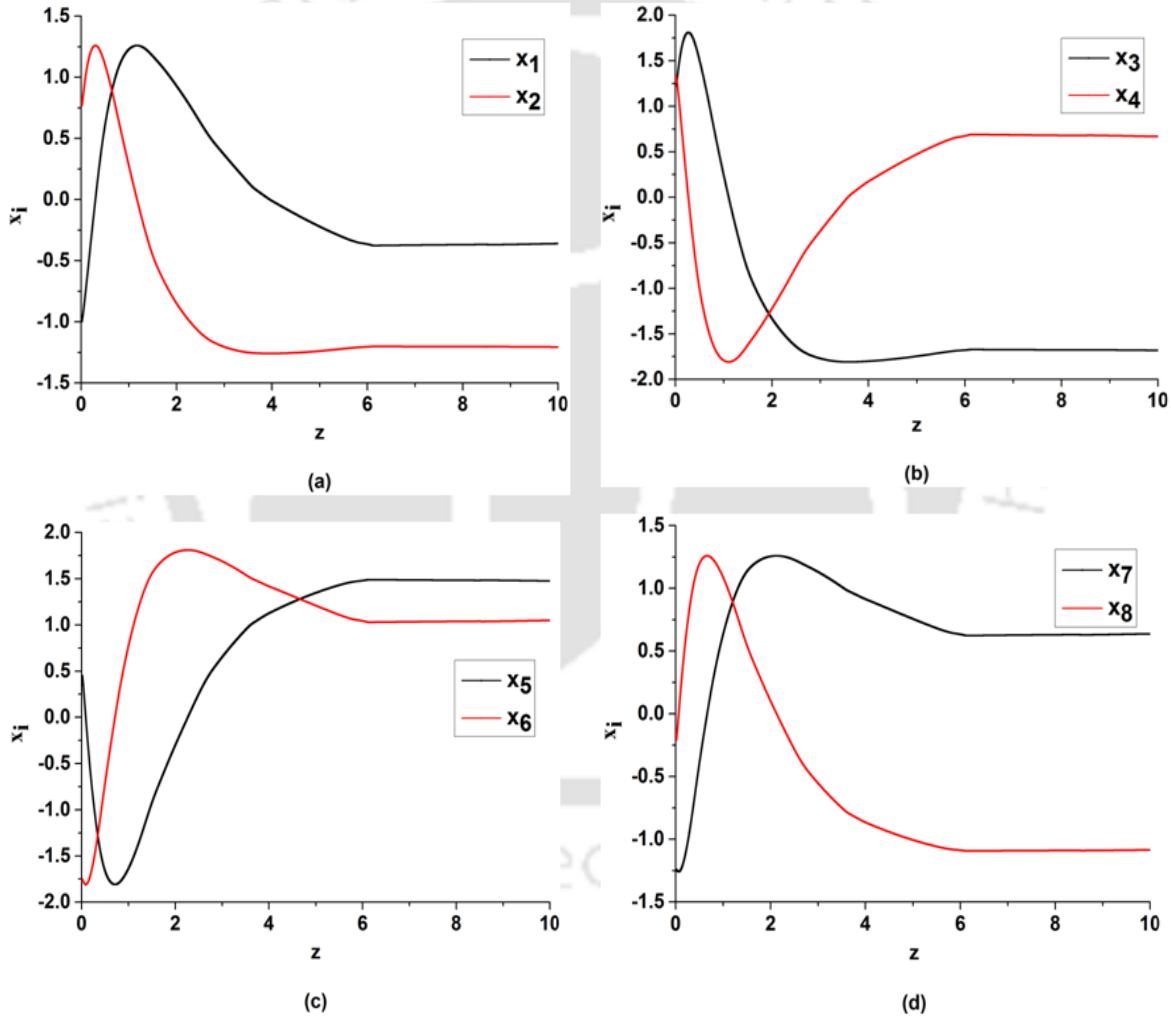

Figure 2.9: Spatial evolution of x_i.

Now it is clear that one can obtain saturation in the optical power along the propagation distance subject to judicious choice of the initial conditions. For instance, in Fig. 2.9 we plot the spatial evolution of optical power, defined as $P_1 = |x_1 + i\,x_2|^2$, in the first waveguide.

It could be seen from Fig. 2.10 that optical power gets saturated in waveguide 1. We find that similar behavior is shown by other three waveguides also. These power saturation behaviors of the system could be attributed to the attractor perspective.

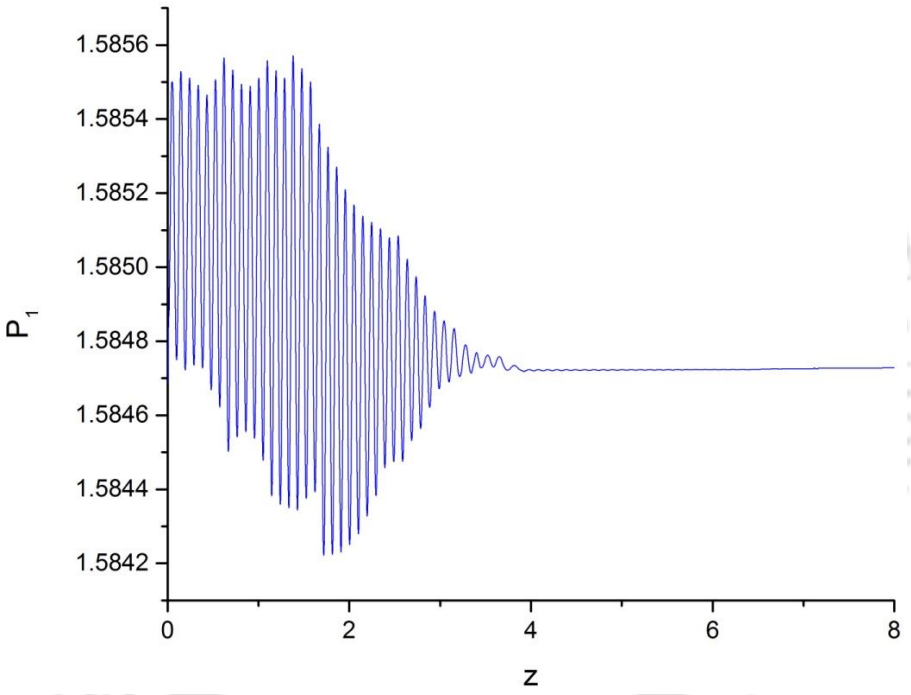

Figure 2.10: Spatial evolution of optical power in the first waveguide.

2.4 Summary of the Chapter

We have studied a closed form PT-symmetric quadrimer optical waveguide structure. The beam dynamics of the structure is studied numerically. The effect of inclusion of nonlinearity and dispersion is also briefly investigated and discussed. The structure considered is

reminiscent to the four-state quantum system found in quantum optics [66]. It is anticipated that, considering the recent interest in quantum-optical analogies [67] and PT-symmetry in atomic medium [68], careful study of such structures might provide lots of insight into the dynamics of more complex configurations or structures. Next, we have considered a closed-form parity-time (PT)-symmetric quadrimer waveguides structure with a specific coupling scheme. From the linear eigen-spectrum of the system it is seen that the system has a narrow window of unbroken PT-symmetric region. In nonlinear regime, for a given value of the gain/loss parameter, we have shown that the system yields stationary solutions that correspond to attractors. A detailed analysis has been provided in confirming the attractor aspect of the stationary solutions. It can be concluded that the power saturation behaviors of the system could be attributed to the attractor perspective.

Chapter 3

Nonlinear waves in Parity-time symmetric Bragg grating structure*

3.1 Introduction

Periodic structures like index gratings in bulk [69] and in optical fibers [70,71], find important applications in obtaining frequency selectivity, high reflectivity and dispersion of significant characteristic properties [72]. Whereas the wave propagation dynamics in the linear periodic structures has found relevance in a variety of areas (solid-state physics, integrated optics) [73], the inclusion of nonlinearity into the system further enriches its dynamical properties and behaviors in terms of chaos, instabilities, pulse compression and solitary waves [74-77]. The study of nonlinear optical periodic structures dates back to 1979 when H. G. Winful et al. investigated the phenomena of optical bistability in a nonlinear distributed feedback structures in continuous-wave approximation [78]. After some years, in a couple of works [79-81], a novel family of solitons classified as Bragg solitons were reported to exist in the similar kind of systems as in [78]. In contrast to the optical solitons in the nonlinear dispersive fibers where they are formed due to the balance between nonlinearity and dispersion, this type of solitons are formed by interlocking of the counter-propagating waves in a nonlinear way [82, 83]. These counter-propagating waves help in creating a defect band within a forbidden band gap which facilitates transport of energy. Among some other efforts in this direction, W. Chen et al. [79] studied the Gap solitons and the nonlinear optical phenomena of super-lattices. D. N. Christodoulides *et al*. [80] have

*Part of the results of this Chapter has been published in the following paper: S. K. Gupta and A. K. Sarma, "*Solitary waves in parity-time (PT)-symmetric Bragg grating structure and the existence of optical rogue waves*," Europhys. Lett. **105**, 44001 (2014).

shown the existence of slow Bragg solitons in nonlinear periodic structures in which it was claimed that the velocity of this type of optical solitons were orders of magnitude lower than nonlinear periodic medium obtaining new non-stationary soliton-like solutions. Meanwhile, it is important to mention that the first-ever experimental demonstration of Bragg grating solitons was reported by B. J. Eggleton et al. [84] in 1996. In the recent times, keeping in mind the enormous amount of research interests using the novel idea of parity-time (PT)-symmetry, there has been growing scientific endeavors to employ this idea to the nonlinear periodic structures. To mention some of them, S. Phang et al. [85] have demonstrated numerically the ultrafast switching behavior in a Bragg grating structure by suddenly switching on the gain in the system. Again, based on a system of passive parity-time (PT)-symmetric grating and nonlinear Silicon distributed Bragg reflector, Y. Xu et al. [86] have shown the unidirectional transmission response at the telecommunication wavelength of 1550 nm while keeping minimum of reflection in a desired direction. In another work by C. Y. Huang et al. type-II modes (perfect absorption and amplification modes) have been shown to exist in combined system of conventional and PT-symmetric Bragg-grating structure [87]. A. K. Sarma [88] has studied the modulation instability in nonlinear complex parity-time symmetric periodic structures in different regimes of PT-symmetry. These studies on the periodic Bragg grating structures have clearly established the importance of revisiting this type of system in the context of PT-symmetry which is capable of novel device applications. In this connection, yet in another investigation by M. A. Miri et al. [89] starting from a modified massive Thirring model [90], have established the existence of closed-form slow Bragg solitons in the complex nonlinear parity-time (PT) symmetric periodic structures. This study shows the dependence of the grating band structures on the PT-symmetric part of the periodic optical refractive index which essentially modifies the coupling between the forward and the backward waves. Yet in a different direction, N. A. Kudryashov et al. [91], in a system of double tunnel-coupled waveguides, have investigated the analytical traveling wave solutions including two periodic and solitary waves and a new nonlinear wave called compacton. In another work by K. Senthilnathan et al. [92], the authors have found bright and dark Bragg soliton solutions. Motivated by these works (in particular [86, 89-91]), we consider a Bragg grating structure with the core having refractive index distribution as

indicated in the section 3.2. For this system we study the traveling wave solutions of the system depending on the system parameters and explore the nature of the solutions in various regimes of PT-symmetry.

3.2 Theoretical model

We consider a nonlinear Bragg grating structure in which the optical fiber-core is associated with the core refractive index distribution given by:

$$n = n_0 + n_{1R}\cos\left(\frac{2\pi z}{\Lambda}\right) + in_{1I}\sin\left(\frac{2\pi z}{\Lambda}\right) + n_2|E|^2 \tag{3.1}$$

Here, n_0 is the refractive index of the background material; n_{1R} and n_{1I} are the real and imaginary parts of the perturbed refractive index distribution; n_2 is the nonlinear Kerr parameter and Λ is the grating period. Other than the n_0 term, the three other terms in Eq. (3.1) can be thought of as small perturbative contributions to n_0. Wave propagation in the medium can be studied by solving the Helmholtz equation:

$$\nabla^2 E + n^2(\omega, z)(\omega^2/c^2)E = 0 \tag{3.2}$$

Since both the forward and backward propagating wave needs to be considered in the grating, we assume:

$$E = E_f(z,t)\exp[\mathrm{i}(\beta_0 z - \omega_0 t)] + E_b(z,t)\exp[-\mathrm{i}(\beta_0 z + \omega_0 t)] \tag{3.3}$$

Here, $\beta_0 = n_0\omega_0/c$, $\omega_0 = 2\pi c/\lambda_0$, and λ_0, ω_0 are the free-space wavelength and the carrier angular frequency respectively. Putting Eq. (3.3) in Eq. (3.2), under the slowly varying envelope approximation, the following coupled differential equations could be obtained [89]:

$$i\left(\frac{\partial E_f}{\partial z} + \frac{1}{v_g}\frac{\partial E_f}{\partial t}\right) + \delta_0 E_f + (k_0 + g_0)E_b + \gamma_0(|E_f|^2 + 2|E_b|^2)E_f = 0 \tag{3.4a}$$

$$i\left(\frac{\partial E_b}{\partial z} + \frac{1}{v_g}\frac{\partial E_b}{\partial t}\right) + \delta_0 E_b - (k_0 - g_0)E_f + \gamma_0(|E_b|^2 + 2|E_f|^2)E_b = 0 \tag{3.4b}$$

Here $E_f(z,t)$ and $E_b(z,t)$ are the slowly-varying amplitudes of the forward and the

backward waves respectively. $v_g = c/n_0$ is the velocity in the background material, $k_0 = \pi n_{1R}/\lambda_0$ is the coupling co-efficient arising from the real Bragg grating and $g_0 = \pi n_{1I}/\lambda_0$ is the anti-symmetric coupling co-efficient arising from the complex PT-potential term. On the other hand, $\delta = (\omega_0 - \omega_B)/v_g$ is the measure of the detuning from the Bragg frequency ω_B. γ_0 is the so called self-phase modulation parameter. In order to simplify our analysis, we adopt the following dimensionless units:

$$\xi = \frac{z}{z_0}, \tilde{E}_f = \frac{E_f}{\sqrt{P_0}}, \tilde{E}_b = \frac{E_b}{\sqrt{P_0}}, \tau = \frac{t}{T_0}, \delta = \delta_0 z_0, k = k_0 z_0, g = g_0 z_0, \gamma = \gamma_0 P_0 z_0 \tag{3.5}$$

where, z_0 , P_0 , and T_0 are the length scale (defined as $z_0 = v_g T_0$), peak power and the pulse width of the laser radiation.

Now, Eq. (3.4) can be rewritten as follows:

$$i\left(\frac{\partial \widetilde{E_f}}{\partial \xi} + \frac{\partial \widetilde{E_f}}{\partial \tau}\right) + \delta \widetilde{E_f} + (k+g)\widetilde{E_b} + \gamma(\left|\widetilde{E_f}\right|^2 + 2\left|\widetilde{E_b}\right|^2)\widetilde{E_f} = 0 \tag{3.6a}$$

$$i\left(\frac{\partial \widetilde{E_b}}{\partial \xi} + \frac{\partial \widetilde{E_b}}{\partial \tau}\right) + \delta \widetilde{E_b} - (k-g)\widetilde{E_f} + \gamma(\left|\widetilde{E_b}\right|^2 + 2\left|\widetilde{E_f}\right|^2)\,\tilde{E}_b = 0 \tag{3.6b}$$

It is worthwhile to mention that in deriving the Eq. (3.6), the coupled-mode theory is employed which has been used with considerable success in diverse contexts [93]. In this method, the forward and the backward waves are considered independently and the Bragg grating provides a coupling bridge between them.

3.3 Analytical traveling wave solutions

To start with, we make the following transformations: $\tilde{E}_{f,b}(\xi,\tau) = a_{f,b}e^{i\phi_{f,b}(\xi,\tau)}, \phi(\xi,\tau) = \phi_f - \phi_b$ in the Eq. (3.2). This results in the following set of equations for the real amplitudes $a_{f,b}(\xi,\tau)$ and real phases $\phi_{f,b}(\xi,\tau)$:

$$\left(\frac{\partial}{\partial \xi} + \frac{\partial}{\partial \tau}\right) a_f = \sin(\phi)\,(k+g)a_b \tag{3.7a}$$

$$\left(\frac{\partial}{\partial \xi} - \frac{\partial}{\partial \tau}\right) a_b = \sin(\phi)\,(k-g)a_f \tag{3.7b}$$

$$a_f\left(\frac{\partial}{\partial\xi}+\frac{\partial}{\partial\tau}\right)\phi_f=\delta a_f+\cos(\phi)\,(k+g)a_b+\gamma(a_f^2+2a_f a_b^2) \tag{3.7c}$$

$$a_b\left(\frac{\partial}{\partial\xi}-\frac{\partial}{\partial\tau}\right)\phi_b=-\delta a_b-\cos(\phi)\,(k-g)a_b-\gamma\left(a_b^2+2a_b a_f^2\right) \tag{3.7d}$$

Now, we introduce the following traveling wave variables in Eq. (3.7):

$$z=\frac{\xi-c_0\tau}{\sqrt{1-c_0^2}},\ a_f=\sqrt{1+c_0}\,u,\ a_b=\sqrt{1-c_0}\,v \tag{3.8}$$

where, c_0 is the dimensionless traveling wave speed.

Due to transformation as in Eq. (3.8) it can be shown that:

$\left(\frac{\partial}{\partial\xi}+\frac{\partial}{\partial\tau}\right)a_f=\sqrt{(1-c_0)}u_z$ and $\left(\frac{\partial}{\partial\xi}-\frac{\partial}{\partial\tau}\right)a_b=\sqrt{(1+c_0)}v_z$, which further gives, from Eq. (3.7a) and (3.7b), the following Eqs. for the amplitudes:

$$u_z=v(k+g)\sin(\phi) \tag{3.9a}$$

$$v_z=u(k-g)\sin(\phi) \tag{3.9b}$$

Again, in a similar way it can be shown that Eq. (3.7c) and (3.7d) give the following Eqs. for the phases:

$$u\phi_{fz}=\delta\,\mu\,u+v(k+g)\cos(\phi)+\vartheta_2 u^3+\vartheta_3 uv^2 \tag{3.10a}$$

$$v\phi_{bz}=-\delta\,\mu^{-1}\,u-u(k-g)\cos(\phi)+\vartheta_2{}'u^3+\vartheta_3{}'vu^2 \tag{3.10b}$$

One can obtain, from Eq. (3.10), the following Eqs.:

$$\phi_z=\gamma'+\frac{\chi_1u^2-c_1}{p_T\varepsilon u\sqrt{u^2-c_1}}\cos(\phi)+\chi_2u^2+\chi_3+\chi_4u^2+\chi_5 \tag{3.11}$$

Here, $\chi_1=p_T^2\eta_1+\eta_2$, $\chi_2=p_T^2\vartheta_2'+\vartheta_2$, $\chi_3=p_T^2c_1\vartheta_2'$, $\chi_4=p_T^2\vartheta_3+\vartheta_3'$, $\chi_5=p_T^2c_1\vartheta_3$,

$\gamma'=\delta(\mu+\mu^{-1})$, $\eta_1=k+g,\eta_2=k-g$, $p_T=\sqrt{\frac{k-g}{k+g}}$, $\vartheta_2=\gamma\frac{(1+c_0)^{3/2}}{\sqrt{(1-c_0)}}$, $\vartheta_2{}'=\frac{(1-c_0)^{3/2}}{\sqrt{(1+c_0)}}$ and $\vartheta_3=\vartheta_3{}'=2\gamma\sqrt{1-c_0^2}$.

In order to keep the rest of the analysis clean, we introduce the following parameters:

$$\alpha = \eta_1 = k + g, \beta = \eta_2 = k - g, \mu = \sqrt{\frac{1+c_0}{1-c_0}} \tag{3.12}$$

Upon dividing u_z by v_z and after doing some straightforward algebra, we obtain:

$$u^2 = v^2 \left(\frac{\alpha}{\beta}\right) + c_1 \tag{3.13}$$

where, c_1 is an integration constant.

Eq. (3.9a) and Eq. (3.13) give:

$$u_z^2 = (u^2 - c_1)\, \alpha^2 \chi^2 sin^2(\phi) \tag{3.14}$$

For $c_1 \neq 0$, from Eq. (3.14) we obtain:

$$\phi_z = \frac{\alpha\, \varepsilon \left[u_{zz}(u^2 - c_1) - u\, u_z^2\right]}{\chi(u^2 - c_1)\left(\sqrt{u^2 - c_1 - u_z^2}\right)} \tag{3.15}$$

where, $\varepsilon = \pm 1,\ \chi = p_T = \sqrt{\beta/\alpha},\ \phi = sin^{-1}\left[\frac{\varepsilon\, u_z}{\alpha\, \chi\sqrt{u^2 - c_1}}\right]$ (3.16)

We now equate the both sides of Eqs. (3.11) and (3.15) to obtain:

$$(uu_{zz} + u_z^2\eta_p^2 - \chi_1 u^2 - c_1)^2 = \left(u^2 + c_1 - u_z^2\eta_p^2\right)\left(u^2\chi_\gamma^2 + 2\chi_\gamma\chi_{24}u^4 + \chi_{24}^2 u^6\right)\eta_1^2$$

Here, $\chi_{24} = \chi_2 + \chi_4, \chi_{35} = \chi_3 + \chi_5, \chi_\gamma = \gamma' + \chi_{35}, \eta_p = \frac{\eta_1}{p_T}$.

Substituting Eq. (3.16) into Eq. (3.15) and using the new variables, defined as follows,

$$E = \frac{\left[u^2 - c_1 - \left(\frac{u_z^2\,\alpha}{\chi}\right)\right]}{u^6},\ r = \sqrt{E},$$

We obtain:

$$\frac{dr}{du} + 4\frac{r}{u} = \varepsilon\alpha\frac{b_1u^2 + b_2}{u^3} \tag{3.17}$$

Here the relevant parameters are defined as follows:

$$b_1 = \chi_{24} = \gamma\left[\chi^2\left(\mu^{-1} + 2\gamma\sqrt{1-c_0^2}\right) + \mu(1+c_0)\right]\left[\chi^2\left(\mu^{-1} + 2\gamma\sqrt{1-c_0^2}\right) + \mu(1+c_0)\right]$$

$$b_2 = \chi_\gamma = \gamma' + \gamma\left[-c_1\chi^2(\mu(1+c_0) + 2\sqrt{1-c^2})\right]$$

$$\gamma' = \delta(\mu + \mu^{-1})\ .$$

Solving Eq. (3.17) and then putting the transformations $r = \sqrt{E}$, $E = \frac{u^2 - c_1 - u_z^2\eta_p^2}{u^6}$, $w = 1/u^2$, following a bit of tedious algebra, under the approximation of weak nonlinearity, we obtain:

$$w_Z^2 = \left[-4c^2w^4 - 4c_1w^3 + 4w^2 - 2c_2\varepsilon\alpha\left(\frac{b_1}{2} + \frac{2b_2w}{3}\right)\right](\chi/\alpha)^2 \tag{3.18}$$

where, c_2 is the constant appearing in the solution of Eq. (3.17).

Now, we write the right hand side of Eq. (3.18) as:

$$f(w) = -2(w-w_1)(w-w_2)(w-w_3)(w-w_4) \tag{3.19}$$

Then, proceeding in the similar way as in Refs. [91, 94], we finally obtain the traveling wave solutions for the forward and backward waves (see *Appendix C*):

$$a_f^2 = (1+c_0)\frac{[\rho + tanh^2(Z)]}{[w_4 + w_3\ tanh^2(Z)]} \tag{3.20a}$$

$$a_b^2 = (1-c_0)\left(\frac{k-g}{k+g}\right)\left(-c_1 + \frac{a_f^2}{1+c_0}\right)\frac{[\rho + tanh^2(Z)]}{[w_4 + w_3\ tanh^2(Z)]} \tag{3.20b}$$

with $Z = \sqrt{\rho}(\sqrt{l}z + C)$. Here, '$f$' stands for forward wave and 'b' stands for backward wave and 'C' is the integration constant. 'l' is the parametric constant which is defined as follows: $l = \frac{w_4^2(1-X_1)(1-X_2)}{2}$ where we have $X_m = w_m/w_4$, with the subscript index $m = 1,2,3,4$; and $\rho = -\frac{w_3}{w_4}$, $c_1 = \rho/w_4$. It is clear that there is an infinite number of traveling wave solutions depending on the values of the parameters. One may obtain either cnoidal wave or solitary wave solutions subject to the parameter values. For the rest of our analysis in this work we take $C = 0.0$. It is worthwhile to mention that at $k = g$, solitary wave solutions as in Eq. (3.20b) do not exist for the chosen set of parameters. This could be due to the fact that in

this case the Bragg grating becomes ineffective since the speed reduction factor tends to unity [93]. Also, equivalently, as evident from the Eq. (3.13), at $k = g$, the solutions simply blow up.

The variation of a_f^2 with $s = \xi - c_0\tau$, for different values of c_0 parameters is shown in Fig. 3.1. We notice that for the right-going waves ($0 < c_0 < 1$) as in Fig. 3.1(a), the amplitudes increase when the traveling wave speed c_0 increases. For the left-going waves, in Fig. 3.1(b), the amplitudes decrease when the absolute values of the traveling wave speed is increased. These results are in conformity with the ones found in Refs. [91, 95].

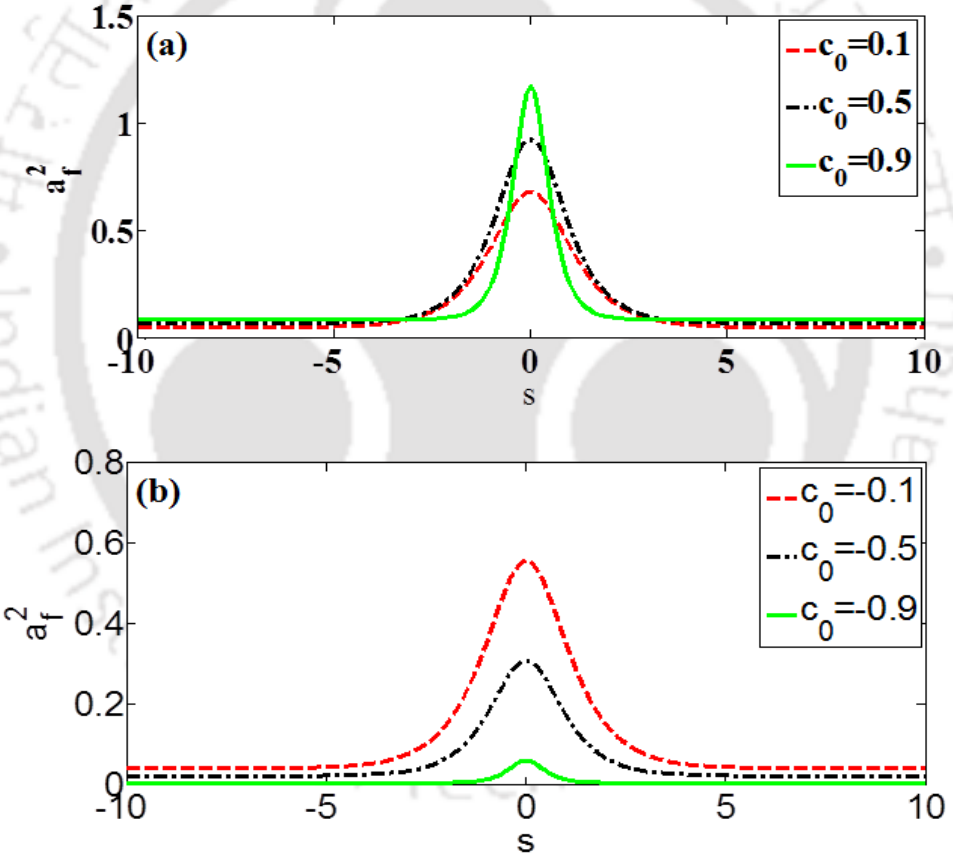

Figure 3.1: Variation of the square of the amplitudes vs. the s parameter for different values of c_0 parameter. k = 1.0, g = 0.9, c_1 = 2.01196.

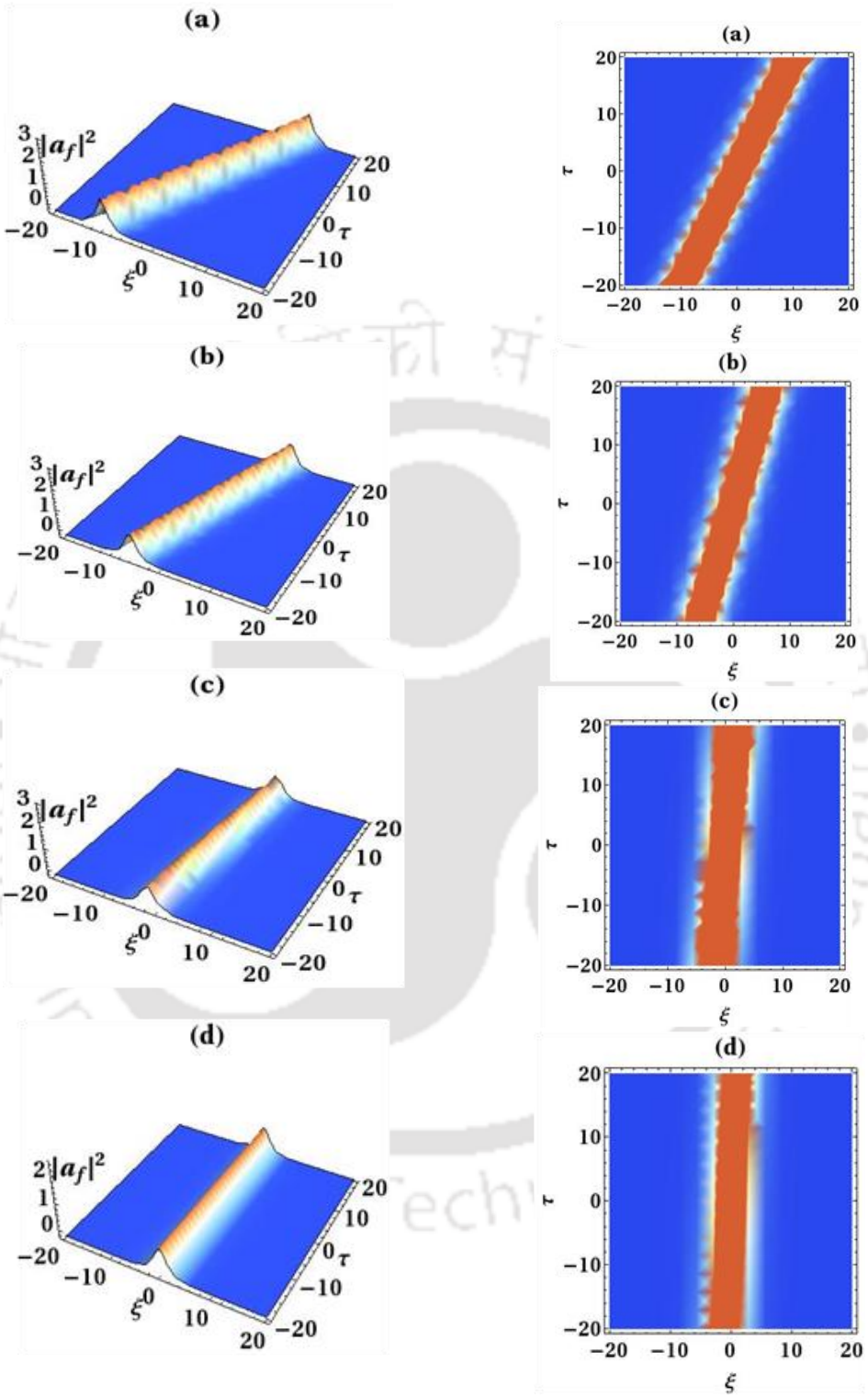

Figure 3.2: Spatio-temporal evolution of the intensity of the forward waves on the left-hand panel. In the right-hand panel density-plots corresponding on the left-hand panel is shown. Different values of c_0 parameter are: (a) c_0 = 0.5, (b) c_0 = 0.3, (c) c_0 = 0.09, (d) c_0 = 0.046. Other parameters are: k = 1.0, g = 0.55, c_1= 0.69884.

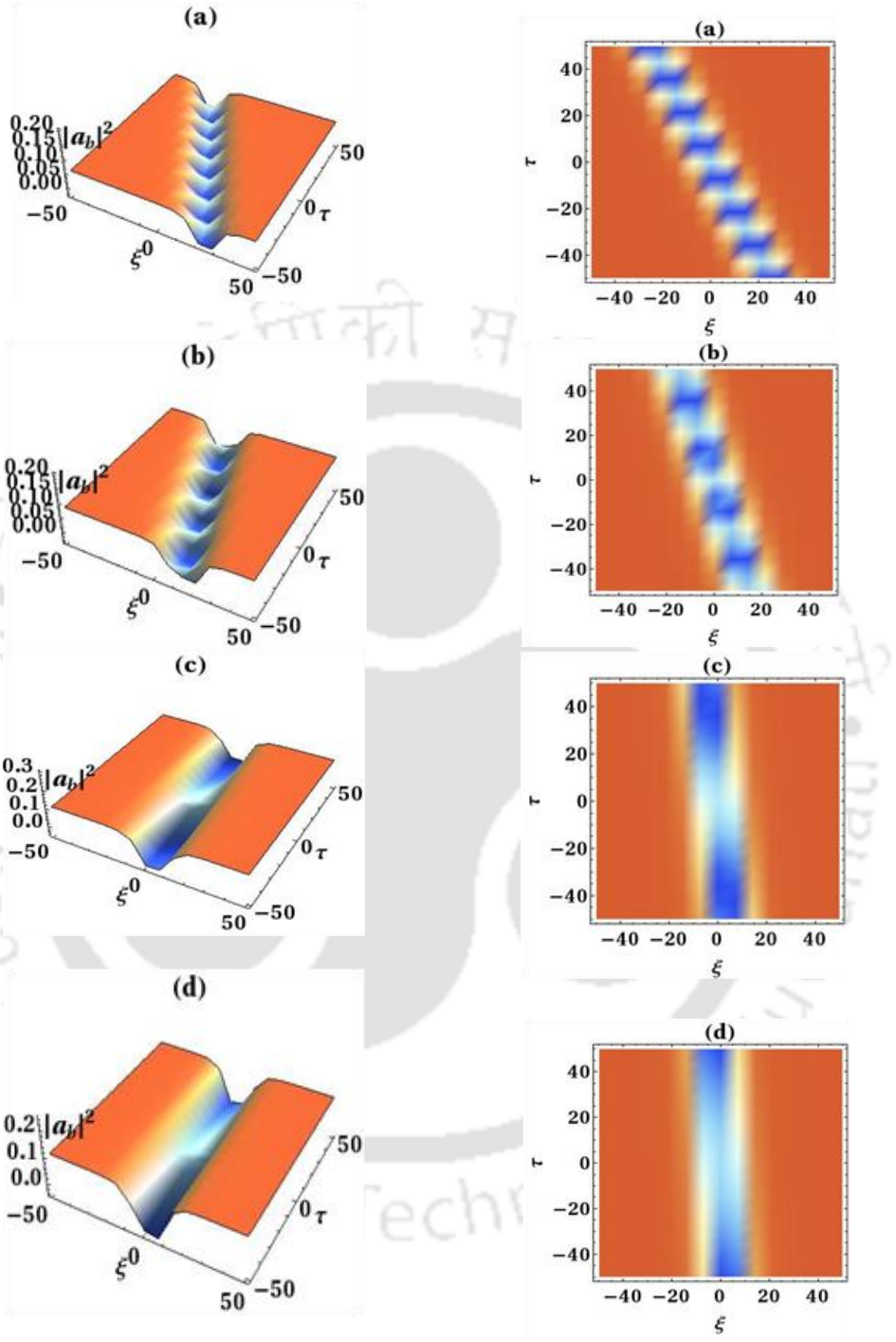

Figure 3.3: Spatio-temporal evolution of the intensity of the backward waves below the PT-threshold (left-hand panel). The corresponding density-plots are shown on the right-hand panel. Different values of parameter are: (a) c_0 = -0.5, (b) c_0 = -0.3, (c) c_0 = -0.09, (d) c_0= - 0.046. Other parameters are: k = 1.0, g = 0.9, c_1 = 2.01196.

3.4.1 Bright and dark solitary waves

We mentioned in Sec. 3.3 that there are many possible solutions to Eq. (3.20) subject to various parameter values. One interesting solution may be of the so called Optical Rogue Waves (ORW). In fact, Eq. (3.20) has close similarity with the solutions reported recently in the context of nonlinear Fiber optics [96]. In this section, we discuss the spatio-temporal evolutions of the forward and the backward waves as found in Eq. (3.20).

The simulations are carried out for two sets of values of the traveling wave speed c_0: one with positive and the other one with negative values. The positive values of c_0 refers to forward wave while the negative ones refers to backward waves. It is quite interesting to find that, below the PT-threshold the system gives rise to bright solitary wave for forward wave while dark solitary wave solution for backward wave for a chosen set of parameters. This could be clearly observed from Figs. 3.2 and 3.3. It should be noted that stable and distortion-free solitary wave propagation occurs for small value of c_0 below the PT-threshold. Also, the solitary wave is shifted towards the positive ξ axis for forward wave while the opposite occurs for backward wave with increase in the value of c_0. The bright as well as dark solitary waves get deformed with increase in the value of the traveling wave speed.

3.4.2 Emergence of Optical Rogue Waves

The spatio-temporal evolution of the intensity for backward waves above the PT-threshold, i.e. the case with k<g, is depicted in Fig. 3.4. Solitary wave with high intensity could be observed from Fig. 3.4(a). If the modulus of the c_0 parameter is decreased significantly then it results in the generation of extremely high intensity backward wave. In fact, Fig. 3.4(c) and 3.4(d) predicts the existence of localized, single solitary waves of large amplitude in the background medium. These occurrences might be explained as follows. As the modulus of the traveling wave speed c_0 is decreased by a little amount, it acts as a perturbation. The perturbation gets amplified via nonlinear processes such as modulation instability, which in turn decreases the soliton-fission threshold. Now, as the soliton-fission sets in, it results in

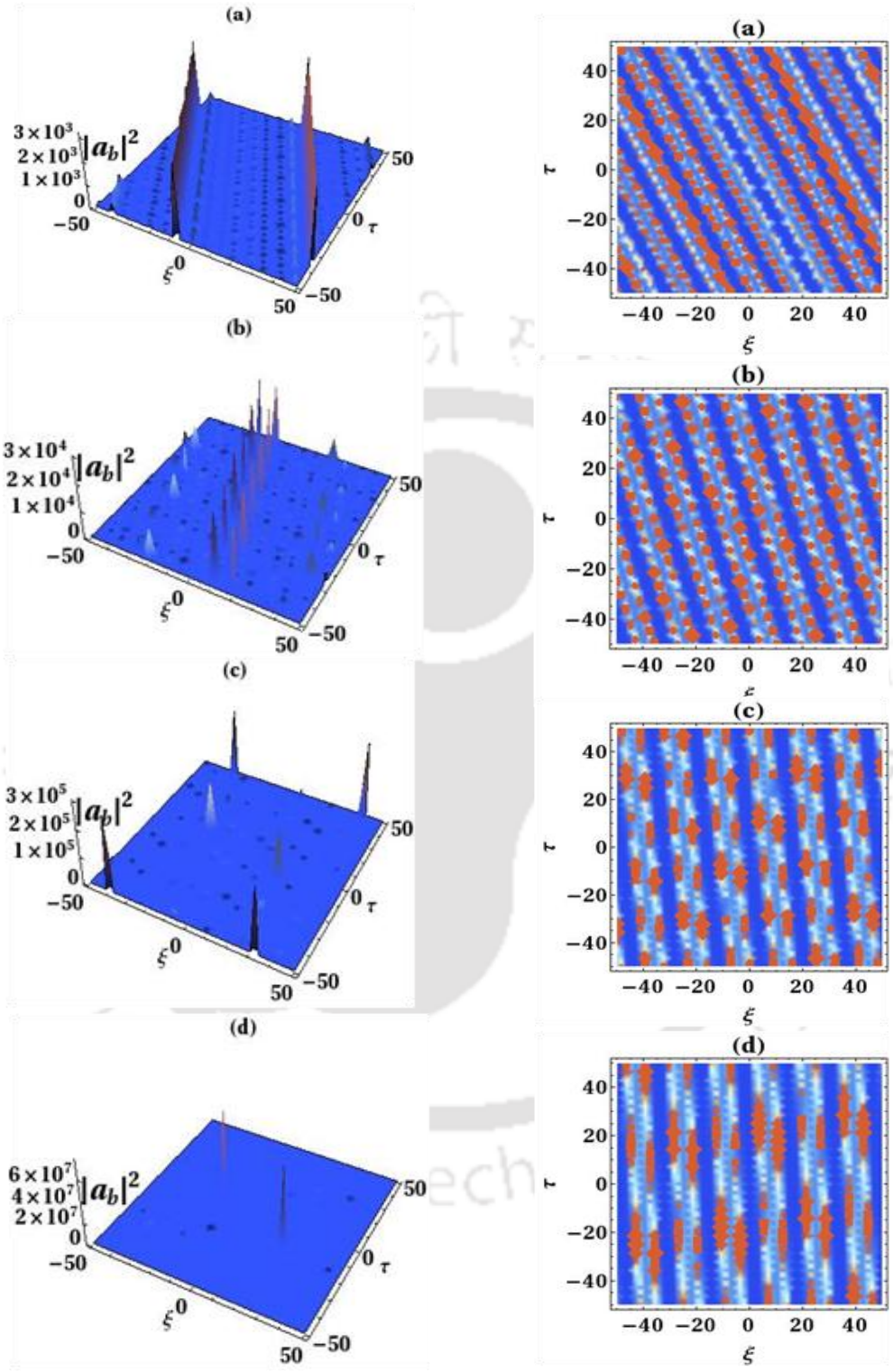

Figure 3.4: Spatio-temporal evolution of the intensity for backward waves above the PT-threshold (left-hand). In the right-hand panel, density-plots corresponding on the right-hand panel is shown. Different values of parameter are: (a) c_0 = -0.5, (b) c_0 = -0.3, (c) c_0 = -0.09, (d) c_0 = -0.046. Other parameters are: k = 1.0, g = 1.2, c_1 = 1.77259i.

the breaking up of the smooth wave and the formation of well-localized group of solitary waves of large amplitudes resembling closely to the so called optical Rogue waves. Physically speaking, with decrease in the modulus of the traveling wave speed, the energy of each of the relatively small-amplitude localized waves starts transferring energy to another one amongst the group of those waves, thus increasing its amplitude rapidly. Interestingly, solutions cease to exist for the forward wave whereas the optical rogue wave solutions are obtained for backward wave above the PT-threshold region. It may be reasonable to say that the absence of the forward wave and the presence of the backward wave are complementary to each other. In passing, it may be appropriate to note that in this work we have assumed the nonlinearity to be weak. Its effects are three-fold: firstly, the approximation of weak nonlinearity is ensuring the simple analytical solutions found in Eq. (3.20), secondly, since the nonlinearity is weak, it is practically not changing the position of the PT-threshold and third, the condition of weak nonlinearity gives rise to modulation instability accounting for the emergence of ORWs. For regular waves, Benjamin-Feir instability [97] is a weakly-nonlinear effect finding equivalent analogues in nonlinear optics. Besides, the weakly-nonlinear theory of the occurrence of rogue waves has been widely suggested as possible explaining tool [98,99], although controversial. As regards some possible applications of the present work, many may be suggested, but one potential application may be to use this PT-symmetric Bragg grating structure in generating high power optical pulses [100].

3.4 Summary of the Chapter

In this work, we have found the analytical traveling solitary wave solutions for the forward and the backward waves in a nonlinear PT-symmetric Bragg grating structure. We observe that there is an infinite number of traveling wave solutions, either solitary or cnoidal-type, depending on the parameter values of the system. The effects of the coupling constant, gain/loss parameter and the traveling wave speed on the evolution dynamics of the solutions have been discussed. We have found bright solitary wave solution below the PT-threshold for forward wave and dark solitary wave solution above the PT-threshold for backward wave. Depending on some suitable choice of the parameter values of the system, the existence of

optical rogue waves has been elucidated. It comes out that the evolutions of the forward and the backward waves crucially depend upon the different system parameters such as traveling wave speed and loss/gain parameter. It is worth mentioning here that the theoretical set-up under consideration can yield, apart from ORWs, various kinds of nonlinear traveling wave solutions based on the parameter values of the system. So, in that regard, this work could be a step forward to the future investigations in the similar systems.

Chapter 4

Peregrine Rogue Wave dynamics in the nonlocal Schrödinger system with parity-time (PT)-symmetric Kerr nonlinearity*

4.1 Introduction

When it comes to the evolutions of the nonlinear waves, integrable equations play an important role. To name a few of those integrable and exactly solvable equations, we may mention: Korteweg-de Vries (*KdV*) equation [101], sine-Gordon equation [102], Kadomstev-Petviashvili (*KP*) equation [103], Nonlinear Schrödinger equation (NLSE) [104] and so on. These equations can be integrated exactly by the inverse scattering transform method [105]. The integrability of such equations refers to infinite numbers of conserved quantities and conservation laws. The solitary waves of this class of equations undergo elastic collisions which amount to saying that there is no change in their shapes or speeds after the collisions. Based on the idea of Lax, Zakharov and Shabat proved the integrability of NLSE [104]. Afterwards, extensive efforts have been made in such integrable systems [106]. In a recent study, Ablowitz and Musslimani [107] have considered an alternative class of highly nonlocal nonlinear Schrödinger equation where the standard third-order nonlinearity $|\psi|^2\psi$ is replaced by its PT-symmetric form: $\psi(x,z)\psi^*(-x,z)\,\psi(x,z)$. The corresponding novel nonlocal nonlinear Schrödinger equation is of the following form:

---

*Part of the results of this Chapter has been published in the following paper: S. K. Gupta and A. K. Sarma, "*Peregrine rogue wave dynamics in the continuous nonlinear Schrödinger system with parity-time symmetric Kerr nonlinearity*," Commun. Nonlin. Sci. Numer. Simulat. **36**, 141 (2016).

$$i\psi_z + \frac{1}{2}\psi_{xx} + \psi(x,z)\psi^*(-x,z)\,\psi(x,z) = 0 \tag{4.1}$$

This equation is parity-time (PT)-symmetric (PTNLSE) in the sense that $V(x) = V^*(-x)$ where $V(x) = \psi^*(-x,z)\,\psi(x,z)$. This equation is nonlocal since the evolution of the optical field at a transverse co-ordinate 'x' always requires the information from the opposite point '-x'. It is worth mentioning here that for the NLSE the nonlocality shows up for sign inversion in only transverse co-ordinate 'x', whereas it can show up due to sign inversions of both the co-ordinates in other integrable equations (e.g. real and complex nonlocal mKdV equations, real nonlocal sine-Gordon equation) [108]. The study also reveals that this equation is fully integrable since it possesses linear Lax pairs and an infinite number of conserved quantities. Here we mention the quasi-power Q and the Hamiltonian H of the system:

$$Q = \int_{-\infty}^{\infty} dx\, \psi(x,z)\psi(-x,z) \tag{4.2}$$

$$H = \frac{1}{2}\int_{-\infty}^{\infty} dx\, [\psi_x(x,z)\psi_x^*(-x,z) - \psi^2(x,z)\psi^{*2}(-x,z) \tag{4.3}$$

Furthermore, it was found that the PTNLSE is Galilean invariant. In another work [8], Ablowitz and Musslimani have the key symmetries of the eigenfunctions and scattering data and conserved quantities of the PTNLSE. It should be noted that nonlinear Schrödinger systems with PT-symmetric linear potentials ($i\psi_z + \frac{1}{2}\psi_{xx} + V(x)\psi + |\psi|^2\psi = 0$) have been studied quite rigorously in the recent past [109-118]. In a nonlinear Schrödinger system, Kerr nonlinearity can dynamically create an effective linear potential which in general may not be PT-symmetric. In consequence, if the even symmetry of the real part of the effective potential gets broken, the system can observe PT-symmetry breaking instability in its wave evolution dynamics. After its inception in [107], there have been investigations pertaining to the novel *PTNLSE*. In their work [119], A. K. Sarma et al. have studied dynamical behaviors of continuous and discrete Schrödinger systems exhibiting parity-time (PT) invariant nonlinearity. The study reveals that the system yields simultaneous bright and dark soliton solutions and that the shift in the transverse co-ordinate 'x' results in the PT-symmetry breaking. This way the wave dynamics of the solitons undergoes instability. It is worthwhile to mention that the idea of parity-time (PT)-symmetry and the transverse shift, in the context

of Rogue waves, have also been explored by a group of researchers [120,121]. Other works in this connection include dark and anti-dark soliton interactions in the nonlocal nonlinear Schrödinger equation with self-induced parity-time (PT)-symmetric potential [122], periodic and hyperbolic soliton solutions in nonlocal PT-symmetric equations [123]. On a different side, as a limiting case of a wide class of solutions to the nonlinear Schrödinger equations, Peregrine solitons (PSs) being localized both in evolution and transverse variables draw fundamental importance [124]. It is also regarded as the limiting case of the transverse coordinate periodic *Akhmediev -Breather (AB)* [124-126] or the longitudinal coordinate periodic *Kuznetsov-Ma* (*KM*) breather [125,127]. In spite of being theoretically predicted in 1983 by H. Peregrine [128], it was not until 2010 by Kibler et al. [127] that the Peregrine soliton has been experimentally demonstrated in nonlinear fiber optics. After that, Peregrine soliton has been studied in numerous contexts such as: Peregrine solitons in a multi-component plasma with negative ions [129], Peregrine soliton generation and breakup in the standard telecommunications fiber [130] [43], interaction of Peregrine solitons [131], breather-like solitons extracted from the Peregrine rogue wave [132], Peregrine solitons and algebraic soliton pairs in Kerr media [133] and so on. Often, the Peregrine soliton is seen as a rogue-wave prototype [134] for its close resemblance to the rogue-wave dynamics. For instance, the maximum amplitude of Peregrine solitons is three times the amplitude of the surrounding unperturbed uniform wave train, whereas statistically speaking, in oceanography a rogue wave is said to form when its height becomes 2.2 times the height of the largest third of waves in a wave record (which is termed as significant wave height (SWH)). It is interesting to note that "Rogue waves" or "freak waves" which are large amplitude "*waves appearing from nowhere and disappearing without a trace*" (*WANDT*) find its roots in hydro-dynamical systems [135,136], nonlinear fiber optics [137], Bose-Einstein condensates [138] etc. Optical rogue waves have been studied in singly resonant parametric oscillators [139], mode-locked lasers [140], in optically injected lasers [141].

In this work, we have considered a Peregrine soliton ansatz to the focusing nonlinear Schrödinger equation with anomalous dispersion with parity-time (PT)-symmetric nonlinearity. We intend to study the dynamics of the *c-PTNLSE* under Peregrine soliton or more generally solitons on finite background (*SFB*) excitation both in unbroken and broken

PT-phases. Since the Peregrine solitons have been seen as a prototype of rogue waves, we study the dynamics of initial PS solution in the *c-PTNLSE* model and see if it can yield Peregrine Rogue (PR) wave in the broken PT-phase. This work may encourage the nonlinear physics community to investigate many other nonlinear systems [142-145] starting with quadratic to power law media with such novel type of nonlinearity.

4.2 Theoretical model

In this work, as stated in the previous section, we are considering the nonlocal nonlinear Schrodinger equation, in normalized units, where the standard third order nonlinearity $|\psi(x,z)|^2\psi(x,z)$ is replaced with its PT symmetric counterpart $\psi(x,z)\psi^*(-x,z)\psi(x,z)$ to obtain:

$$i\psi_z + \tfrac{1}{2}\psi_{xx} + \psi(x,z)\psi^*(-x,z)\psi(x,z) = 0 \tag{4.4}$$

Here $\psi(x,z)$ is the dimensionless field. x and z are transverse co-ordinate and normalized propagation distance (evolution variable). It is straightforward to show that Eq. (4.4) possesses the following solitons on finite background (SFB) solutions:

$$\psi(x,z) = \left[\frac{(1-4\,a)\cosh(bz)+\sqrt{2a}\cos(\Omega\,x)+i\,b\sinh(bz)}{\sqrt{2a}\cos(\Omega\,x)-\cosh(bz)}\right] \tag{4.5}$$

Here, Ω is the dimensionless spatial modulation frequency, $a = 1/2(1-\Omega^2/4)$ with $0 < a < 1/2$ determines the frequencies experiencing gain and $b = \sqrt{\{8a(1-2a)\}}$ is the instability growth parameter. For $a \to 1/2$, the above solution reduces to the rational soliton form i.e. Peregrine soliton:

$$\psi(x,z) = \left[1 - \frac{4(1+2iz)}{1+4x^2+4z^2}\right]e^{iz} \tag{4.6}$$

4.3 Numerical simulations and analysis

In order to analyze the continuous *PTNLSE* numerically, in the context of *SFB* solutions, we have taken the following initial excitation from Eq. (4.5): $\psi(x,0) = \left[\frac{(1-4\,a)+\sqrt{2a}\cos(\Omega\,x)}{\sqrt{2a}\cos(\Omega\,x)-1}\right]$.

Eq. (4.4) is solved numerically by using the so-called split-operator method. A detailed discussion of the method can be found in Ref. [146]. In a recent work [119] it is shown that introduction of the shift, ε, in the transverse co-ordinate, x, may give rise to instability in the wave dynamics. This happens because the self-induced potential $V\,(x,z)$ starts to have the imaginary contribution, due to the transverse shift, which once goes beyond a critical value results in instability of the wave dynamics. This motivates us to consider various cases with regard to broken and unbroken PT-phases.

4.3.1 Without any transverse shift

We first consider the case without transverse shift. Fig. 4.1 exhibits the dynamical evolutions of the intensity of the optical field under the *SFB* excitation. As can be observed from Fig. 4.1 (a)-(b), we find existence of *Kuznetsov-Ma* (*KM*) solitons periodic in the evolution variable 'z'. *KM* soliton is dependent on the modulation parameter 'a'. The spatial periodicity of KM solitons keeps on increasing with increase in the modulation parameter 'a'. The spatial periodicity of *KM* solitons keeps on increasing with increase in the modulation parameter 'a' and results in the Peregrine solitons as $a \to 1/2$, as could be seen from Fig. 4.1 (c)-(d). In passing, it is worth noting that the standard NLSE supports *Akhmediev Breather* (*AB*) solutions, which become more and more localized both in 'z' and transverse co-ordinates 'x' with the increase of the modulation parameter 'a' [127].

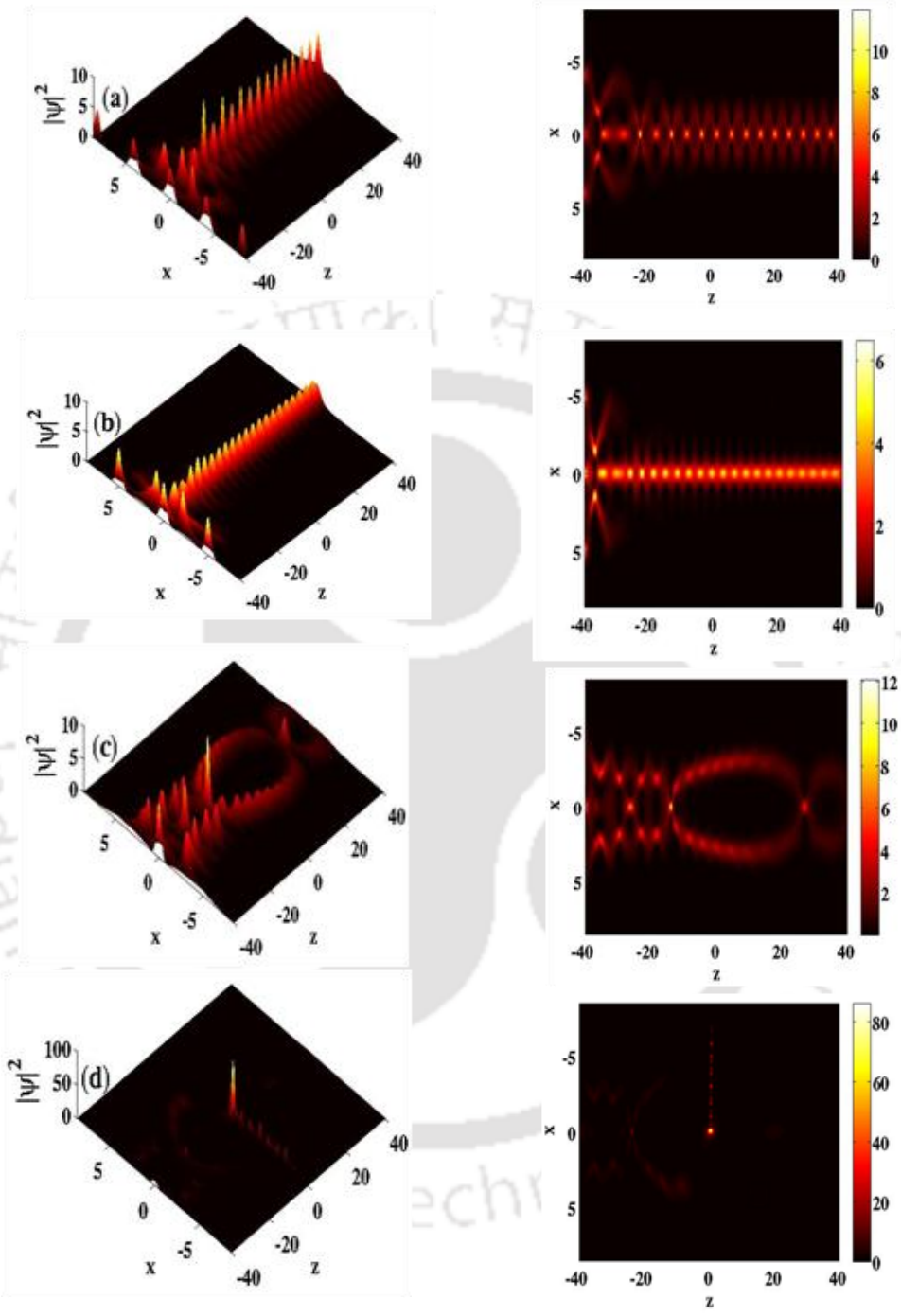

Figure 4.1: Left hand panel: Evolutions of optical intensity in the z-x plane. Right hand panel: corresponding 3D density plots. (a) $a = 0.20$, (b) $a = 0.30$, (c) $a = 0.45$, (d) $a = 0.47$. $\varepsilon = 0$.

4.3.2 With a small but nonzero transverse shift

Fig. 4.2 elucidates the effect of shift in the transverse co-ordinate 'x' on the evolution of the optical field dynamics. From Fig. 4.2, we can infer that with the increase in the transverse shift parameter, the optical field dynamics tend to be more localized in the z-x plane. The role of the transverse shift is two-fold: first, in triggering the PT-instability, and second, ensuring the nonlinear interactions between localized modes. That is why, in Fig. 4.2 (a) and 4.2 (b), although we see presence of a dominant single second-order kind of PS with a wing-like structure, in Fig. 4.2 (c), we find appearance of another second-order type of PS in the *CW* background. It is worthwhile to note that a strict mathematical definition of second order *PS* soliton for the continuous Schrodinger equation considered in this work, unlike some other nonlinear systems [121], is not available. Our assumption of second order PS is based on plots resulting from numerical simulations. More interestingly, in Fig. 4.2 (d), we finally observe one *PS* in the *CW* background. This is simply because in Fig. 4.2 (d), further increase of the transverse shift acts as a perturbation which gets amplified via modulation instability and through nonlinear wave-mixing processes the multiple PS profiles interact with each other to transfer energy from one to the other resulting into giant Peregrine rogue wave. One crucial point to mention here is that the occurrence of the *PRW* depends on very definite parameter values, which is quite evident as far as the rarity of the rogue wave phenomenon is concerned. In the corresponding density plot of Fig. 4.2(d), we also observe occurrence of certain radiation states alongside the Peregrine rogue wave profile.

It is worthwhile to mention here that in a recent work in the context of PT-symmetric coupled waveguides, occurrence of two *KM* solitons trains hinged upon a second-order Peregrine soliton creating a wing-like shape has been reported [125]. Our study on *c-PTNLSE* model also reveals existence of similar wing-like *KM* soliton trains hinged upon a second-order Peregrine soliton as is evident from Fig. 4.2 (a)-(b).

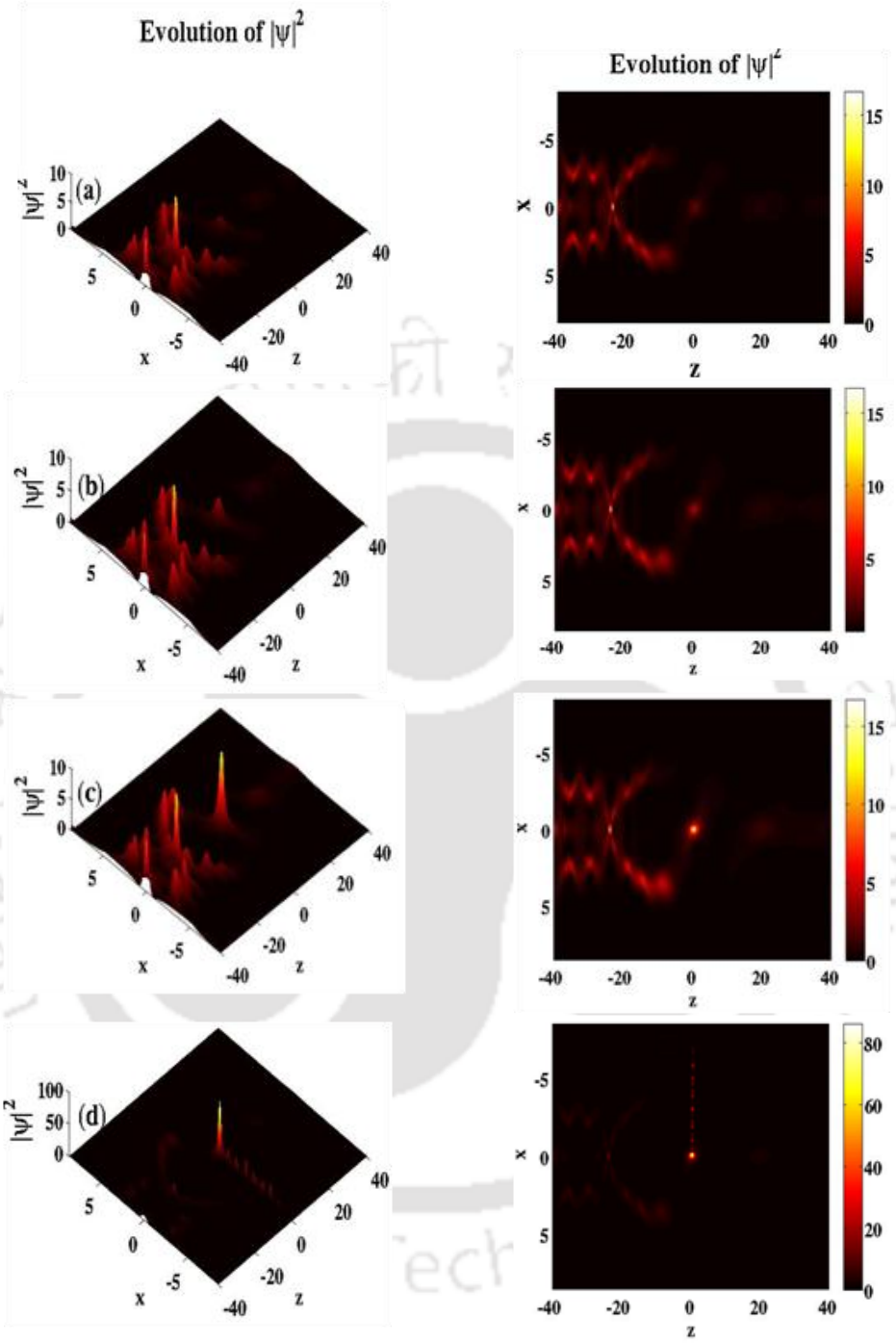

Figure 4.2: Left hand panel: Evolutions of optical intensity in the z-x plane. Right hand panel: corresponding 3D density plots. (a) $\varepsilon = 2 \times 10^{-6}$, (b) $\varepsilon = 3 \times 10^{-6}$, (c) $\varepsilon = 4 \times 10^{-6}$, (d) $\varepsilon = 4.53 \times 10^{-6}$. Other parameter value: $a = 0.47$.

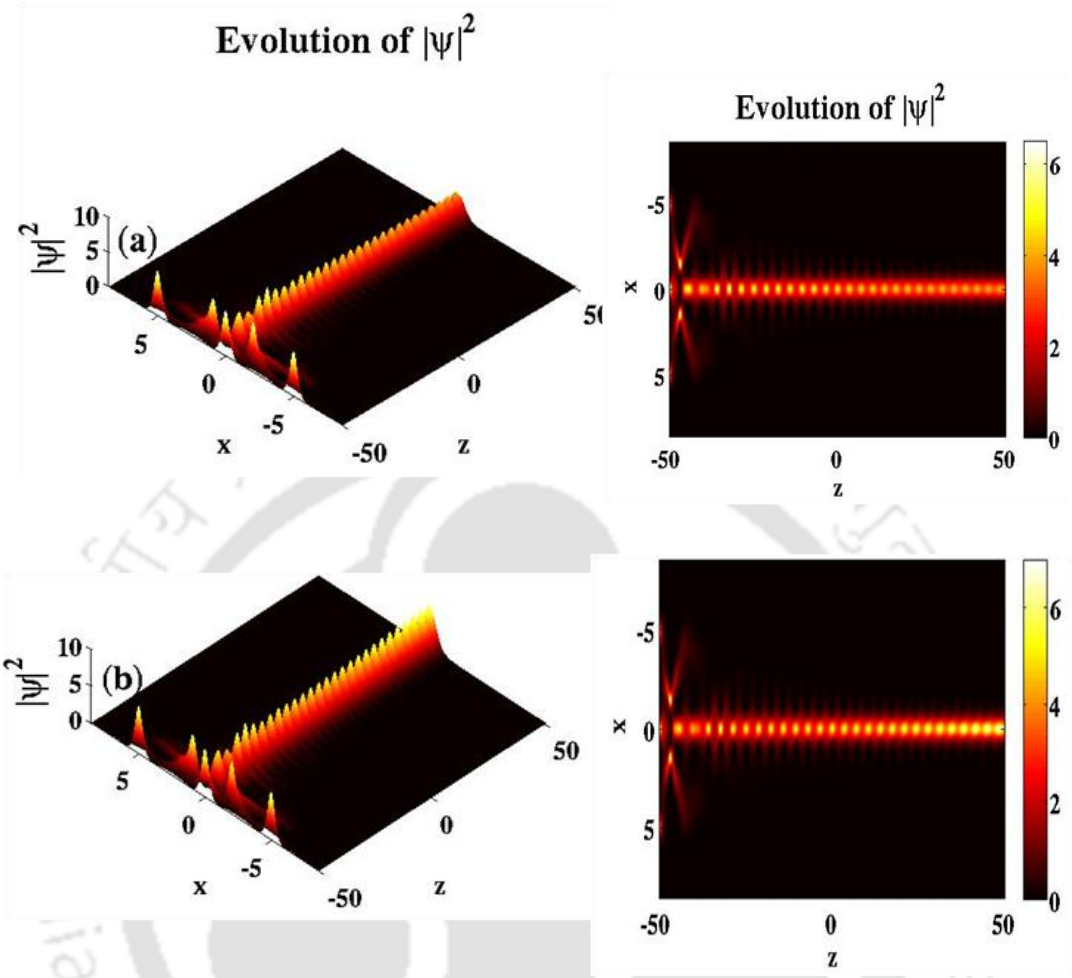

Figure 4.3: Left hand panel: Evolutions of optical intensity in the z-x plane. Right hand panel: corresponding 3D density plots. (a) $\varepsilon = 0$, (b) $\varepsilon = 3 \times 10^{-3}$. Other parameter value: $a = 0.30$.

The fact that inclusion of a nonzero shift in the transverse co-ordinate results in the instability in the wave dynamics, as suggested in [119], could be clearly seen from Fig. 4.3. This instability can be attributed to the induction of an imaginary part in the self-induced potential, which goes beyond a critical value. In Fig. 4.3 (b) and its corresponding density plot shows the onset of instability in the optical field dynamics in presence of the transverse shift. The intensity of the optical field keeps on increasing with the normalized propagation distance. Without any transverse shift, in Fig. 4.4(a) we observe two lines of peaks of *KM* soliton trains along the z-axis, existing at different locations. These two lines of peaks of *KM*

soliton trains are hinged upon a second order Peregrine soliton. Fig. 4.4(c) depicts the corresponding power along the propagation distance. Now, quite interestingly, we find that for the same set of parameter values but with a nonzero shift in the transverse co-ordinate, the system supports robust (with respect to the transverse shift parameter in the range $\varepsilon = [4.5,4.605] \times 10^{-6}$) Peregrine soliton solution with enhanced intensity, strongly localized in the z-x plane, as is clear from Fig. 4.4 (b) and (d). This enhancement in the intensity of the optical field is owing to the broken PT-symmetry of the self-induced potential. Due to the prototypical analogy between Peregrine soliton and the Peregrine rogue wave, we can qualitatively argue that the enhanced PS dynamics resemble to the Peregrine rogue waves.

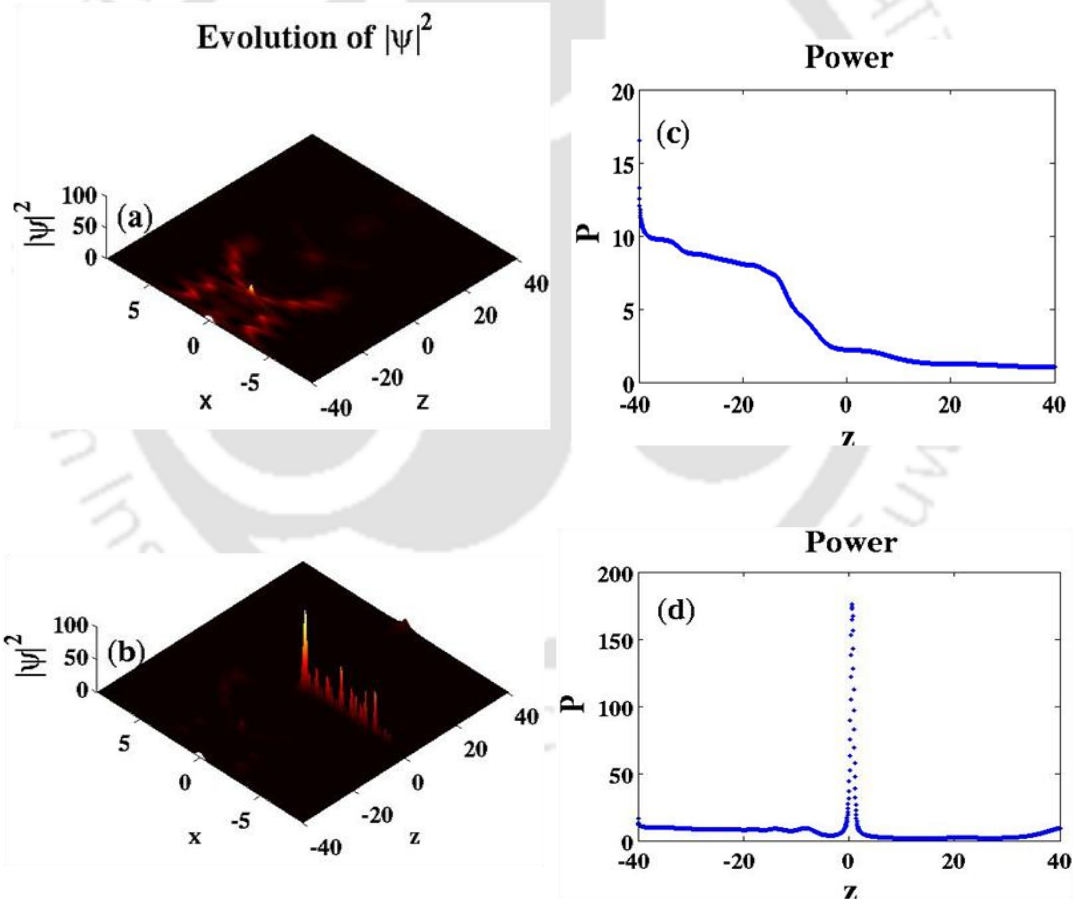

Figure 4.4: Left hand panel: Evolutions of optical intensity in the z-x plane. Right hand panel: Corresponding power along the propagation distance. (a), (c): $\varepsilon = 0$ and (b),(d): $\varepsilon = 4.605 \times 10^{-6}$. Other parameter value: $a = 0.47$.

4.4 Summary of the Chapter

We have carried out a numerical study of continuous nonlinear Schrodinger equation with parity-time symmetric nonlinearity with special emphasis given to the Peregrine soliton dynamics. The general solitons on the finite background ansatz is taken as the initial excitation. Since, the Peregrine solitons have been seen as a rogue-wave prototype for a long time, we numerically confirmed that an initial PS excitation could yield *PRW* in the broken PT-phase. Upon numerical computation, we observe the appearance of low-intense *Kuznetsov-Ma* (*KM*) soliton trains in the absence of transverse shift and well-localized high-intense Peregrine Rogue waves in the presence of transverse shift in a definite parametric regime. In the earlier case, the PT-symmetry is unbroken, whereas in the later case the PT-symmetry is broken. It is to be noted that such nonlocal parity-time (PT)-symmetric nonlinearity may be obtainable in the wave mixing phenomena with proper PT-symmetric environments [119]. As has been pointed out in [119] that nonlocal nonlinearities are all-pervasive in nature, to mention a few among them: it may be found in the BECs with spatially and temporally fluctuating trapping potentials, in atomic vapors for diffusion processes [147,148]; in waveguide arrays due to random variations in the refractive index, size or waveguide spacing [149], long-range molecular interactions in nematic liquid crystals [150] etc. This work may boost further investigation of optical rogue waves and its dynamics in the context of nonlocal nonlinear systems that may be more useful if such nonlinearity can be found testable in real physical settings.

भारतीय प्रौद्योगिकी संस्थान गुवाहाटी
Indian Institute of Technology Guwahati

Chapter 5

Controllable chaotic dynamics in a nonlinear fiber ring resonators with balanced gain and loss*

5.1 Introduction

Chaotic systems exhibit sensitivity to the initial conditions. In such systems any uncertainty, no matter how small, in the beginning will produce rapidly escalating and compounding errors in the prediction of the future of the system behavior. It implies that two trajectories emerging out from two distinct but nearby initial conditions diverge exponentially from each other with the passage of time. The idea of chaos is studied quite extensively in natural sciences, especially in chemistry [151-153], electronics [154,155], fluid dynamics [156] and nonlinear optics [157-163]. We mention a few of them here in the following. In the review paper [157] by A. D. Stone the scientific endeavors in the direction of studying the interface between chaos and the quantum mechanics was chronologically shown. In this connection, the study of classical chaos in the microscopic systems [158] have witnessed in recent times the chaos-assisted tunneling of directional emission from micro-billiards structure [159]. In a system of two coupled lasers with modulated parameters, numerical investigation shows that although the phases of the electric fields involved were synchronized but there might be chaotic variations in the amplitudes [160]. H. G. Winful et al. [161] showed that in a system of array of lasers a subset of it can produce spatio-temporal chaos beyond a critical coupling strength when synchronization fails. S. Zaitsev et al. [162] studied the nonlinear dynamics of a micro resonator in an optical resonance cavity where it was shown that the coupling of the resonator to the optical cavity introduces corrections to the linear and the nonlinear dissipations and the nonlinear elastic constants. M. J. Akram et al. [163] have investigated

*Part of the work is published in *Nonlinear Dynamics (Springer) DOI: 10.1007/S11071-016-3102-9*

upon the chaotic dynamics of the kicked nanomechanical membrane in the optomechanical system under judicious control of the system parameters. It should be noted that, a discrete time dynamical system known as the Ikeda map, proposed by K. Ikeda, model optical field dynamics in nonlinear optical resonators [164,165]. K. Ikeda showed that the stationary state of the transmitted light exhibits chaotic behavior over a wide range of some system parameter values [164]. Ikeda et al. in a subsequent paper [165] demonstrated that the stationary state of the transmitted light from the nonlinear dielectric medium containing ring cavity system can make transition into the periodic and the nonperiodic states with the increase in the input intensity. The nonperiodic states were shown to be associated with the chaotic dynamics.

In this context, dynamical pulse shaping and period-doubling bifurcations have been studied in nonlinear fiber ring resonator systems both theoretically and experimentally [166-172]. Among them, in a system of a ring cavity containing an optical fiber the period-doubling route to chaos was shown to exist near the zero dispersion wavelength of the fiber [166]. M. Haelterman [167] later proposed a new theoretical approach to study the period-doubling bifurcation and the transverse effects in the nonlinear ring cavity. The existence of dissipative spatial stationary structures was predicted as a result of interplay between the diffraction and the nonlinearity. In another paper G. Steinmeyer et al. [168] studied the dynamical pulse shaping in a nonlinear ring resonator containing an optical fiber. The study showed that the pulse shapes can give rise to substructure which can be periodic, stationary or chaotic. In an experimental setting of an all-fiber ring cavity [169], the temporal instabilities were shown to exist in the resonant pulse train from a dye laser. In another work, in a nonlinear ring cavity with fiber dispersion the periodic oscillation of the intensity was reported as a consequence of modulation instability [170]. M. B. van der Mark [171] experimentally demonstrated the occurrence of hysteresis, period doubling and the chaotic behavior of picoseconds pulses in a nonlinear optical ring cavity. In another experimental work by S. Coen at al., [172] the authors have studied the nonlinear dynamics of the synchronously pumped all-fiber passive ring cavity where it was emphasized that the modulation instability plays a vital role in the dynamics of the ring cavity. So far we see that although the roles played by the fiber dispersion, nonlinearity, modulation instability in the ring resonator systems in the context of

nonlinear dynamics have been studied and investigated with due relevance over times, but the role of optical losses was not addressed in detail. Of particular interest may lie in the fundamental question: what happens in these systems when there is simultaneous and balanced presence of gain and loss. As a matter of fact, we know that balanced presence of gain and loss in the optical structures gives rise to the concept of PT-symmetry that shows interesting physical behaviors. It is to be noted that our system is not PT-symmetric as there is no axis of symmetry. Still, this work can trigger further explorations in similar or more sophisticated systems in the context of PT-symmetry. Here, we study the effects of the balanced gain and loss profile upon the evolution dynamics of the input optical pulse over a sufficiently large number of round-trips in the ring cavity. It is found that input light above a certain threshold power can give rise to chaos due to the interference between the input field and the cavity field.

5.2 Theoretical model

In an optical fiber coupler, the coupled mode equations governing the dynamics of the field amplitudes are given by:

$$i\frac{da_1}{dz} = \beta_1 a_1 + C a_2 \tag{5.1a}$$

$$i\frac{da_1}{dz} = \beta_2 a_2 + C a_1 \tag{5.1b}$$

Here, a_1 and a_2 are field amplitudes in fiber 1 and fiber 2 respectively. β_1 and β_2 are the propagation constants of the two waveguides and C is the coupling coefficient. For identical fibers, $\beta_1 = \beta_2$ and analytical solution of these equations yield the following transfer matrix:

$$\begin{pmatrix} a_1(z) \\ a_2(z) \end{pmatrix} = \begin{pmatrix} \cos(Cz) & i\sin(Cz) \\ i\sin(Cz) & \cos(Cz) \end{pmatrix} \begin{pmatrix} a_1(0) \\ a_2(0) \end{pmatrix} \tag{5.2}$$

The transfer matrix can be rewritten, defining the intensity splitting ratio, $k \equiv (\sin(CL))^2$ where L is the coupling length, as follows [173]:

$$A = \begin{pmatrix} \sqrt{1-k} & i\sqrt{k} \\ i\sqrt{k} & \sqrt{1-k} \end{pmatrix} \tag{5.3}$$

For a 50:50 directional coupler, $k = \frac{1}{2}$. Hence, the transfer matrix for 50:50 directional couplers is given by:

$$A = \frac{1}{\sqrt{2}} \begin{pmatrix} 1 & i \\ i & 1 \end{pmatrix} \tag{5.4}$$

The fiber coupler considered in this work is inspired by the parity-time (PT) synthetic coupler introduced in Refs. [174,175]. The coupler comprises a passive coupling region and two channels of waveguides, one of which provides amplification and the other provides an equal amount of attenuation. It is worthwhile to note that optical fibers can be synthesized to amplify as well as attenuate optical power by suitably tailoring their refractive index profile. Suppose the refractive index profile of an optical fiber is $n = n_r + in_I$. If $n_I < 0$, the light input will undergo amplification, whereas if $n_I > 0$, it will suffer attenuation. The two channels are connected to the passive coupling region as shown in Fig. 5.1. This configuration served as the building block of *PT* symmetric optical mesh lattices in the aforementioned works. In this work, we consider the same *PT synthetic coupler* but with a slight modification (as shown in Fig.5.1).

The system has been modified in such a way that the output port from the loss channel has been fed back into its input. And we consider the loss channel to be a nonlinear dielectric medium. This provides us with a loss resonator channel and we can write the transfer matrix as follows:

$$M = \begin{pmatrix} e^{\frac{\gamma}{2}} & 0 \\ 0 & e^{-\frac{\gamma}{2}} \end{pmatrix} \frac{1}{\sqrt{2}} \begin{pmatrix} 1 & i \\ i & 1 \end{pmatrix} \begin{pmatrix} e^{\frac{\gamma}{2}} & 0 \\ 0 & e^{-\frac{\gamma}{2}} \end{pmatrix} \tag{5.5}$$

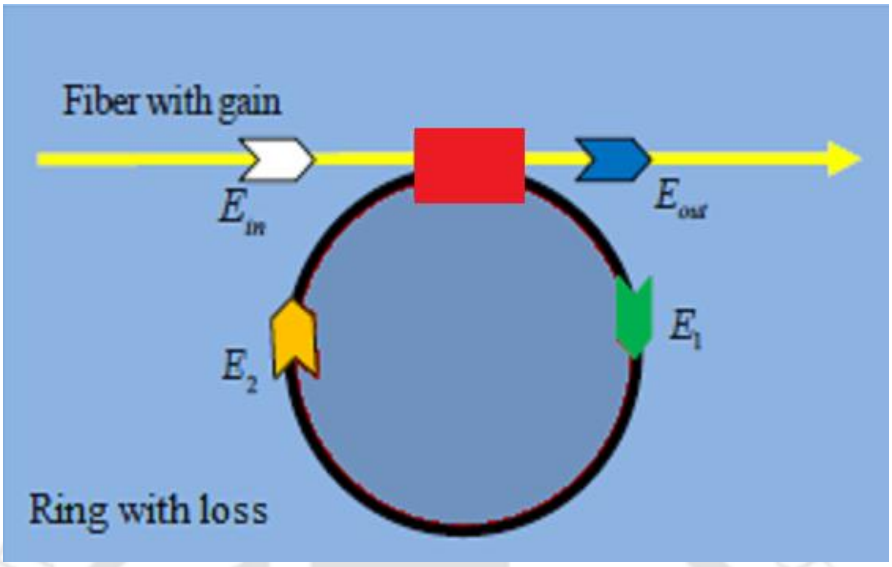

Figure 5.1: Schematic diagram of the SFR resonator structure. The yellow-color region represents the fiber with gain, the black-color ring represents the resonator with loss and the red-color rectangular block is the passive coupling region. E_{in} is the input light.

Here, $'\gamma'$ is defined as the loss parameter. And it must be noted here that there is no evanescent coupling between the optical fibers. It can be seen from Eq. (5.5) that the matrix in the middle is that of 50:50 directional coupler and the matrix on the left and right are that of two optical fibers, one of which amplifies light amplitude by a factor of $e^{\frac{\gamma}{2}}$ and the other attenuates the same by a factor of $e^{-\frac{\gamma}{2}}$. In a nutshell, we can say that our system couples an amplified and an attenuated light input via a 50:50 directional coupler and redirects one output back into directional coupler after it has traversed a lossy nonlinear resonating channel and the other output is sent to a detector to study the evolution dynamics in the system.

Using the transfer matrix, M, we can write the output amplitudes in terms of the input amplitudes as follows:

$$\begin{pmatrix} E_{out} \\ E_1 \end{pmatrix} = \frac{1}{\sqrt{2}} \begin{pmatrix} e^{\gamma} & i \\ i & e^{-\gamma} \end{pmatrix} \begin{pmatrix} E_{in} \\ E_2 \end{pmatrix} \tag{5.6}$$

The field suffers a nonlinear phase shift, $\emptyset_{NL}$, when it travels one complete loop across the ring. So, we can write: $E_2 = E_1 e^{i\emptyset}$ where $\emptyset = \emptyset_L + \emptyset_{NL}$ is the total phase shift suffered by the field. $\emptyset_L$ is the linear phase shift. The round-trip time for one complete loop of the electromagnetic wave around the resonator is given by: $t_R = nL/c$. L is the length of the resonator, *'n'* is the effective refractive index in the resonator. The nonlinear phase shift:

$\emptyset_{NL}$, is given by:

$$\emptyset_{NL} = \frac{2Ln_2\pi}{A_{eff}\lambda_o}\left|E_j\right|^2 \tag{5.7}$$

Here n_2 is the nonlinear refractive index coefficient, A_{eff} is the effective core area of the fiber and λ_0 is the wavelength of the propagating light in vacuum. Using Eq. (5.6) we can write the discretized field amplitude evolution equation in the resonator taking time steps equal to t_R in the form of an iterative equation:

$$E_{j+1} = A + BE_j exp\big(i(\emptyset_{NL} + \emptyset_L)\big) \tag{5.8}$$

where $A = iE_{in}/\sqrt{2}$ and $B = e^{-\gamma}/\sqrt{2}$. Without any loss of generality, taking $\emptyset_L = 0$, we can rewrite Eq. (5.8) as:

$$E_{j+1} = A + BE_j e^{i|E_j|^2} \tag{5.9}$$

It is straightforward to work out the resonator field intensity from Eq. (5.6), given as:

$$P_2 = \frac{|E_{in}|^2}{e^{-2\gamma}+2-2\sqrt{2}e^{-\gamma}\cos(\emptyset)} \tag{5.10}$$

At resonance, $\emptyset = 2\pi m$, where m is an integer. Using Eq. (5.7) and setting $g = \frac{n_2}{A_{eff}\lambda_0}$, the resonance condition is found to be: $m = Lg|E_2|^2$. Here g is the nonlinear parameter.

5.3 Results and discussions

The system displays rich behavior in the context of nonlinear dynamics. The number of round trips (or iterations) light takes in the resonator shows how the field intensity evolves in the resonator. This evolution is governed by Eq. (5.6). Now because the ring is an absorbing medium, the intensity gets attenuated in it. As the iteration progresses, the system slowly enters the steady state. Now depending on the value of γ, the ring can either be in a chaotic state or contain a single intensity, which are primarily the fixed points of Eq. (5.6). Taking a fixed value of γ, we carried out 1000 iterations and discarded the first 900 as transients and plot the remaining 100 steady state iterations. Fig. 5.2 depicts the output intensity as a function of the input amplitude for $\gamma = 1.0$.

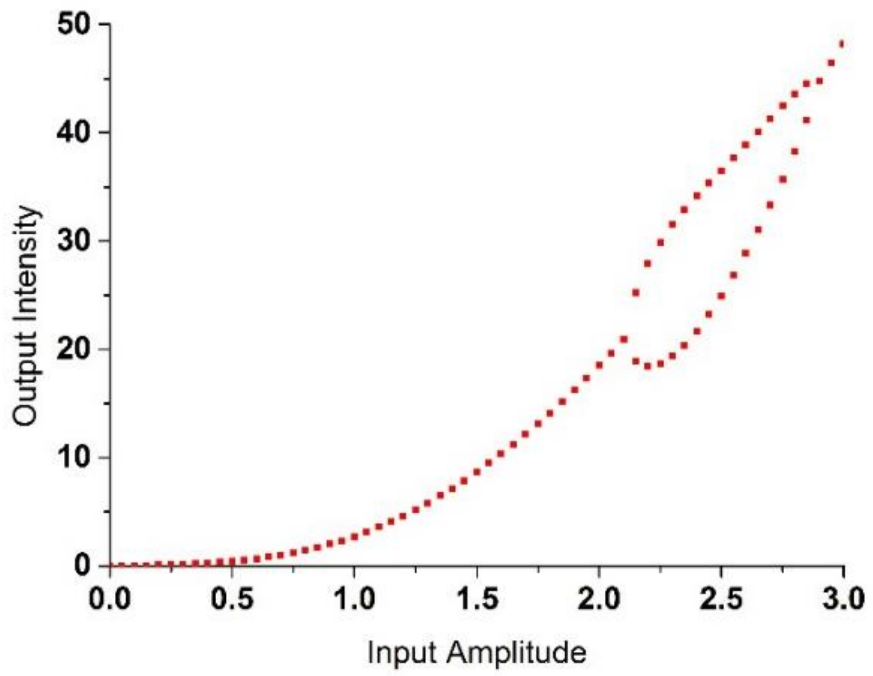

Figure 5.2: Field Intensity in the Output port vs. Input Field Amplitude E_{in} for γ=1.0.

It can be seen that the output intensity gets highly amplified as input amplitude increases. We also observe two different field intensities for a certain range of E_{in}. It is worth noting that if

we increase γ, the bifurcation behavior will cease to exist beyond a certain limit. On the other hand, if we proceed to increase E_{in} beyond 3.0, as depicted in Fig. 5.3, we encounter a chaotic region beyond a certain point because $\gamma = 1.0$ is not sufficient to counteract the chaotic behavior of the system. The reason for this can be attributed to the fact that the ring resonator in our configuration is an intensity absorber.

So, up to certain input amplitude, the resonator can attenuate the influx of energy and prevent the system from going to a chaotic state. But beyond a certain value, it fails in this aspect and we observe chaotic transmission of field intensity in the output port. The role of the loss parameter γ can be illustrated by plotting a bifurcation diagram of intensity in the resonator against the loss parameter γ, as shown in Fig. 5.4. As γ decreases, the resonator field intensity has two distinct values, which goes to four on further decrease in γ and eventually

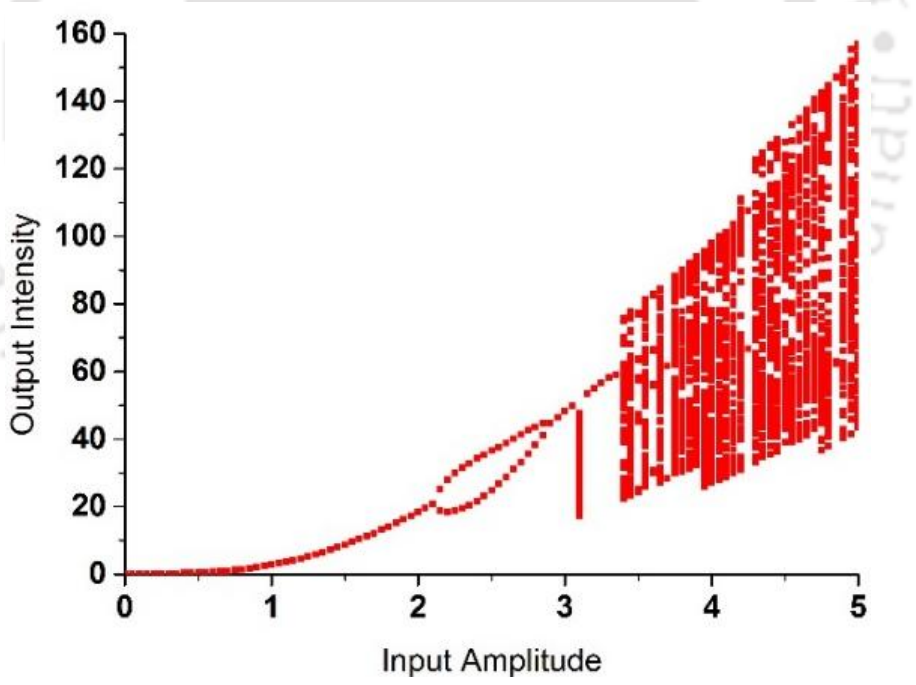

Figure 5.3: Output intensity versus the input amplitude plot showing the chaotic behavior of the system for E_{in} beyond 3.0.

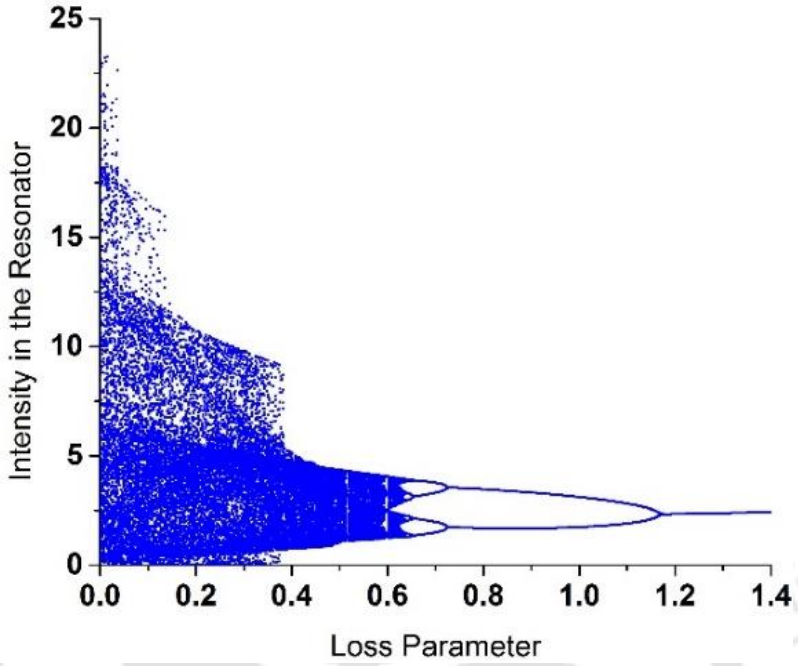

Figure 5.4: Bifurcation diagram of the Resonator Field Intensity vs. γ for $E_{in} = 2.5$.

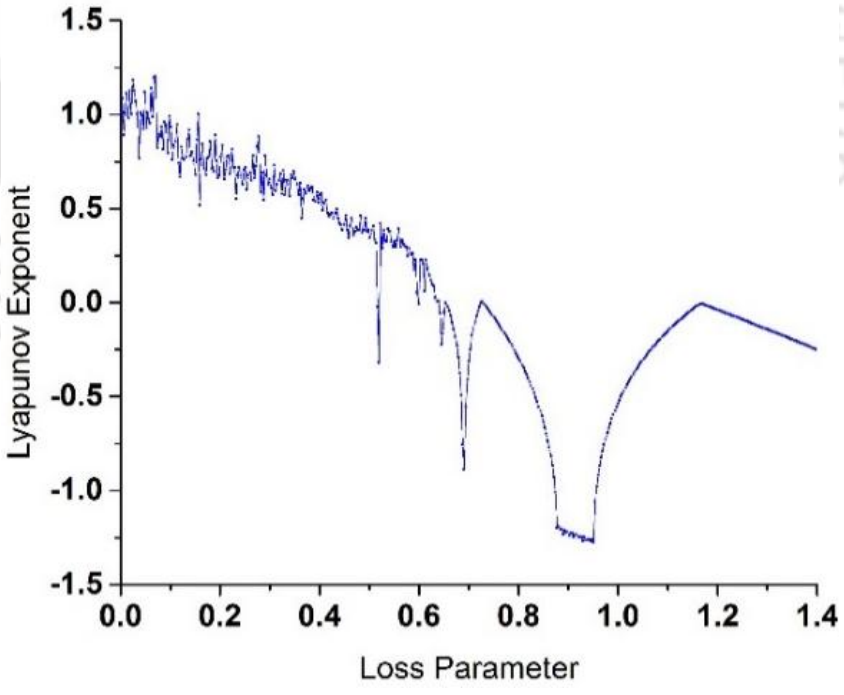

Figure 5.5: Largest Lyapunov exponent vs. γ for $E_{in} = 2.5$.

we enter into a region of chaotic behavior. It is clearly evident that the period doubling point lies close to $\gamma = 1.2$. γ plays a crucial role in the transition of the system to a chaotic state. We can claim that γ plays the role of a chaos control parameter. A plot of the largest Lyapunov exponent against the loss parameter γ, shown in Fig. 5.5, validates our above-mentioned claim.

For γ above 1.2, the system has negative Lyapunov exponents. This implies that the ring contains a single intensity, as is evident from the bifurcation diagram. In the region of γ from 0 to 0.6, the Lyapunov exponents are positive indicating that the system is in chaotic state. Now, a numerical algorithm can be designed which computes the value of γ at which period doubling takes place for different values of E_{in}. This presents us with a set of γ corresponding to the input amplitude E_{in}, as depicted in Fig. 5.6.

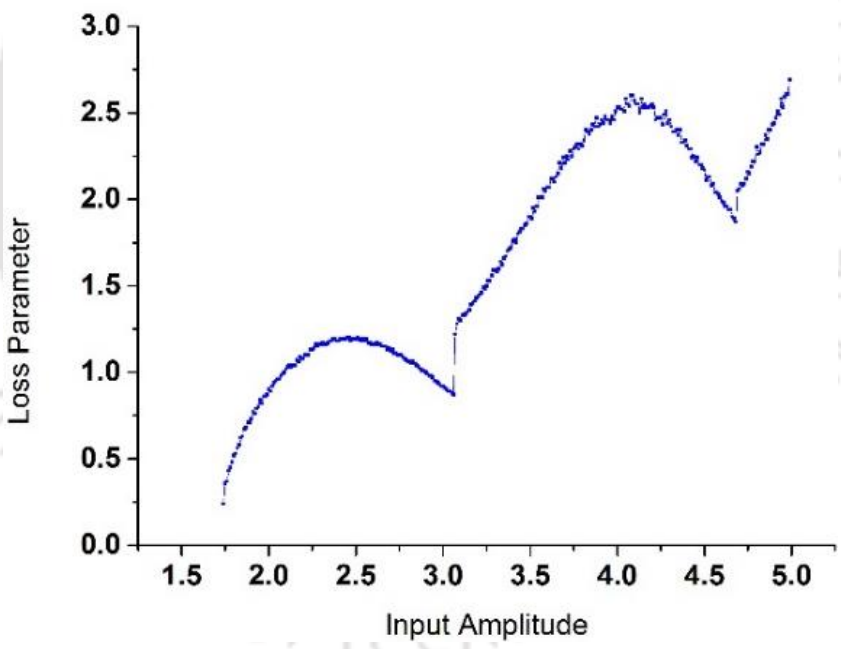

Figure 5.6: Period doubling point vs. E_{in}.

The period doubling point shifts its value in accordance with E_{in}. Fig. 5.6 gives us an idea about how the system should be designed so as to observe a single intensity in the output. A single stable intensity in the resonator will ensure the same in the output. The period

doubling point as calculated numerically for each value of E_{in} corresponds to a maximal limit of γ, beyond which fluctuation in the resonator field intensity has been observed to be of the order of 10^{-5}. Some of the values of E_{in} and γ used to plot Fig. 5.6 are (2.0, 0.90), (2.5, 1.19), (3.0, 0.92), (3.5, 1.90) and (4.0, 2.53). Typically, for a Gaussian modal distribution, if the nonlinear refractive index n_2 is chosen to be on the order of $10^{-20}\, m^2W^{-1}$, g takes values in the range of $10^{-3} - 10^{-2}\, W^{-1}/m$. Moreover, the nonlinear parameter g can be increased by decreasing A_{eff} . Taking these parameter values under consideration, the resonance spectrum can be estimated using Eq. (5.7). Numerically, $g = 0.92$ has been found to restore the resonator intensity dynamics into a steady state when $E_{in} = 3.0$. The resonance spectrum for this particular case has been shown in Fig.5.7, which depicts the resonance profile with wavelength range chosen in the visible spectrum.

The resonator field intensity peaks around 550-600 nm indicating that this configuration, if properly engineered, can be utilized for practical purposes.

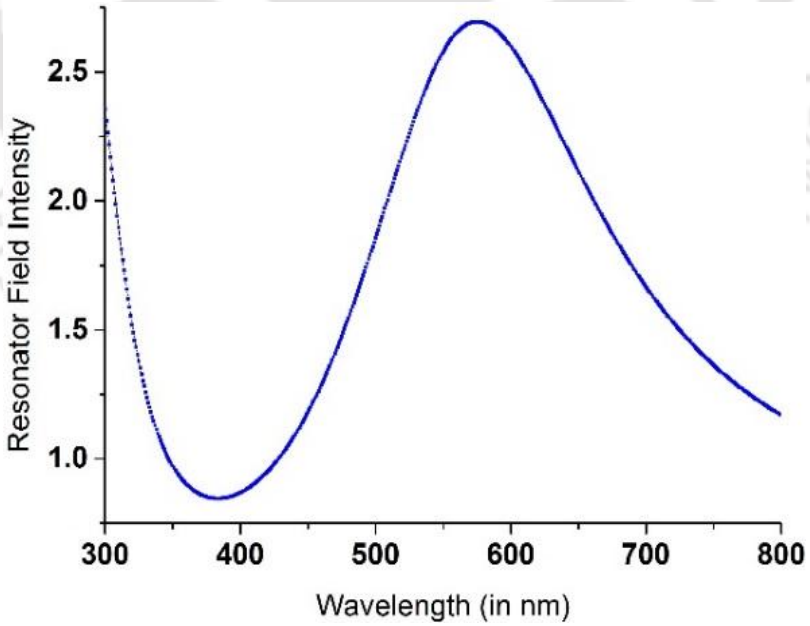

Figure 5.7: The resonance profile for $E_{in} = 3.0$ and γ = 0.92. The parameters chosen are: $n_2 = 2.6 \times 10^{-20}\, m^2W^{-1}$, $A_{eff} = 10^{14}m^2$, $L = 0.5\, m$.

In Fig. 5.8 the intensity in the resonator has been plotted against the number of iterations of the optical fields. It can be seen that the resonator behaves like a damped harmonic oscillator, but the intensity does not decay down to zero owing to the fact that there is a constant influx of light, which is being fed to the resonator.

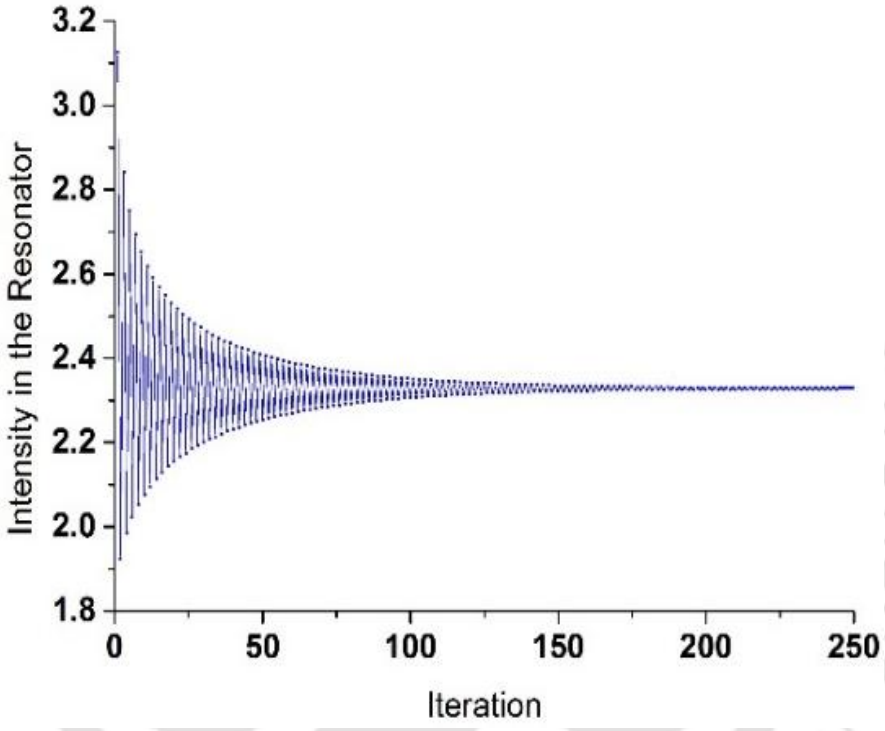

Figure 5.8: Intensity Evolution in the resonator vs. iteration for $E_{in} = 2.5$ and $\gamma = 1.19$.

The loss ring plays the role of a dampening medium and the input amplitude acts as the driving force in the system. Moreover, we have considered the ring to be a nonlinear dielectric medium. These elements are also a part of the pulse driven nonlinear oscillator equation [175], from which the Ikeda map is derivable and this justifies the behavior shown in Fig. 5.8. Hence, we can infer from the above plots that γ plays the role of a chaos control parameter in our configuration. This work so far, on firm grounds, has validated the fact that the idea of a *PT* synthetic coupler can be converted into a simple fiber ring resonator with a control parameter that is solely dependent on the fiber characteristics. In addition to this, the

fluctuations in the field intensity at the output port could be controlled with a judicious choice of the value of γ.

5.4 Summary of the Chapter

In conclusion, we find that simple alterations in the parity time symmetric synthetic coupler structures could result in a dynamically controllable algorithm for the chaotic dynamics inherent in the system. We have also shown the dependence of the period doubling point on the input amplitude, emphasizing on the dynamical aspects. Moreover, the fact that the resonator essentially plays the role of a damped and driven harmonic oscillator has been elucidated with the non-zero intensity inside the resonator due to constant influx of input light. It should be noted that the system considered in this work do not exhibit PT-symmetry owing to the lack of an axis of symmetry in the configuration of the system. However, the objective of this study is to understand the dynamical aspects of such system configuration with respect to balanced presence of loss and gain. It may also trigger further studies in the resonator systems with other configurations which can shed more light as regards the role of PT-symmetry is concerned.

Chapter 6

Optical parametric amplification in parity-time-symmetric negative-index metamaterials

6.1 Introduction

"*In a very potent way, metamaterials ignited the world at the beginning of the last decade, and the flame was fanned by the idea of embracing negative refractive index materials, …*" we quote Allan Boardman with regard to metamaterials in one of his review papers [176]. Metamaterials are artificially engineered materials made of sub-wavelength structures from composite substances such as metals or plastics which derive their astonishingly peculiar properties from the spatial or topological arrangements of the materials in repetitious patterns. This way the metamaterials influence the manipulation of the electromagnetic or acoustic waves which are otherwise impossible in conventional bulk materials [177,178]. Of particular importance are metamaterials which possess negative index of refraction for specific wavelengths (e.g. gold and silver at shorter wavelengths). These are termed as negative index metamaterials (NIMs), left-handed metamaterials (LHMs), and double-negative metamaterials (DNGs). In these materials, both the permittivity (ε) and the permeability (μ) are negative for which the index of refraction turns out to be negative. Due to this reason, in NIMs a backward wave is generated. It is worth mentioning here that the metamaterials were first termed as LHMs in the pioneering work by Victor Veselago [179] since the electric field, magnetic field and the wave vector form a left-handed triplet. It was theoretically argued that the phase velocity could be made anti-parallel to the Pointing vector. Insofar the practical realization of the NIMs was concerned, it was Sir John Pendry who was the first to propose the idea of constructing a LHMs in an array of wires and rings [180,181]. Subsequently, Shelby et al. [182] demonstrated the experimental realization of the much

speculated negative refraction in a split ring resonators and thin wires system at microwave frequency.

This was followed by other experimental reports of negative index metamaterials [177,183-185]. It is worthwhile to note that optical metamaterials with negative refractive index, known as optical negative index metamaterials (NIM), when demonstrated created quite a promise owing to its various potential future applications [186,187]. It is speculated that metamaterials with negative refraction may lead to the development of a superlens capable of beating the so called diffraction limit, thereby enabling imaging objects and fine structures that are much smaller than the wavelength of light. Also, it may take us into a new domain of exploration and thus promise to create entirely new prospects for manipulating light, with revolutionary impacts on present-day optical technologies [186]. However, soon it turns out that loss inherent in optical NIMs stand as the biggest restriction even to attempt to realize the aforementioned possible applications since most NIMs depend upon the resonant meta-atoms that suffer high losses. In recent years research in optical negative index metamaterials is primarily directed towards resolving this issue. Shalaev and his collaborators experimentally demonstrated that the incorporation of gain material in the high-local-field areas of a metamaterial makes it possible to fabricate an extremely low-loss and active optical NIM [188]. Another idea to compensate losses in NIMs is through by the so-called optical parametric amplification [189]. It is to be noted that the technique of transformation optics based on the foundations of Maxwell's equations is pivotal in designing and structuring the metamaterials [190-194]. On the other side, recently, parity-time symmetry is explored even in the context of optical metamaterials [17, 20]. H. Alaeain et al. [17] have studied the parity-time-symmetric three dimensional metamaterials system made of plasmonic waveguides. In an attempt to compensate for the propagation and the coupling losses the plasmonic modes of the system were subjected to the parity-time (PT)-symmetric potentials. The study reveals the intriguing properties such as Bloch power oscillation, double negative refraction, and unidirectional invisibility. In another experimental demonstration, L. Feng et al. [20] showed that the electromagnetic reflection could be significantly reduced unidirectionally at the optical frequency in a parity-time metamaterial

near to the exceptional point. These studies show that PT-symmetry ideas can be exploited in metamaterials for practical applications in the wavelength and the subwavelength domains paving the way for novel class of synthetic materials. It is interesting to note that recently N. Engheta et al. have even extended the transformation optics paradigm to deal with electromagnetic metamaterials characterized by balanced loss and gain with parity-time symmetry [195, 196].

In this work, we report our study on a parity-time (PT)-symmetric optical parametric amplifier. We have already discussed earlier that *PT* symmetry allows a controlled interplay between gain and loss resulting in new ways of achieving optical behavior that is at present unattainable with standard arrangements. We propose that if the amplifier is operated above the so-called parity-time symmetric threshold it is possible to achieve significant enhancement in the signal strength. It should be noted that recently parametric amplification process is addressed in the context of parity-time anti-symmetry [197]. In our discussion, we will use the terms metamaterials and negative index materials (NIM) interchangeably.

6.2 Theoretical model

We consider a metamaterial waveguide doped with a $\chi^{(2)}$ material such that the signal experiences a negative refractive index while both the idler and the pump see positive refractive index. It is useful to recall that in an optical parametric amplification (OPA) process, strong pump frequency (ω_p) are down-converted into signal (ω_s) and idler (ω_i) via the relation: $\omega_p = \omega_s + \omega_i$ [198]. The spatial evolution of the complex amplitudes, in the waveguide, of the pump (E_p), the signal (E_s), and the idler (E_i) along the z-direction, could be modeled by the following set of coupled equations [198]:

$$i\frac{dE_p}{dz} = -\kappa_p E_s E_i e^{-i\Delta kz} \tag{6.1}$$

$$i\frac{dE_s}{dz} = \kappa_s E_p E_i^* e^{i\Delta kz} \tag{6.2}$$

$$i\frac{dE_i}{dz} = -\kappa_i E_p E_s^* e^{i\Delta kz} \tag{6.3}$$

Here, $\kappa_j = \omega_j \chi^{(2)} \mu(\omega_j)/2c\mu_0 n_j$, with $j = p, s, i$ and $\Delta k = k_p - k_s - k_i$.

We assume that the pump is not getting depleted in the parametric amplification process, known as the undepleted pump approximation, i.e. E_p =constant [198]. Eq. (6.2) and (6.3) can be rewritten, with $E_\alpha = (\frac{\mu_\alpha}{\varepsilon_\alpha})^{1/4}\sqrt{\omega_\alpha} A_\alpha$, as follows:

$$i\frac{dA_s}{dz} = \kappa A_i^* e^{i\Delta kz} + ig_0 A_s \tag{6.4}$$

$$i\frac{dA_i^*}{dz} = \kappa A_s e^{-i\Delta kz} - ig_0 A_i^* \tag{6.5}$$

g_0 is the so-called loss/gain parameter. $\kappa = \left(\frac{\mu_s \mu_i}{\varepsilon_s \varepsilon_i}\right)^{\frac{1}{4}} \sqrt{\omega_s \omega_i} (\frac{E_p \chi^{(2)}}{2c\mu_0})$ is the coupling parameter. μ_s and μ_i are magnetic permeability of the signal and idler respectively while ε_s and ε_i are the corresponding electric permittivity. $\chi^{(2)}$ is the second order nonlinear susceptibility. Under the perfect phase-matched condition, i.e. $\Delta k = 0$, it is easy to see that the system is now described by the PT-symmetric Hamiltonian:

$$H = \begin{pmatrix} ig_0 & \kappa \\ \kappa & -ig_0 \end{pmatrix} \tag{6.6}$$

Here, the parity operator is given by $P = \begin{pmatrix} 0 & 1 \\ 1 & 0 \end{pmatrix}$. The Hamiltonian has eigenvalues $E = \pm\sqrt{\kappa^2 - {g_0}^2}$. Clearly, the PT-threshold of the system is given by $\kappa = \pm g_0$.

In passing, it is useful to comment on the optical parametric amplification due to third order nonlinear $\chi^{(3)}$ process in a negative index material. Let us consider the four-wave mixing process: $\omega_s + \omega_i = \omega_c + \omega_g$, in a metamaterial waveguide doped with $\chi^{(3)}$ material such that the signal frequency, ω_s, experiences negative refractive index, while all the other frequencies, say ω_i, ω_c and ω_g see positive refractive index. As discussed in Ref. [199] and assuming that the signal experiences amplification while the idler suffers equal amount of loss or attenuation, in a quantum controlled four-wave interaction process, it is possible to derive coupled differential equations exactly similar to the ones in Eqs. (6.4) and (6.5).

Hence the analysis carried out in this work may be applicable to an optical parametric amplification process, in a NIM, initiated by cubic nonlinearity also.

6.3 Results and discussions

We can solve Eqs. (6.4) and (6.5) analytically, subject to the following general boundary conditions: $A_s(z=L)=A_{SL}$ and $A_i(z=0)=A_{i0}$. Following a tedious but straightforward algebra, one can obtain the following solutions for the signal and the idler fields:

$$A_s(z)=\alpha\, exp\left[i\left(\gamma+\tfrac{\Delta k}{2}\right)z\right]+\beta exp\left[-i\left(\gamma-\tfrac{\Delta k}{2}\right)z\right] \tag{6.7a}$$

$$A_i^*(z)=p\alpha\, exp\left[i\left(\gamma-\tfrac{\Delta k}{2}\right)z\right]+q\beta exp\left[-i\left(\gamma+\tfrac{\Delta k}{2}\right)z\right] \tag{6.7b}$$

Here, $\gamma=\sqrt{\kappa^2-\gamma_0^2}$, $\gamma_0=g_0-i\frac{\Delta k}{2}$, $p=(\gamma+i\gamma_0)/\kappa$, $q=(-\gamma+i\gamma_0)/\kappa$,

$\alpha=r\left(qA_{SL}-A_{i0}^* exp\left[-i\left(\gamma-\frac{\Delta k}{2}\right)L\right]\right)$, $\beta=-r\left(pA_{SL}-A_{i0}^* exp\left[i\left(\gamma+\frac{\Delta k}{2}\right)L\right]\right)$, $r=\left(q\, exp\left[i\left(\gamma+\frac{\Delta k}{2}\right)L\right]-p exp\left[-i\left(\gamma-\frac{\Delta k}{2}\right)L\right]\right)^{-1}$.

To simplify our analysis, we assume that the input interface has zero idler fields, i.e. $A_i(z=0)=A_{i0}=0$. The amplification factor for the negative-index signal wave is defined as: $G_s(z)=|A_s(z)/A_s(z=L)|^2$. On the other hand, the conversion factor for the positive-index idler, generated owing to difference frequency generation, is given by: $C_I(z)=|A_i^*(z)/A_s(z=L)|^2$. Let us first consider the parametric amplification process for the system described by the PT symmetric Hamiltonian, i.e. for the case $\Delta k=0$. In Figs. 6.1-6.3 we depict the amplification factor for the signal wave and the conversion factor for the idler wave in all the three parity-time symmetric regimes, namely, below the PT-threshold, at the PT-threshold and above the PT-threshold. The corresponding field profiles for both the signal and the idler are also depicted. We have assumed, for our numerical simulation, a temporal Gaussian field profile for the signal at $z=L$, defined as $A_s(z=L)=exp(-t^2/2T_0^2)$ where T_0 is the pulse width. In plotting the field profiles, we define normalized time as $\tau=t/T_0$.

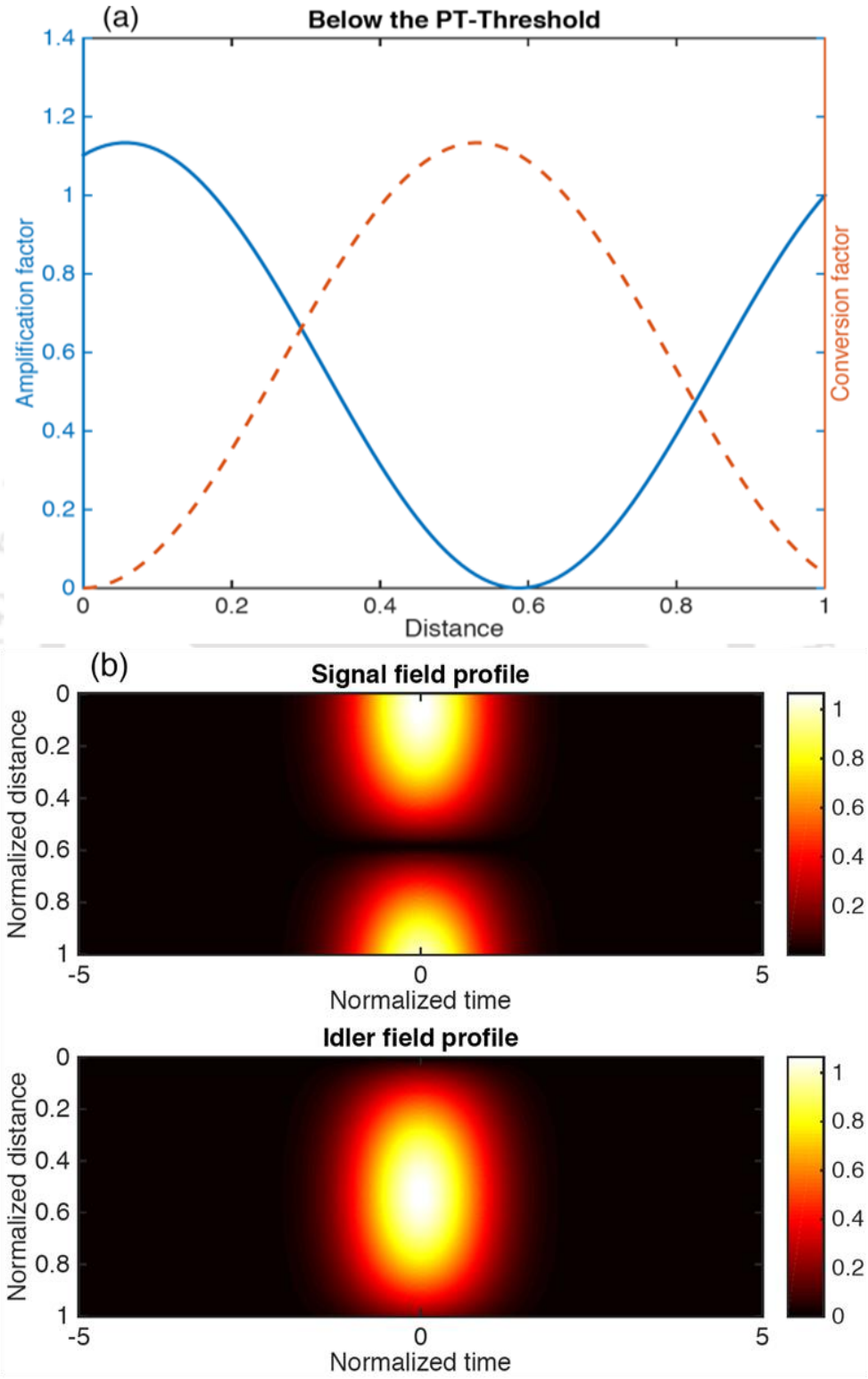

Figure 6.1: (a) Spatial profile of the amplification factor of the signal and conversion factor of the idler field with $\kappa = 3.0$ and $g_0 = 1.0$. (b) Corresponding field profiles of the signal and idler wave.

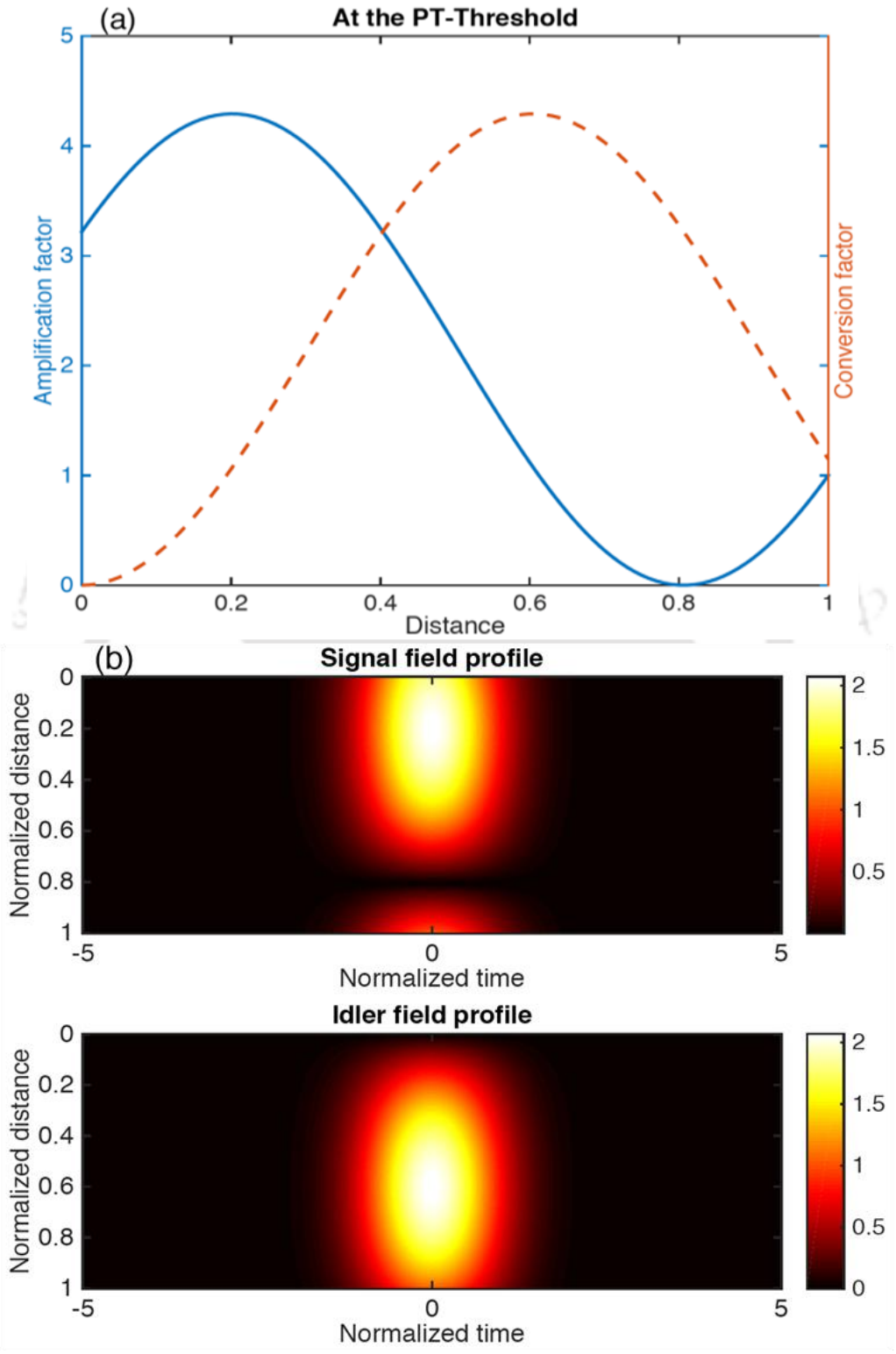

Figure 6.2: (a) Spatial profile of the amplification factor of the signal and conversion factor of the idler field with $\kappa = 3.0$ and $g_0 = 3.0$. (b) Corresponding field profiles of the signal and idler wave.

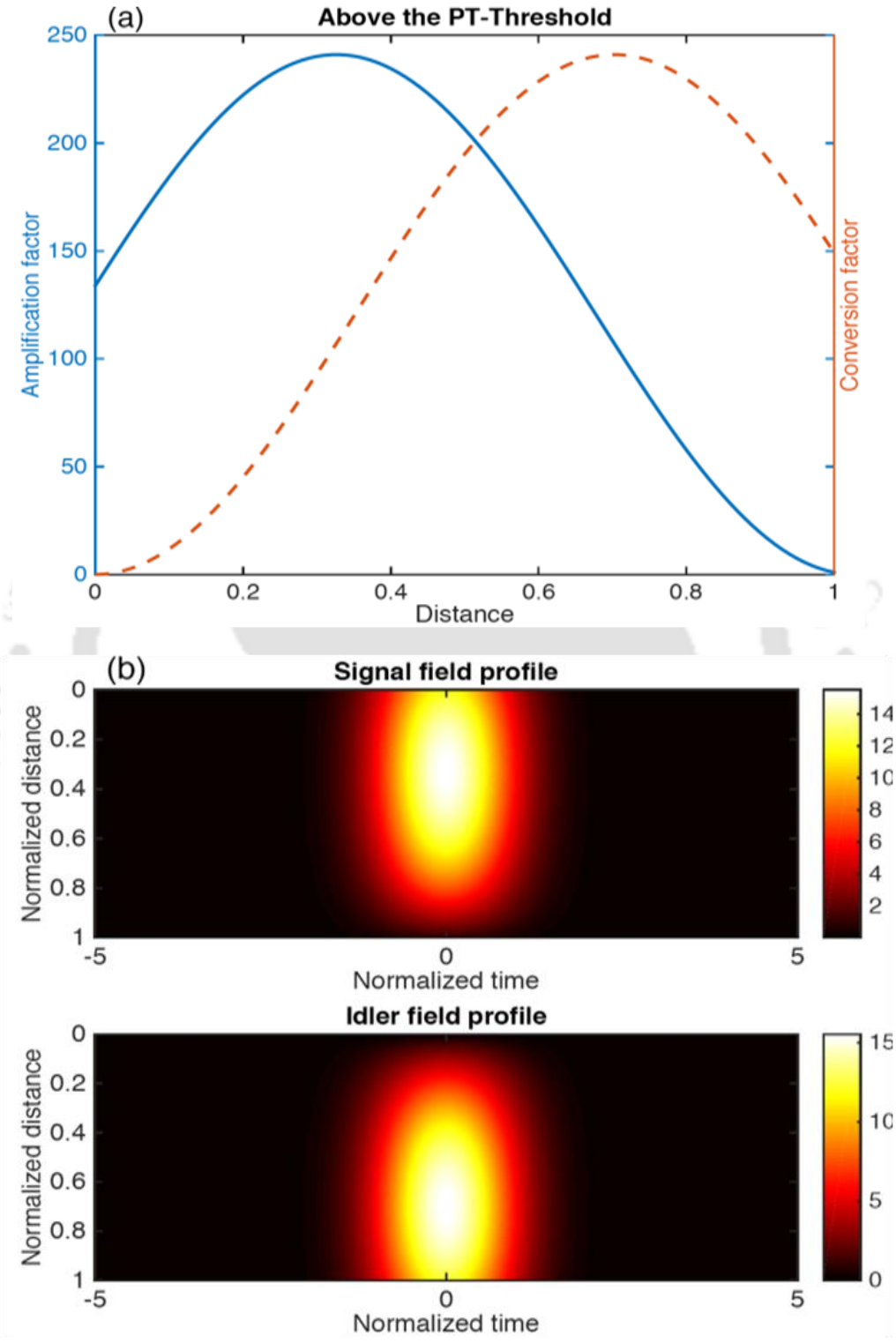

Figure 6.3: (a) Spatial profile of the amplification factor of the signal and conversion factor of the idler field with $\kappa = 3.0$ and $g_0 = 4.0$. (b) Corresponding field profiles of the signal and idler wave.

It must be noted that the signal and the idler are travelling in opposite directions and their behavior is governed by the boundary conditions on the opposite sides of the nonlinear negative index material. We observe that the signal and the idler exhibit oscillatory behavior. When operated below the PT-symmetric threshold, the signal gets amplified slightly at the left end of the metamaterial. As we approach the threshold, the amplification gets enhanced more than three times. However, significant enhancement is obtained when one operates above the PT-symmetric threshold. And this can be considered as a very useful result if one aims at compensating losses in an optical metamaterials. The corresponding field profiles obtained from numerical simulation supports this claim.

In a real experimental scenario, one may not be able to achieve the exact phase-matched condition $\Delta k = 0$. This is also the condition for the Hamiltonian describing the system to be PT-symmetric. Hence, it is important to check the robustness of this behavior if one deviates slightly from the phase-matched condition. In order to investigate the robustness of the amplification and the conversion factor of the signal and the idler respectively, in Fig. 6.4, we plot the contour plot of these quantities with slight variation in the phase-mismatch parameter.

We observe from Fig. 6.4 that if we deviate from the phase-matched condition by 2% or so, we will still be able to have significant enhancement in the signal strength. Thus, the issue of parity-time (PT) symmetry could certainly be exploited to compensate losses in an optical metamaterial. As we have mentioned earlier, similar conclusions could also be arrived at if one exploits $\chi^{(3)}$ nonlinearity.

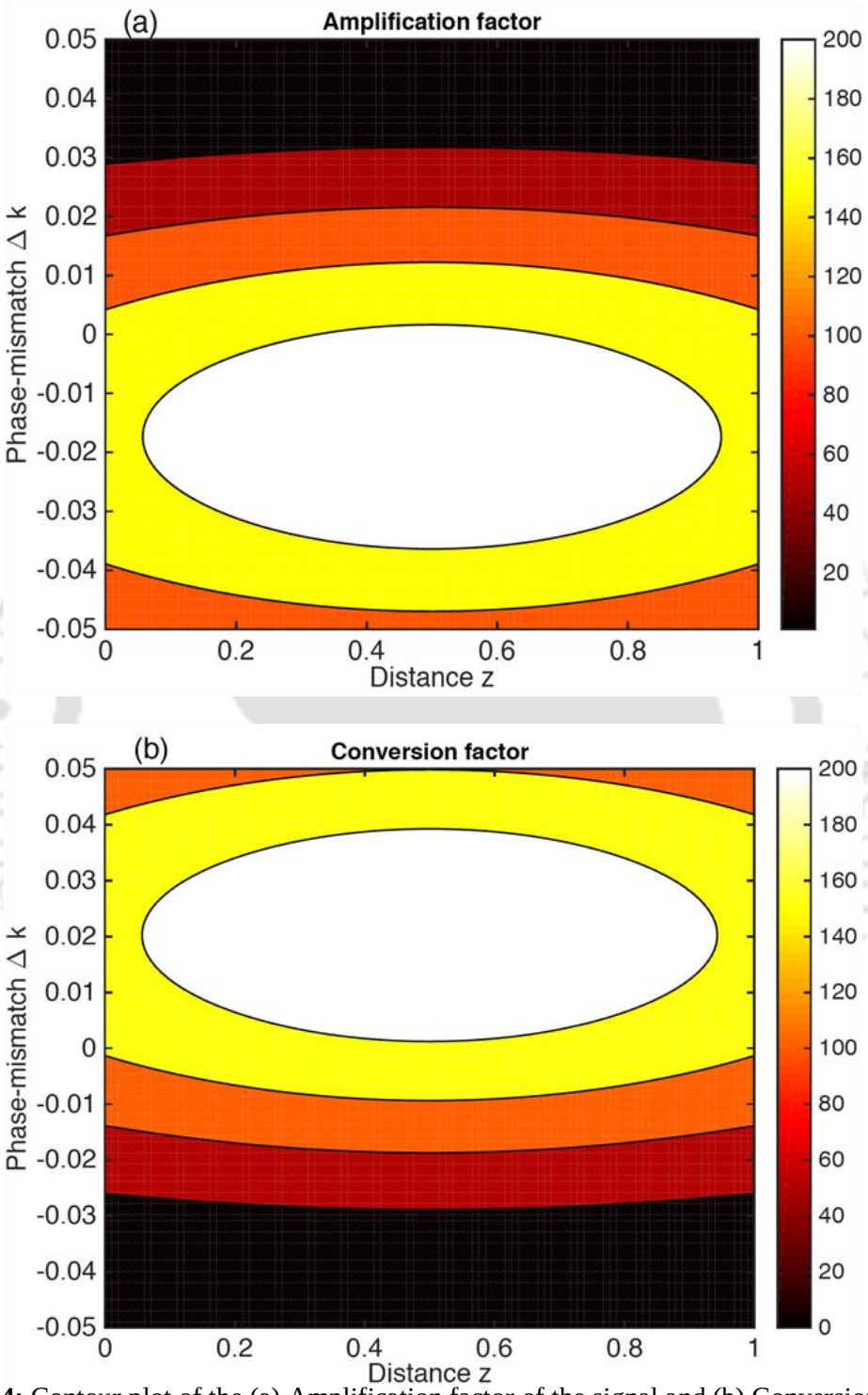

Figure 6.4: Contour plot of the (a) Amplification factor of the signal and (b) Conversion factor of the idler field as a function of distance, z, and phase-mismatch parameter, $\Delta\kappa$, with $\kappa = 3.0$ and $g_0 = 4.0$.

6.4 Summary of the Chapter

To conclude, we have studied optical parametric amplification in parity-time symmetric negative refractive index metamaterials with $\chi^{(2)}$ nonlinearity. The system exhibits *PT*-symmetry in the phase-matched condition. OPA is studied in all the three parity-time (PT)-symmetric regimes, namely below the *PT*-threshold, at the *PT*-threshold and above the *PT*-threshold. It is shown that the signal can be amplified hugely if the system is operated beyond the parity-time symmetric threshold. These observations are found to be in conformity with the field profiles of the signal and the idler found from numerical simulation. It is shown that even if one deviates from the exact phase-match condition, the amplification of the signal is pretty robust. It is anticipated that similar conclusions can be drawn for a negative index material doped with cubic nonlinearity.

भारतीय प्रौद्योगिकी संस्थान गुवाहाटी
Indian Institute of Technology Guwahati

Chapter 7

Summary and the Future directions of Research

7.1 Summary of the Thesis

This thesis work has explored the idea of parity-time-symmetry in different types of optical structures and systems in the context of nonlinear optics. These include coupled waveguide arrays in the quadrimer configurations, nonlinear Bragg structure, ring-resonator systems, nonlocal Schrödinger system and the negative-index metamaterials in parametric amplifier settings. Our studies on the quadrimer configurations investigate upon the effects of the nonlinearity and the dispersions on the PT-phase transition. It is shown that the nonlinearity changes the PT-phase transition threshold point towards a lower value. On the other hand, depending on the nature of dispersion (i.e. normal or anomalous) on various sites of the quadrimer system, the system may or may not exhibit PT-symmetry. The combined effect of nonlinearity and anomalous dispersion may result in stable soliton propagation in the system. In another nonlinear quadrimer configuration, with a different coupling scheme, we have addressed the issue of parity-time symmetry from attractor perspective. It is concluded that the power saturation behaviors of the system could be attributed to the presence of attractor. Next, we have found the analytical traveling solitary wave solutions for the forward and the backward waves in a nonlinear PT-symmetric Bragg grating structure. We observe that there is an infinite number of traveling wave solutions, either solitary or cnoidal-type, depending on the parameter values of the system. The effects of the coupling constant, gain/loss parameter and the traveling wave speed on the evolution dynamics of the solutions have been discussed. It predicts the existence of bright solitary wave solution below the PT-threshold for forward wave and dark solitary wave solution above the PT-threshold for backward wave. In a definite parametric regime, the existence of optical rogue waves has been elucidated. It turns out that the evolutions of the forward and the backward waves crucially depend on the

different system parameters such as: traveling wave speed and loss/gain parameter. It is worth mentioning here that the theoretical set-up under consideration can yield, apart from ORWs, various kinds of nonlinear traveling wave solutions based on the parameter values of the system. So, in that regard, this work could a step forward to the future investigations in the similar systems. In another work, in the continuous *PTNLSE* model, taking the general solitons on the finite background ansatz as the initial excitation, a numerical study has been carried out with special emphasis given to the Peregrine Soliton dynamics. Due to prototypical analogy between the Peregrine solitons and the rogue waves, we numerically confirm that an initial PS excitation could yield Peregrine rogue wave in the broken PT-phase. Upon numerical computation, we observe the appearance of low-intense *Kuznetsov-Ma* (*KM*) soliton trains in the absence of transverse shift and well-localized high-intense Peregrine Rogue waves in the presence of transverse shift in a specific parametric regime. In the earlier case, the PT-symmetry is unbroken, whereas in the later case the PT-symmetry is broken. Fundamentally this work may boost further investigation of optical rogue waves and its dynamics in the context of nonlocal nonlinear systems that may be more useful if such nonlinearity can be found testable in real physical settings. In the single ring resonator system, we find that simple alterations in the parity-time (PT) symmetric synthetic coupler structures could result in a dynamically controllable algorithm for the chaotic dynamics inherent in the system. We have also shown the dependence of the period doubling point upon the input amplitude, emphasizing on the dynamical aspects. Moreover, the fact that the resonator essentially plays the role of a damped and driven harmonic oscillator has been elucidated with the non-zero intensity inside the resonator due to constant influx of input light. Finally, a theoretical study has been performed in order to explore the parity-time (PT)-symmetry in optical negative-index materials with parametric amplifier settings. In this study we have exploited the notion of parity-time (PT)-symmetry in order to address the issue of optical loss, which stands as a hindrance in realizing such materials for practical applications. It has been found that the strength of the signal can be significantly enhanced if the system is operated beyond the PT-threshold point. It is shown that the aforementioned behavior is robust against small deviation from the exact phase-matching condition or the PT-symmetry.

7.2 Future aspects

Research activities in Physics, involving the idea of non-Hermitian Hamiltonians and parity-time (PT)-symmetry are growing at a tremendous rate with experimental verifications of earlier theoretical predictions. PT-Symmetry is now explored in optics, condensed matter physics, quantum field theory and quantum mechanics. More interestingly, it is finding its new cross-disciplinary ramifications. To mention a few among them: the eigen-spectra and the localization properties of the non-Hermitian random matrices occurring in the sparse neural networks [200], antigen-antibody systems where it was theoretically proposed that small injection of a second antigen can even cure the serious disease in the broken PT-phase [201]. In optics PT-Symmetry has witnessed a large spectrum of physical systems, models and settings in which this novel idea has been theoretically predicted, experimentally realized and technologically applied. This way we can say that an integrated scientific pursuit involving this idea can always be of fundamental and applied importance. The vast range of systems and models considered in this thesis are liable to yielding more potential aspects worth studying in future.

For example, the studies devoted to the quadrimer systems can be further extended to the more sophisticated systems and lattice models where these configurations can act as basic building blocks. In similar tune with the study carried out in the Bragg structure, efforts may be employed to search for more general solutions for different types of nonlinear waves. Especially, the rogue wave aspect can be studied more rigorously. Such extreme phenomena may be studied in the coupled waveguide arrays also. The nonlocal Schrödinger system can be revisited to look into further exotic complex dynamical aspects, one of them could well be the interaction of first and higher order Peregrine solitons. Another, important search may be to look for real physical systems where PT-symmetry with nonlocal nonlinearity could be realized. It has been suggested that it might be realized in some nonlinear frequency mixing processes [119].

Our work on the nonlinear single ring resonator system can further be taken up for even more structural complexity and more importantly where the connection can be made between the

dynamics of the system and the PT symmetry. In this connection, on theoretical front, a more rigorous Hamiltonian optics formalism [202] may be adopted to extract useful physical information. Finally, our efforts in looking for compensating the optical losses in the negative-index media with PT-symmetric parametric amplifier settings can be studied more extensively. Also the evolution dynamics of the solitary waves and the modulation instability can be investigated in characterizing the solutions in different parametric regimes. On a different note, it is worth mentioning that the future directions of research involving the idea of parity-time (PT)-symmetry may well include exploring PT-symmetry in the coherent atomic medium [203-205], whispering-gallery mode resonators [206,207], metamaterials [17] and the manipulation of light in PT-symmetric optical potentials [59,208-210]. These issues have not been addressed in this thesis work. But these topics of research encompass a variety of physical behaviors and have tremendous fundamental and technological significance.

Appendices

Appendix A

It contains the proof of the PT-symmetry of the Hamiltonian as in Eq. (2.2) in Chapter 2.

The Hamiltonian and the parity operator for the system are as under:

$$H = \begin{bmatrix} ig & -k & -\gamma & -\beta \\ -k & -ig & -\delta & -\eta \\ -\gamma & -\delta & ig & -\alpha \\ -\beta & -\eta & -\alpha & -ig \end{bmatrix}, \; P = \begin{bmatrix} 0 & 0 & 0 & 1 \\ 0 & 0 & 1 & 0 \\ 0 & 1 & 0 & 0 \\ 1 & 0 & 0 & 0 \end{bmatrix} \tag{A.1}$$

This Hamiltonian is PT-symmetric if it commutes with the PT operator, i.e.

$$[H, PT] = 0 \tag{A.2}$$

Let us choose an arbitrary four-component state vector as:

$$X = \begin{bmatrix} x_1 \\ x_2 \\ x_3 \\ x_4 \end{bmatrix} \tag{A.3}$$

So, calculating

$$PTX = \begin{bmatrix} 0 & 0 & 0 & 1 \\ 0 & 0 & 1 & 0 \\ 0 & 1 & 0 & 0 \\ 1 & 0 & 0 & 0 \end{bmatrix} \begin{bmatrix} x_1 \\ x_2 \\ x_3 \\ x_4 \end{bmatrix}^* = \begin{bmatrix} x_4^* \\ x_3^* \\ x_2^* \\ x_1^* \end{bmatrix} \text{ and } HPTX = \begin{bmatrix} igx_4^* - kx_3^* - \gamma x_2^* - \beta x_1^* \\ -kx_4^* - igx_3^* - \delta x_2^* - \eta x_1^* \\ -\gamma x_4^* - \delta x_3^* + igx_2^* - \alpha x_1^* \\ -\beta x_4^* - \eta x_3^* - \alpha x_2^* - igx_1^* \end{bmatrix} \tag{A.4}$$

$$\text{Similarly one can calculate, } PTHX = \begin{bmatrix} -\beta x_1^* - \eta x_2^* - \alpha x_3^* + igx_4^* \\ -\gamma x_1^* - \delta x_2^* - igx_3^* - \alpha x_4^* \\ -kx_1^* + igx_2^* - \delta x_3^* - \eta x_4^* \\ -igx_1^* - kx_2^* - \gamma x_3^* - \beta x_4^* \end{bmatrix} \tag{A.5}$$

Therefore, from A.4 and A.5 we can have in order to have [H, PT] = 0, the following condition to be satisfied:

$$k = \alpha\ , \gamma = \eta \tag{A.6}$$

Appendix B

It contains the calculation for supermodes for Eqs. (2.4) and Eqs. (2.5) in Chapter 2.

Now we ignore the coupling between specific waveguides so that $\beta = \delta = 0$.

Now our Hamiltonian is:

$$H = \begin{bmatrix} ig & -k & -\gamma & 0 \\ -k & -ig & 0 & -\eta \\ -\gamma & 0 & ig & -\alpha \\ 0 & -\eta & -\alpha & -ig \end{bmatrix} \tag{B.1}$$

The eigenvalues of this Hamiltonian are as under:

$$\lambda = \pm\gamma \pm \sqrt{k^2 - g^2} \tag{B. 2}$$

Therefore,

$$\lambda_1 = \gamma + \sqrt{k^2 - g^2}, \lambda_2 = \gamma - \sqrt{k^2 - g^2},\ \lambda_3 = -\gamma + \sqrt{k^2 - g^2},\ \lambda_4 = -\gamma - \sqrt{k^2 - g^2} \tag{B. 3}$$

Below the threshold (when k > g), $\sin\theta = \frac{g}{k}$, therefore

$$\lambda_1 = \gamma + \sqrt{k^2 - g^2} = k\left(\frac{\gamma}{k} + \cos\theta\right) \tag{B. 4}$$

So, solving for the eigenfunction X_1corresponding to the eigenvalue $\lambda_1$by $HX_1 = \lambda_1 X_1$with $X_1 = \begin{bmatrix} x_1 \\ x_2 \\ x_3 \\ x_4 \end{bmatrix}$, we obtain the following set of four algebraic equations ($\varepsilon = \frac{\gamma}{k}$):

$$\left.\begin{aligned} x_1\left(\varepsilon + e^{-i\theta}\right) + x_2 + \varepsilon x_3 &= 0 \\ x_1 + x_2\left(\varepsilon + e^{i\theta}\right) + \varepsilon x_4 &= 0 \\ \varepsilon x_1 + x_3\left(\varepsilon + e^{-i\theta}\right) + x_4 &= 0 \\ \varepsilon x_2 + x_3 + x_4\left(\varepsilon + e^{i\theta}\right) &= 0 \end{aligned}\right\} \quad \text{(B.5)}$$

Now substituting x_3 from the fourth of Eqs. (B.5) to the first of Eqs. (B.5) we get

$$x_1\left(\varepsilon + e^{-i\theta}\right) + x_2 + \varepsilon\left(-\varepsilon x_2 - x_4\left(\varepsilon + e^{i\theta}\right)\right) = 0 \quad \text{(B.6)}$$

Now substituting x_4 in Eq. (B.6) from the second of Eqs. (B.5) we get

$$x_1\left(\varepsilon + e^{-i\theta}\right) + x_2(1 - \varepsilon^2) + \left(\varepsilon + e^{i\theta}\right)\left(x_1 + x_2\left(\varepsilon + e^{i\theta}\right)\right) = 0 \quad \text{(B.7)}$$

Which upon further simplification reads as

$$2x_1(\varepsilon + \cos\theta) + x_2 e^{i\theta}(e^{i\theta} + e^{-i\theta} + 2\varepsilon) = 0 \quad \text{(B.8)}$$

$$x_1 + x_2 e^{i\theta} = 0 \quad \text{(B.9)}$$

Similarly substituting x_4 from the third of Eqs. (B.5) to the second of Eqs. (B.5) we get

$$x_1 + x_2\left(\varepsilon + e^{i\theta}\right) + \varepsilon\left(-\varepsilon x_1 - x_3\left(\varepsilon + e^{-i\theta}\right)\right) = 0 \quad \text{(B.10)}$$

Now substituting x_3 in Eq. (B.10) from the first of Eqs. (B.5) we get

$$x_1(1 - \varepsilon^2) + x_2\left(\varepsilon + e^{i\theta}\right) + \left(\varepsilon + e^{-i\theta}\right)\left(x_2 + x_1\left(\varepsilon + e^{-i\theta}\right)\right) = 0 \quad \text{(B.11)}$$

Which upon further simplification gives

$$2x_2(\varepsilon + \cos\theta) + x_1 e^{-i\theta}(e^{i\theta} + e^{-i\theta} + 2\varepsilon) = 0 \quad \text{(B.12)}$$

$$x_2 + x_1 e^{-i\theta} = 0 \quad \text{(B.13)}$$

So, taking an arbitrary value for $x_2 = 1$

$$x_1 = -e^{-i\theta} \tag{B.14}$$

Now with these values of $x_1$and x_2 we can calculate the values of $x_3$and $x_4$from the first two equations of Eqs. (B.5):

$$x_3 = e^{i\theta} \text{ and } x_4 = -1 \tag{B.15}$$

Therefore, the supermode corresponding to the eigenvalue $\lambda_1$below the PT-threshold can be written as:

$$X_1 = \begin{bmatrix} -e^{i\theta} \\ 1 \\ e^{i\theta} \\ -1 \end{bmatrix} \tag{B.16}$$

Similarly, other supermodes below the PT-threshold case can be found as stated in Eq. 2.4.

For above the PT-threshold case (k < g), we need to take $\cosh\theta = \frac{g}{k}$ and following similar procedure as for the below threshold case we can derive the supermodes as stated in Eq. (2.5) as well.

Appendix C

This contains the derivation details of the Eq. (3.20) in Chapter 3.

The solution of the Eq. (3.17) is of the below form:

$$r(u) = \frac{c_2}{u^4} + \frac{\varepsilon\alpha\left(\frac{b_1 u^8}{8} + \frac{u^6 b_2}{6}\right)}{u^4} \tag{C.1}$$

Now we recall the relations as mentioned above the Eq. (3.17) in Chapter 3, $r(u) = \sqrt{E}$ and

$E = \frac{\left(u^2 - c_1 - \frac{u_z^2 \alpha}{\chi}\right)}{u^6}$, we get from Eq. (C.1)

$\frac{\left(u^2-c_1-\frac{u_z^2\alpha}{\chi}\right)}{u^6}=\left(\frac{c_2}{u^4}+\frac{\varepsilon\alpha\left(\frac{b_1u^8}{8}+\frac{u^6b_2}{6}\right)}{u^4}\right)^2$, which now can be simplified as:

$$u_z^2=(u^2+c_1)\left(\frac{\alpha}{\chi}\right)^2-\frac{\left(\left(c_2+\varepsilon\alpha\left(\frac{b_1u^8}{8}+\frac{u^6b_2}{6}\right)\right)\right)^2}{u^2}$$

$$=-\frac{c_2^2}{u^2}\frac{\chi}{\alpha}+\frac{(u^2+c_1)\chi^2}{\alpha^2}-\frac{2\varepsilon\alpha c_2\chi^2}{\alpha^2}\left(\frac{b_1u^6}{8}+\frac{b_2u^4}{6}\right)+\frac{b_1^2}{64\alpha^2}u^{14}\chi^2+\frac{b_1b_2u^{12}\chi^2}{24\alpha^2}+\frac{b_2^2u^{10}\chi^2}{36\alpha^2} \quad \text{(C.2)}$$

If we now take the transformation $u^2=w^{-1}$, taking derivative w.r.t. 'z' gives:

$$2uu_z=-w^{-2}w_z \text{ , or } u_z^2=\frac{w_z^2}{4w^3} \quad \text{(C.3)}$$

Eq. (C.2) and Eq. (C.3) gives the following equation:

$$w_z^2=\left(-4c_2^2w^4+4w^2+4c_1w^3-2\varepsilon\alpha c_2\left(\frac{b_1}{2}+\frac{2b_2}{3}w\right)+\frac{b_1^2}{16w^4}+\frac{b_1b_2}{6w^3}+\frac{b_2^2}{9w^2}\right)\left(\frac{\chi}{\alpha}\right)^2 \quad \text{(C.4)}$$

Under the condition of weak nonlinearity the last three terms can be neglected to yield:

$$w_z^2=\left(-4c_2^2w^4+4w^2+4c_1w^3-2\varepsilon\alpha c_2\left(\frac{b_1}{2}+\frac{2b_2}{3}w\right)\right)\left(\frac{\chi}{\alpha}\right)^2 \quad \text{(C.5)}$$

Now this Eq. (C.5) can be written as:

$$w_z^2=(w-w_1)(w-w_2)(w-w_3)(w-w_4) \quad \text{(C.6)}$$

Comparing Eq. (C.5) and Eq. (C.6) we can have four equations in terms of four unknown quantities:

$w_1+w_2+w_3+w_4=4c_1\left(\frac{\chi}{\alpha}\right)^2$, $w_1w_3+w_1w_4+w_2w_3+w_2w_4+w_3w_4+w_1w_2=-4\left(\frac{\chi}{\alpha}\right)^2$,

$w_1w_3w_4+w_2w_3w_4+w_1w_2w_3+w_1w_2w_4=-\frac{4\varepsilon\alpha c_1b_2}{3}\left(\frac{\chi}{\alpha}\right)^2$, $w_1w_1w_1w_1=\varepsilon c_1b_1\left(\frac{\chi}{\alpha}\right)^2$

Now let us define some transformations:

$X = \frac{w}{w_4}$ and $X_m = \frac{w_m}{w_4}, m = 1,2,3,4.$ (C.7)

So, $X_z^2 = \frac{w_z^2}{w_4^2}$, and the Eq. (C.6) becomes following Eq. (C.7) as under

$$X_z^2 = 2w_4^2(X - X_1)(X - X_2)(X - X_3)(X_4 - X) \quad \text{(C.8)}$$

$$X_z^2 = 2w_4^2(X - X_1)(X - X_2)(X - X_3)(1 - X) \quad \text{(C.9)}$$

Let, $X = 1 + (X_3 - 1)sin^2Y$ (C.10)

$$X_z = 2\sin Y \cos Y\,(X_3 - 1)Y_z \quad \text{(C.11)}$$

Using Eq. (C.10) and Eq. (C.11) into Eq. (C.8) we get after some simplifications

$$Y_z^2 = \frac{w_4^2(1-X_1)(1-X_2)}{2}\left[1 - \frac{(1-X_3)}{(1-X_1)}sin^2Y\right]\left[1 - \frac{(1-X_3)}{(1-X_2)}sin^2Y\right] \quad \text{(C.12)}$$

We define

$$k_1^2 = \frac{(1-X_3)}{(1-X_1)}, k_2^2 = \frac{(1-X_3)}{(1-X_2)}, l = \frac{w_4^2(1-X_1)(1-X_2)}{2} \quad \text{(C.13)}$$

$$Y_z^2 = l\,(1 - k_1^2\,sin^2Y)(1 - k_2^2\,sin^2Y)\text{ , or, } Y_z = \sqrt{l}\sqrt{(1 - k_1^2\,sin^2Y)}\sqrt{(1 - k_2^2\,sin^2Y)} \quad \text{(C.14)}$$

$$\sqrt{l}\,z = \int_0^Y \frac{ds}{\sqrt{(1-k_1^2\,sin^2s)}\sqrt{(1-k_2^2\,sin^2s)}} \quad \text{(C.15)}$$

Which for $X_1 = X_2 = 0$ (and so, $k_1^2 = k_2^2 = 1 - X_3 = k_0^2$), becomes:

$$\sqrt{l}\,z + C = \int_0^Y \frac{ds}{(1-k_0^2 sin^2 s)} = \frac{-tan^{-1}\left(2i\,(k_0^2-1)tan\,Y\right)/\sqrt{(k_0^2-1)}}{\sqrt{(k_0^2-1)}},$$ 'C' is an integration constant.

Which gives:

$$\tan Y = \frac{\left(\tan i\sqrt{(k_0^2-1)}\,(\sqrt{l}z+C)\right)}{\sqrt{(k_0^2-1)}} \quad \text{(C.16)}$$

Now from Eq. (C.10) and Eq. (C.16) and using the fact that $sin^2Y = \frac{tan^2Y}{1+tan^2Y}$ we get:

$$X = 1 + (X_3 - 1)sin^2Y = X = 1 + (X_3 - 1)\frac{tan^2Y}{1+tan^2Y}$$

Which using the transformation defined in Eq. (C.7) it becomes:

$$w = \frac{w_3\, tan^2\left(i\sqrt{(k_0^2-1)}\,(\sqrt{l}z+C)\right)+w_4}{(k_0^2-1)+tan^2\left(i\sqrt{(k_0^2-1)}\,(\sqrt{l}z+C)\right)} \tag{C.17}$$

Using the transformation as stated above the Eq. (C.3) $u^2 = w^{-1}$, and using relation mentioned in Eq. (3.8) of the Chapter 3 we obtain:

$$a_f^2 = (1+c_0)u^2 = \frac{(1+c_0)}{w} = (1+c_0)\frac{(k_0^2-1)+tan^2\left(i\sqrt{(k_0^2-1)}\,(\sqrt{l}z+C)\right)}{w_3\, tan^2\left(i\sqrt{(k_0^2-1)}\,(\sqrt{l}z+C)\right)+w_4}$$

$$a_f^2 = (1+c_0)\frac{\rho+tanh^2\left(\sqrt{\rho}\,(\sqrt{l}z+C)\right)}{w_3\, tanh^2\left(\sqrt{\rho}\,(\sqrt{l}z+C)\right)+w_4} = (1+c_0)\frac{\rho+tanh^2(Z)}{w_3\, tanh^2(Z)+w_4} \tag{C.18}$$

Where, $\sqrt{\rho}\,(\sqrt{l}z + C) = \rho.$ (C.19)

From Eq. (3.13) of Chapter 3 now a_b^2 can be calculated to be:

$$a_b^2 = (1-c_0)\left(\frac{k-g}{k+g}\right)\left(-c_1 + \frac{a_f^2}{1+c_0}\right)\frac{\rho+tanh^2(Z)}{w_3\, tanh^2(Z)+w_4} \tag{C.20}$$

Publications

A. Peer Reviewed Journals:

1. **Samit Kumar Gupta** and Amarendra K. Sarma, "Peregrine rogue wave dynamics in the nonlocal nonlinear Schrödinger system with parity-time (PT)-symmetric Kerr nonlinearity," ***Communications in Nonlinear Science and Numerical Simulations 36****, 141 (2016)* (Elsevier)
2. **Samit Kumar Gupta,** Jyoti P. Deka and Amarendra K. Sarma, "Nonlinear Parity-Time (PT)-symmetric closed-form optical quadrimer waveguides: Attractor perspective," ***European Physical Journal D 69****, 199 (2015)* (Springer)
3. **Samit Kumar Gupta** and Amarendra K. Sarma, "Solitary waves in Parity-time (PT) symmetric Bragg-grating structure and the existence of Optical Rogue Waves," ***Europhysics Letters 105****, 44001 (2014)* (IOP)
4. **Samit Kumar Gupta** and Amarendra K. Sarma, "Parity-time-symmetric closed form optical quadrimer waveguides," ***Journal of Modern Optics 61****, 227 (2014)*). (Taylor & Francis)
5. Jyoti P. Deka, **Samit Kumar Gupta** and Amarendra K. Sarma, "Controllable chaotic dynamics in a nonlinear fiber ring resonators with balanced gain and loss," ***Nonlinear Dynamics*** (Published online) DOI: 10.1007/S11071-016-3102-9 (2016) (Springer)
6. **Samit Kumar Gupta** and Amarendra K. Sarma, "Optical parametric amplification in parity-time symmetric negative index materials," ***under review***.

B. Peer Reviewed proceedings

1. **Samit Kumar Gupta** and Amarendra K. Sarma, "Parity-time symmetric closed-form quadrimer waveguides with focusing and defocusing nonlinearity," ***Proc. SPIE***, **9654**, p. 96541Y-1 (2015)

2. **Samit Kumar Gupta** and Amarendra K. Sarma, "Periodic optical rogue waves in parity-time (PT) symmetric Bragg-grating structure," ***AIP Conference Proceedings***, Vol. **1620**, p. 452 (2014).

C. Conference presentations

1. **Samit Kumar Gupta** and Amarendra K. Sarma, "PT-symmetric three coupled waveguides system," XXXVII *National Symposium of Optical Society of India, OSI 2013*, 23-25 Jan. 2013, Pondicherry University, India. (***S.K. Gupta got the best presentation award for this work***)
2. **Samit Kumar Gupta** and Amarendra K. Sarma, "PT-symmetric quadrimer: closed-form structure," *National Focused discussion meeting on Metamaterials and Photonic Nano-structures*, 16-17 August 2013, IIT Kanpur.
3. **Samit Kumar Gupta** and Amarendra K. Sarma, "Coherent population transfer in a parity-time (PT)-symmetric two-level atomic system with Gaussian pulses," International Conference on Optics and Opto-electronics (*ICOL-2014*), 05-08 March, 2014, IRDE Dehradun.
4. **Samit Kumar Gupta** and Amarendra K. Sarma, "Periodic optical rogue waves (PORWs) in parity-time (PT)-symmetric Bragg grating structure," International Conference on Light (*OPTICS-2014*), 19-21 March 2014, NIT Calicut (***S. K. Gupta got the Best Paper Award for this work***).
5. **Samit Kumar Gupta** and Amarendra K. Sarma, "Parity-time (PT)-symmetric closed-form quadrimer waveguides with focusing and defocusing nonlinearity", International Conference on Optics and Photonics (*ICOP-2015*)," 20-22 February, 2015, the University of Calcutta. (***S.K. Gupta got the OSA best student poster award for this work*).**
6. **Samit Kumar Gupta** and Amarendra K. Sarma, "Exploring Parity-time (PT)-symmetric closed-form quadrimer waveguides (N-type) in nonlinear regime," Second National Symposium on Nonlinear and Complex Phenomena (*NSNCP-2015*), 26-28 March 2015, IASST Guwahati, Gauhati University, organized by IASST Guwahati and CPP-IPR Sonapur.

7. **Samit Kumar Gupta** and Amarendra K. Sarma, "Peregrine Rogue Wave dynamics in the continuous nonlinear Schrödinger system with parity-time (PT)-symmetric Kerr nonlinearity," South Asian Workshop on Optics and Photonics *SAWOP-2015*, UNESCO New Delhi Office Celebration, 17-18 November 2015, organized by Dept. of Physics, IIT Guwahati.

8. **Samit Kumar Gupta** and Amarendra K. Sarma, "Dynamics of interactions of two Peregrine solitons in the continuous Schrödinger system with parity-time (PT)-symmetric nonlinearity," Progress in Quantum Physics with Non-Hermitian Operators (PHHQP16), 08-12 August 2016, Yukawa Institute for Theoretical Physics, Kyoto University, Japan.

भारतीय प्रौद्योगिकी संस्थान गुवाहाटी
Indian Institute of Technology Guwahati

Vita

The author, Mr. Samit Kumar Gupta was born on the 9th January, 1989 at *Sriniketan*, in the state of West Bengal, India. He did his Bachelor of Science (B. Sc.) with Physics as major and Mathematics and Chemistry as the subsidiary subjects in 2009 and Master of Science (M. Sc.) in Physics in 2011 from *Siksha Bhavana* (Institute of Science), *Visva-Bharati*, *Santiniketan*. He joined the Department of Physics, Indian Institute of Technology Guwahati in 2011 as the as a regular Ph.D. student. He was awarded the Junior Research Fellowship in 2011 and Senior Research Fellowship in 2013 by the Ministry of Human Resource and Development, Government of India.

Bibliography

[1] http://pirsa.org/10110055.

[2] D. Bessis (private communication). This problem was the result of discussions between D. Bessis and J. Zinn-Justin.

[3] C. M. Bender, Contemporary Physics **46**, 277 (2005).

[4] R. Brower, M. Furman, and M. Moshe, Phys. Lett. B **76**, 213 (1978); B. Harms, S. Jones, and C. –I. Tan, Nucl. Phys. 171, 392 (1990); Phys. Lett. B **91**, 291 (1980).

[5] E. Caliceti, S. Graffi, and M. Maioli, Comm. Math. Phys. **75**, 51 (1980).

[6] C. M. Bender and S. Boettcher, Phys. Rev. Lett. **80**, 5243 (1998).

[7] C. M. Bender, K. A. Milton, S. S. Pinsky, et al., J. Math. Phys. **30**, 1447 (1989).

[8] C. M. Bender, S. Boettcher, and P. N. Meisinger, J. Math. Phys. **40**, 2201 (1999).

[9] C. M. Bender, D. C. Brody, and H. F. Jones, Phys. Rev. Lett. **89**, 270401 (2002).

[10] C. M. Bender, Rep. Prog. Phys. **70**, 947 (2007).

[11] A. Mostafazadeh, J. Phys. A. **36**, 7081 (2003).

[12] C. M. Bender, D. C. Brody, and H. F. Jones, Phys. Rev. D **70**, 025001 (2004).

[13] A. Guo, G. J. Salamo, D. Duchesne, R. Morandotti, M. Volatier-Ravat, V. Aimez, G. A. Siviloglou, D. N. Christodoulides, Phys. Rev. Lett. **103**, 093902 (2009).

[14] Y. Goldsheid, Y. and B. A. Khoruzhenko, Phys. Rev. Lett. **80**, 2897 (1998).

[15] I. Rotter, J. Phys. A 42, 1_**51** (2009).

[16] Dembowski, C. et al., Phys. Rev. Lett. **90**, 034101 (2003).

[17] H. Alaeian and J. A. Dionne, Phys. Rev. A **89**, 033829 (2014).

[18] C. E. Rüter, K.G. Makris, R. El-Ganainy, D. N. Christodoulides, M. Segev, D. Kip, Nat. Phys. **6**, 192 (2010).

[19] A. Regensburger, C. Bersch, M. -A. Miri, G. Onischukov, D. N. Christodoulides, U. Peschel, Nature **488**, 167 (2012).

[20] L. Feng, Y. -L. Xu, W. S. Fegadolli, M. -H. Lu, J. E. B. Oliveira, V. R. Almeida, Y. -F. Chen, A. Scherer, Nature Mater. **12**, 108 (2013).

[21] J. Schindler, A. Li, M. C. Zheng, F. M. Ellis, T. Kottos, Phys. Rev. A 84, 040101 (R) (2011).

[22] N. Bender et al., Phys. Rev. Lett. **110**, 234101 (2013).

[23] S. Bitner, B. Dietz, U. Günther, H. L. Harney, M. Miski-Oglu, A. Richter, F. Schäfer, Phys. Rev. Lett. **108**, 024101 (2012).

[24] N. M. Chtchelkatchev et al., Phys. Rev. Lett. **109**, 150405 (2012).

[25] A. Ruschhaupt, F. Delgado, J. G. Muga, J. Phys. A **38**, L171 (2005).

[26] C. Thompson, Y. N. Joglekar and G. Vemuri, Phys. Rev. A **43**, 043822 (2012).

[27] Y. N. Joglekar, C. Thospson and G. Vemuri, Phys. Rev. A **83**, 063817 (2011).

[28] Y. N. Joglekar, C. Thospson, D. D. Scot and G. Vemuri, Eur. Phys. J. Appl. Phys. **63**, 30001 (2013).

[29] K. G. Makris, R. El-Ganainy, D. N. Christodoulides, and Z. H. Musslimani, Phys. Rev. Lett. **100**, 103904 (2008).

[30] Z. Lin, H. Ramayana, T. Eichelkraut, T. Kottos, H. Cao, and D. N. Christodoulides, Phys. Rev. Lett. **106**, 213901(2011).

[31] M. A. Miri, P. LiKam Wa, and D. N. Christodoulides, Opt. Lett. **37**, 764(2012).

[32] Y. D. Chong, L. Ge and A. D. Stone, Phys. Rev. Lett. **106**, 093902 (2011).

[33] S. Longhi, Phys. Rev. A **82**, 031801 (2010).

[34] M. Liertzer, L. Ge, A. Cerjan, A.D. Stone, H.E. Tureci and S. Rotter, Phys. Rev. Lett. **108**, 173901(2012).

[35] Z. H. Musslimani, K. G. Makris, R. El-Ganainy, and D. N. Christodoulides, Phys. Rev. Lett. **100**, 030402 (2008).

[36] Yu. V. Bludov, V.V. Konotop and B. A. Malomed, Phys. Rev. A **87**, 013816(2013).

[37] S. V. Suchkov, B. A. Malomed, S. V. Dmitriev and Y. S. Kivshar, Phys. Rev. E **84**, 046609 (2011).

[38] M. A. Miri, A. B. Aceves, T. Kottos, V. Kovanis, and D. N. Christodoulides, Phys. Rev. A **86**, 033801(2012).

[39] J. D. Jackson, *Classical Electrodynamics*, Third Edn. (Wiley, California, 1998).

[40] C.M. Bender, B.K. Bertson, D. Parker and E. Samuel. Am. J. Phys. **81**,173 (2013).

[41] K. Li and P. G. Kevrekidis, Phys. Rev. E **83**, 066608 (2011).

[42] M. Duanmu, K. Li, R. L. Horne, P. G. Kevrekidis and N. Whitaker, Phil. Trans. Roy. Soc. A **371**, 20120171 (2013).

[43] K. Li, P. G. Kevrekidis, D. J. Frantzeskakis, C. E. Ruter and D. Kip, J. Phys. A **46**, 375304 (2013).

[44] J. D'Ambroise, P. G. Kevrekidis, and B. A. Malomed, Phys. Rev. E **91**, 033207 (2015).

[45] W. Walasik and N. M. Litchinister, Sci. Rep. **6**, 19826 (2016).

[46] F. Battelli, J. Diblik, M. Fečkan, J. Picton, M. Pospíšil, H. Susanto, Nonlin. Dyn. **81**, 353 (2015).

[47] S. Suchkov, B. A. Malomed, S. V. Dmitriev, and Y. S. Kivshar, Phys. Rev. E **84**, 046609 (2011).

[48] V.V. Konotop, D.D. Pelinovsky and D.A. Zezyulin, Europhys. Lett. **100**, 56006 (2012).

[49] K. Li, P. G. Kevrekidis, B. A. Malomed and U. Günther, J. Phys. A **45**, 444021 (2012).

[50] D.A. Zezyulin and V.V. Konotop, Phys. Rev. Lett. **108**, 213906 (2012).

[51] K. Li , D.A. Zezyulin, V.V. Konotop and P. G. Kevrekidis, Phys. Rev. A **87**, 033812(2013).

[52] I.V. Barashenkov, L. Baker and N. V. Alexeeva, Phys. Rev. A **87**, 033819 (2013).

[53] Y. Lumer, Y. Plotnik, M. C. Rechtsman, M. Segev, Phys. Rev. Lett.**111**, 263901 (2013).

[54] S. Longhi, Ann. Phys. **360**, 150 (2015).

[55] H. Ramezani, T. Kottos, E. El-Ganainy, D. N. Christodoulides, Phys. Rev. A **82**, 043803 (2010).

[56] P. G. Kevrekidis, D. E. Pelinovsky, D. Y. Tyugin, J. Phys. A **46**, 365201 (2013).

[57] I. V. Barashenkov, G. S. Jackson, S. Flach, Phys. Rev. A **88**, 053817 (2013).

[58] J. Auslander, N. P. Bhatia, P. Seibert, Bol. Soc. Mat. Mex. **9**, 55 (1964); J. Milnor, Comm. Math. Phys. 99, 177 (1985a); J. Milnor, Comm. Math. Phys. **102**, 517 (1985b); D. Ruelle, F. Takens, Comm. Math. Phys. **20**, 167 (1971).

[59] K. G. Makris, R. El-Ganainy, D. N. Christodoulides, and Z. H. Musslimani, Int. J. Theor. Phys. **50**, (2011) 1019.

[60] A. Guo, G. J. Salamo, D. Duchesne, R. Morandotti, M. Volatier-Ravat, V. Aimez, G. A. Siviloglou and D. N. Christodoulides, Phys. Rev. Lett. **103**, 093902 (2009).

[61] C. M. Bender, B. K. Berntson, D. Parker and E. Samuel, Am. J. Phys. **81**, 173 (2013).

[62] G. P. Agrawal, *Nonlinear Fiber Optics*, 4th Edn. (Academic Press, San Diego, 2007).

[63] F. Nazari, M. Nazari and M. K. Moravvej-Farshi, Opt. Lett. **36**, (2011) 4368.

[64] G. P. Agrawal, *Applications of Nonlinear Fiber Optics*, 2nd Edn. (Academic Press, San Diego, 2007).

[65] R. Driben and B. A. Malomed, Opt. Lett. **36**, 4323 (2011).

[66] H. Suchowski, Y. Silberberg and D. B. Uskov, Phys. Rev. A **84**, 013414 (2011).

[67] S. Longhi, Laser & Photon. Rev. **3**, 243 (2009).

[68] C. Hang, G. Huang and V. V. Konotop, Phys. Rev. Lett. **110**, 083604 (2013).

[69] P. Yeh, *Optical Waves in Layered Media* (Wiley, New York, 1984).

[70] K. O. Hill, Y. Fujii, D. C. John, and B. S. Kawasaki, Appl. Phys. Lett. **32**, 647 (1978).

[71] T. Erdogan, J. Lightwave Tech. J. **48**2, 909 (1969).

[72] A. Yariv and P. Yeh, *Optical Waves in Crystals* (Wiley, New York, 1984).

[73] L. Brillouin, *Wave propagation in periodic structures* (McGraw-Hill, New York, 1946); H. G. Kogelnik and C. V. Shank, J. Appl. Phys. **43**, 2327 (1972); A. Yariv and M. Nakamura, IEEE J. Quantum Electron. **13**, 233 (1977).

[74] Y. Silberberg and I. Bar-Joseph, Phys. Rev. Lett. **48**, 1541 (1982).

[75] H. G. Winful and G. D. Cooperman, Appl. Phys. Lett. **40**, 298 (1982); H. G. Winful, Appl. Phys. Lett. **46**, 527 (1985).

[76] J. E. Sipe and H. G. Winful, Opt. Lett. **13**, 132 (1988).

[77] C. M. de Sterke and J. E. Sipe, Phys. Rev. A **38**, 5149 (1988).

[78] H. G. Winful, J. H. Marburger, and E. Garmire, Appl. Phys. Lett. **35**, 379 (1979).

[79] W. Chen and D. L. Mills, Phys. Rev. Lett. **58**, 160 (1987).

[80] D. N. Christodoulides and R. I. Joseph, Phys. Rev. Lett. **62**, 1746 (1989).

[81] A. Aceves and S. Wabnitz, Phys. Lett. A 141, **37** (1989).

[82] C. M. de Sterke and J. E. Sipe, Progress in Optics, Vol. **XXXIII**, 203-260 (1994); C. M. de Sterke, K. R. Jackson, and B. D. Robert, J. Opt. Soc. Am. B **8**, 403 (1991).

[83] C. Conti and S. Trillo, Phys. Rev. E **64**, 036617 (2001).

[84] B. J. Eggleton, R. E. Slusher, C. M. de Sterke, P. A. Krug, J. E. Sipe, Phys. Rev. Lett. **76**, 1627 (1996).

[85] S. Phang, A. Vukovic, H. Susanto, T. M. Benson, and P. Sewell, J. Opt. Soc. Am. B **30**, 2984 (2013).

[86] Y. Xu, L. Feng, M. Mu, Y. Chen, IEEE Photonics Journal **6**, 0600507 (2014).

[87] C. Y. Huang, R. Zhang, J. L. Han, J. Zheng, and J. Q. Xu, Phys. Rev. A **89**, 023842 (2014).

[88] A. K. Sarma, J. Opt. Soc. Am. B **31**, 1861 (2014).

[89] M. –A. Miri, A. B. Aceves, T. Kottos, V. Kovanis, and D. N. Christodoulides, Phys. Rev. A **86**, 033801 (2012).

[90] W. E. Thirring, Ann. Phys. **3**, 91 (1958).

[91] N. A. Kudryashov, A. I. Maimistov, D. I. Sinelshchikov, Phys. Lett. A **376**, 3658 (2012).

[92] K. Senthilnathan, K. Porsezian, P. Ramesh Babu, and V. Santhanam, IEEE J. Quantum Electron. **39**, 1492 (2003).

[93] G. P. Agrawal, *Applications of Nonlinear Fiber Optics* (Academic Press, New York, 2001).

[94] J. Billingham and A. C. King, *Wave Motion* (Cambridge University Press, Birmingham, 2000).

[95] E. V. Kazantseva, A. I. Maimistov and S. S. Ozhenko, Phys. Rev. A **80**,043833 (2009).

[96] C. N. Kumar, R. Gupta, A. Goyal, S. Loomba, T. S. Raju and P. K. Panigrahi, Phys. Rev. A **86**, 025802 (2012).

[97] T. B. Benjamin and J.E. Feir, Theory. J. Fluid Mechanics **27**, 417 (1967).

[98] D. H. Peregrine, J. Aust. Math. Soc. Ser. B **25** , 16 (1983).

[99] P. A. E. M. Janssen, J. Physical Oceanography **33**, 863 (2003).

[100] G. Yang, L. Li, S. Jia, D. Mihalache, Rom. Rep. Phys. **65**, 391 (2013).

[101] D. J. Korteweg and G. de Vries, Phil. Mag. **39**, 422 (1895).

[102] J. Weiss, J. Math. Phys. **25**, 2226 (1984).

[103] B. B. Kadomtsev and V. I. Petviashvili, Sov. Phys. Dokl. **15**, 539 (1970).

[104] V. E. Zakharov and A. B. Shabat, Sov. Phys. JETP **34**, 62 (1972).

[105] P. Lax, Commun. Pure Appl. Math. **21**, 467 (1968).

[106] J. Yang, *Nonlinear Waves in Integrable and Nonintegrable Systems* (SIAM, Burlington, 2010).

[107] M. J. Ablowitz and Z. H. Musslimani, Phys. Rev. Lett. **110**, 064105 (2013).

[108] M. J. Ablowitz and Z. H. Musslimani, Nonlinearity **29**, 915 (2016).

[109] S.K. Gupta and A. K. Sarma, Europhys. Lett. **105**, 44001 (2014).

[110] H. Ramezani, T. Kottos, R. El-Ganainy, and D. N. Christodoulides, Phys. Rev. A **82**, 043803 (2010).

[111] K. Li, and P. G. Kevrekidis, Phys. Rev. E **83**, 066608 (2011).

[112] N. V. Alexeeva, I. V. Barashenkov, A. A. Sukhorukov, and Y. S. Kivshar, Phys. Rev. A **85**, 063837 (2012).

[113] M. –A. Miri, A. B. Aceves, T. Kottos, V. Kovanis, D. N. Christodoulides, Phys. Rev. A **86**, 033801 (2012).

[114] S.V. Suchkov, B.A. Malomed, S.V. Dmitriev, Y.S. Kivshar, Phys. Rev. E **84**, 046609 (2011).

[115] A. A. Sukhorukov, Z. Xu, and Y.S. Kivshar, Phys. Rev. A **82**, 043818 (2010).

[116] Z. H. Musslimani, K.G. Makris, R. El-Ganainy, D. N. Christodoulides, Phys. Rev. Lett **100**, 030402 (2008).

[117] R. Driben, B. A. Malomed, Opt. Lett. **36**, 4323 (2011).

[118] Y.V. Bludov, V. V. Konotop, B.A. Malomed, Phys. Rev. A **87**, 013816 (2013).

[119] A. K. Sarma, M. –A. Miri, Z. H. Musslimani, and D. N. Christodoulides, Phys. Rev. E **89**, 052918 (2014).

[120] W. P. Zhong, M. R. Belic, and T. Huang, Nonlinear Dyn. **70**, 2027 (2012).

[121] W. P. Zhong, M. R. Belic, Y. Zhang, Opt. Exp. **23**, 3708 (2015).

[122] M. Li, T. Xu, Phys. Rev. E **91**, 033202 (2015).

[123] A. Khare, A. Saxena, J. Math. Phys. **56**, 032104 (2015).

[124] B. Kibler, J. Fatome, C. Finot, G. Millot, F. Dias, G. Genty, N. Akhmediev, J. M. Dudley, Nat. Phys. **6**, 790 (2010).

[125] C. Dai, Y. Wang, X. Zhang, Opt. Exp. **22**, 29862 (2014).

[126] J. M. Dudley, G. Genty, F. Dias, B. Kibler, N. Akhmediev, Opt. Exp. **17**, 21497 (2009).

[127] B. Kibler, J. Fatome, C. Finot, G. Millot, G. Genty, B. Wetzel, N. Akhmediev, F. Dias, J. M. Dudley, Sci. Rep. **2**, 463 (2012).

[128] D. H. Peregrine, J. Aust. Math. Soc. Ser. B **25**, 16 (1983).

[129] H. Bailung, S. K. Sharma, Y. Nakamura, Phys. Rev. Lett. **107**, 255005 (2011).

[130] K. Hammani, B. Kibler, C. Finot, P. Morin, J. Fatome, J. M. Dudley, G. Millot, Opt. Lett. **36**, 112 (2011).

[131] W. Zhen-Kun, Z. Yun-Zhe, H. Yi, W. Feng, Z. Yi-Qi, Z. Yan-Peng, Chinesse Phys. Lett. **31**, 090502 (2014).

[132] G. Yang, Y. Wang, Z. Qin, B. A. Malomed, D. Mihalache, L. Li, Phys. Rev. E **90**, 062909 (2014).

[133] S. Chen, L. Song, Phys. Lett. A **378**, 1228 (2014).

[134] V. I. Shrira, V. V. Geogjaev, J. Eng. Math. **67**, 11 (2010).

[135] A. I. Dyachenko, and V. E. Zakharov, JETP Lett. **81**, 255 (2005).

[136] A. Chabchoub, N. P. Hoffmann, N. Akhmediev, Phys. Rev. Lett. **106**, 204502 (2011).

[137] D. R. Solli, C. Ropers, P. Koonath and B. Jalali, Nature **450**, 1054 (2007).

[138] Y. V. Bludov, V.V. Konotop, N. Akhmediev, Phys. Rev. A **80**, 033610 (2009).

[139] G. Oppo, A. M. Yao, D. Cuozzo, Phys. Rev. A **88**, 043813 (2013).

[140] J. Zamora-Munt, B. Garbin, S. Barland, M. Giudici, J. R. R. Leite, C. Masoller, J. R. Tredicce, Phys. Rev. A **87,** 035802 (2013).

[141] A. Zaviyalov, O. Egorov, R. Iliew, F. Lederer, Phys. Rev. A **85**, 013828 (2012).

[142] A. K. Sarma, M. Saha, J. Opt. Soc. Am. B **28**, 944 (2011).

[143] M. Saha, A. K. Sarma, A. Biswas, Phys. Lett. A **373**, 4438 (2009).

[144] A. K. Sarma, Commun Nonlinear Sci. Numer. Simulat. **14**, 3215 (2009).

[145] K. K. De , A. Goyal, C. N. Kumar, and A. K. Sarma, Commun. Nonlin. Sci Numer Simulat. **20**, 629 (2015).

[146] G. P. Agrawal, *Nonlinear Fiber Optics*, 5th Ed. (Academic Press, San Diego, 2013).

[147] F. Maucher, E. Siminos,W. Krolikowski, and S. Skupin, New J. Phys. **15**, 083055 (2013).

[148] S. P. Cockburn, H. E. Nistazakis, T. P. Horikis, P. G. Kevrekidis,N. P. Proukakis, and D. J. Frantzeskakis, Phys. Rev. Lett. **104**,174101 (2010).

[149] T. Pertsch, U. Peschel, J. Kobelke, K. Schuster, H. Bartelt, S.Nolte, A. Tunnermann, and F. Lederer, Phys. Rev. Lett. **93**,053901 (2004).

[150] C. Conti, M. Peccianti, and G. Assanto, Phys. Rev. Lett. **92**,113902 (2004).

[151] L. Gyorgi and R. J. Field, Nature **355**, 808 (1992).

[152] V. Petrov, V. Gaspar, J. Masere, and K. Showalter, Nature **361**, 240 (1993).

[153] L. Gyorgi and R. J. Field, J. Phys. Chem. **95**, 6594 (1991).

[154] T. Matsumoto, IEEE Trans. Circuits Syst. **31**, 1055 (1984).

[155] G. Ablay, Nonlinear Dyn. **81**, 1795 (2015).

[156] D. A. Egolf, I. V. Melnikov, W. Pesch, and R. E. Ecke, Nature **404**, 733 (2000).

[157] A. D. Stone, Nature **465**, 696 (2010).

[158] M. C. Gutzwiller et al., Am. J. Phys. **66**, 304 (1998).

[159] S. Shinohara, T. Harayama, T. Fukushima, M. Hentschel, T. Sasaki, and E. E. Narimanov, Phys. Rev. Lett. **104**, 163902 (2010).

[160] P. Ashwin, J. R. Terry, K. S. Thornburg Jr., and R. Roy, Phys. Rev. E **58**, 7186 (1998).

[161] H. G. Winful and L. Rahman, Phys. Rev. Lett. **65**, 1575 (1990).

[162] S. Zaitsev, O. Gottlieb and E. Buks, Nonlinear Dyn. **69**, 1589 (2012).

[163] M. J. Akram and F. Saif, Nonlinear Dyn. **83**, 963 (2016).

[164] K. Ikeda, Opt. Commun. **30**, 257 (1979).

[165] K. Ikeda and H. Daido, Phys. Rev. Lett. **45**, 709 (1980).

[166] G. Steinmeyer, D. Jaspert, and F. Mitschke, Opt. Commun. **104**, 379 (1994).

[167] M. Haelterman, Opt. Lett. **17**, 792 (1992).

[168] G. Steinmeyer, A. Buchholz, M. Hansel, M. Heuer, A. Schwache, and F. Mitschke, Phys. Rev. A **52**, 830 (1995).

[169] R. Vallée, Opt. Commun. **81**, 419 (1991).

[170] M. Nakazawa, K. Suzuki, and H. A. Haus, Phys. Rev. A **38**, 5193 (1988).

[171] M. B. van der Mark, J. M. Schins, and A. Lagendijk, Opt. Commun. **98**, 120 (1993).

[172] S. Coen, M. Haelterman, and Ph. Emplit, L. Delage, L. M. Simohamed, and F. Reynaud, J. Opt. Soc. Am. B **15**, 2283 (1998).

[173] A. Regensburger et al., Nature **488**, 167 (2012).

[174] M. A. Miri, A. Regensburger, U. Peschel, and D. N. Christodoulides, Phys. Rev. A **86**, 023807 (2012).

[175] A. P. Kuznetsov, A.V. Savin, D.V. Savin, Physica A **387**, 1464-1474 (2008).

[176] A. Boardman, J. Opt. **13**, 020401 (2011).

[177] N. Engheta and R. W. Ziolkowski, Metamaterials: Physics and engineering explorations (Wiley, Philadelphia, 2006).

[178] S. Zouhdi, A. Sihvola, A. P. Vonogradov, *Metamaterilas and Plasmonics: Fundamentals, Modeling, Applications* (Springer-Verlag, New York, 2006).

[179] V. G. Veselago, Sov. Phys. Usp. **10**, 509 (1968).

[180] D.K. Lynch, *Atmospheric Phenomena* (San Fransisco, CA: Freeman, 1980).

[181] A. D. Boardman, N. King and L. Velasco, Electromagnetics **25**, 365 (2005).

[182] R. A. Shelby, D. Smith and S. Schultz, Science **292**, 77 (2001).

[183] K. B. Alici and E. Özbay, Phys. Status Solidi (b) **244**, 1192 (2007).

[184] P. V. Parini, W. T. Lu, P. Vodo, and S. Sridhar, Nature **426**, 404 (2003).

[185] A. Grbic, G. V. Eleftherides, Phys. Rev. Lett. **92**, 117403 (2004).

[186] W. Cai and V. Shalaev, *Optical Metamaterials: Fundamentals and applications*, (Springer, New York, 2010).

[187] J. B. Pendry, Contemporay Physics **45**, 191 (2004).

[188] S. Xiao et al., Nature **466**, 735 (2010).

[189] A.K. Popov and V.M. Shalaev, Opt. Lett. **31**, 2169 (2006).

[190] E. G. Post, *Formal Structure of Electromagnetics: General Covariance and Electromagnetics* (Interscience, New York, 1962).

[191] M. Lax, D. F. Nelson, Phys. Rev. Lett. **13**, 1777 (1962).

[192] A. J. Ward, J. B. Pendry, J. Mod. Opt. **43**, 773 (1996).

[193] U. Leonhardt, Science **312**, 1777 (2006).

[194] J. B. Pendry, D. Schurig, D. R. Smith, Science **312**, 1780 (2006).

[195] S. Savoia, G. Castaldi, V. Galdi, A. Alu and N. Engheta, Phys. Rev. B **89**, 085105 (2014).

[196] G. Castaldi, S. Savoia, V. Galdi, A. Alu and N. Engheta, Phys. Rev. Lett. 110, 173901 (2016).

[197] D. A. Antonosyan, A. S. Solntsev and A. A. Sukhorukov, Opt. Lett. **40**, 4575 (2015).

[198] R.W. Boyd, *Nonlinear Optics*, 3rd ed. (New York, Academic Press, 2008).

[199] A.K. Popov, S.A. Myslivets and V.M. Shalaev, Appl. Phys. B **96**, 315 (2009).

[200] A. Amir, N. Hatano, and D. R. Nelson, Phys. Rev. E **93**, 042310 (2016).

[201] C. M. Bender, A. Ghatak, M. Gianfreda, arXiv:1604.03928v1 [nlin.CD].

[202] X. Sun, Z. Yang, X. Liu, C. Li, Y. Dong, L. Xie, and J. E. Sipe, Opt. Exp. **19**, 7176 (2011).

[203] H. Li, J. Dou, and G. Huang, Opt. Exp. **21**, 32053 (2013).

[204] X. Wang and J. Wu, Opt. Exp. **24**, 4289 (2016).

[205] Z. Zhang, Y. Zhang, J. Sheng, L. Yang, M. -A. Miri, D. N. Christodoulides, B. He, Y. Zhang, M. Xiao, arXiv: 1604.04025 [physics. optics].

[206] B. Peng, S. Kaya, Ö. Fuchuan, L. F. Monif, M. Gianfreda, G. L. Long, S. Fan, F. Nori, C. M. Bender, L. Yang, Nat. Phys. **10**, 394 (2014).

[207] L. Chang, X. Jiang, S. Hua, C. Yang, J. Wen, L. Jiang, G. Li, G. Wang, and M. Xiao, Nat. Photon. **8**, 524 (2014).

[208] L. Ge, M. Shen, C. Ma, T. Zang, and L. Dai, Opt. Exp. **22**, 29435 (2014).

[209] C.-Q. Dai, X.-G. Wang, Nonlin. Dyn. **77**, 1133 (2014).

[210] B. Midya, Nonlin. Dyn. **79**, 409 (2015).